Determinants of trafficking, conduction, and disease within a K^+ channel revealed through multiparametric deep mutational scanning

Short Title: Multiparametric Deep Mutational Scanning in the Inward Rectifier Kir2.1

Authors: Willow Coyote-Maestas[1#], David Nedrud[1], Yungui He[2], Daniel Schmidt[2§]

Affiliations: [1]Department of Biochemistry, Molecular Biology & Biophysics, University of Minnesota, Minneapolis, MN, 55455, USA; [2] Department of Genetics, Cell Biology & Development, University of Minnesota, Minneapolis, MN, 55455, USA

[#]Present address: Department of Bioengineering and Therapeutic Science and Quantitative Biosciences Institute, University of California, San Francisco, San Francisco, CA, 94158

[§]Correspondence and requests for materials should be addressed to D.S. (email: schmida@umn.edu)

Abstract:

A longstanding goal in protein science and clinical genetics is to develop quantitative models of sequence, structure, and function relationships and delineate the mechanisms by which mutations cause disease. Deep Mutational Scanning (DMS) is a promising strategy to map how amino acids contribute to protein structure and function and to advance clinical variant interpretation. Here, we introduce 7,429 single residue missense mutation into the Inward Rectifier K^+ channel Kir2.1 and determine how this affects folding, assembly, and trafficking, as well as regulation by allosteric ligands and ion conduction. Our data provides high-resolution information on a cotranslationally-folded biogenic unit, trafficking and quality control signals, and segregated roles of different structural elements in fold-stability and function. We show that Kir2.1 trafficking mutants are underrepresented in variant effect databases, which has implications for clinical practice. By comparing fitness scores with expert-reviewed variant effects, we can predict the pathogenicity of 'variants of unknown significance' and disease mechanisms of know pathogenic mutations. Our study in Kir2.1 provides a blueprint for how multiparametric DMS can help us understand the mechanistic basis of genetic disorders and the structure-function relationships of proteins.

Introduction

Inward rectifier K^+ (Kir) play a central role in physiology by setting, maintaining, and regulating a cell's resting membrane potential [1]. Misregulated Kir cause neurological disorders (alcohol and opiate addiction[2–4], Down's syndrome [5], epilepsy [6], Parkinsons [7]), cardiac disorders (Long QT syndrome [8]), hereditary renal diseases[9], and diabetes [10].

While some mechanisms that underlie disease-causing Kir variants involve aberrant function (gating, ion permeation, ligand binding [11]) or transcript processing [12], disease-causing variants are often linked to trafficking defects. For example, over half the missense mutations investigated in Kir1.1 (ROMK1) affected surface expression, often caused by proteosomal degradation of folding-deficient or mistrafficked channels [13,14]. A comparison of mutation hotspots in the Kir C-terminal domain (CTD) revealed that ~60% of variants could be linked to impaired surface expression [15,16]. Many mutations linked to neonatal diabetes reduced Kir6.2 surface expression to varying degrees [17]. Beyond known trafficking signals (e.g., ER and Golgi-export signal sequences [18–23]), mutations along the entire Kir primary sequence can disrupt surface expression [16]. Several additional factors control surface expression, such as protein stability, interactions with trafficking partners, and complexes that stabilize channels in the membrane [20,24,25].

The apparent prevalence of Kir trafficking phenotypes has a significant caveat: phenotypes are experimentally determined for a small fraction of possible or clinically observed variants. Of the 8,113 possible missense mutations for KCNJ2/Kir2.1 only 163 are represented in ClinVar– a database of clinically observed variation and phenotypes [26] (**Fig. 1A, Supplementary Fig. 1**). Most studies focus on common natural variants observed in human genomes or exomes. Rare genetic variants vastly outnumber common variants [27] and are implicated in a substantial portion of complex human disease [28]. Rarity means that clinical significance (benign or pathogenic) of most variants cannot be established using genome-wide association studies due to low statistical power for calling pathogenic variants. For KCNJ2/Kir2.1 ClinVar reports 144 missense mutations, but most (72%) have "uncertain significance" or conflicting or no interpretation (**Fig. 1A**). Computational algorithms (PolyPhen-2 [29], SIFT [30], EVE [31] etc.) are currently filling this gap by predicting the consequence of mutations. However, computational approaches work best in conserved regions of genes and cannot predict mechanism of pathogenicity.

Despite a central role for Kir trafficking and function in disease etiology, there are no large-scale studies that comprehensively study sequence determinants of K_{IR} trafficking and function. Previous studies focused on a small subset of common natural variants, while systematic variation is needed for a global picture of Kir trafficking and function. Beyond explaining disease, large-scale mutational studies can reveal intrinsic properties of proteins [32–34], determine protein structures [35], and inform mechanistic models of protein structure function relationships [36].

Here, we combine programmable mutagenesis library generation with multi-parametric sequencing-based assays for surface expression and function of Kir2.1. Our data reveal distinct determinants for Kir trafficking, folding, tetramerization, and function. The phenotype of most clinically observed variants can be explained by impacting function, which may be related to the essential role of Kir2.1 in human physiology. We also find further support for the hypothesis that a hierarchical organization of ion channels structure balances stability and flexibility for folding and function [34].

A multi-parametric deep mutational scan of kir2.1

For Kir2.1 to fulfill its roles in cellular physiology, it must be ER targeted, folded, tetramerized, and surface trafficked (**Fig. 1B**). Once trafficked to the cell surface, Kir2.1 must be sensitive to Phosphatidylinositol 4,5-bisphosphate (PIP_2) [1,37], undergo gating associated conformational transitions (pore opening and closing), and selectively conduct K^+.

To probe how Kir2.1 mutations affect these processes, we use a programmable deep mutagenesis approach (SPINE [38,39]) and mutated residues 2-392 of mouse Kir2.1 (Uniprot P35561) to every other amino acid (**Fig. 1C**). We included synonymous mutations in 20 Kir2.1 positions as an internal standard to determine wildtype fitness. From this DMS library, we generated a stable single copy library cell line using BxBI-mediated recombination [40] for stringent genotype-phenotype linkage. Endogenous channel currents in HEK293 are negligible when compared to those of exogenous channel driven from a strong constitutive promoter (CAG) [41].

Since mutations can affect any of the abovementioned processes, multi-parametric assessment of phenotypes is required to develop a comprehensive mechanistic understanding of Kir2.1 variation. We focused on separating a mutations effect on secretion, folding, and trafficking (‘surface expression’) and allosteric regulation and ion conductance (‘function’). Considering the

library size of variants (391x19 = 7,429 variants), assays that assess surface-expression and function must be high-throughput. Cell-based assays coupled to fluorescently activated cell sorting that can separate cell population (and the genotypes encoding in population) based on a phenotype reported by fluorescent reporters are immensely flexible.

Mutations that interfere with secretion, folding, or trafficking will cause reduced Kir2.1 surface expression [42–44]. To measure Kir2.1 surface expression in cells we inserted an epitope tag into the extracellular loop (T115 [45]). Cells with surface trafficked variants can be separated from poorly expressed variants based on antibody-labeling and fluorescence-activated cell sorting (FACS) (**Supplementary Fig. 2**). Phenotypes can be linked to genotype by NGS. We've extensively used this method in FACS-based genotype-phenotype assays [34,38,46].

Functional Kir2.1 hyperpolarizes HEK293 cells by driving the resting membrane potential (RMP) towards the reversal potential of K^+ (-80mV) while non-functional Kir2.1 variants do not affect the RMP (-35mV). We can measure RMP with voltage sensitive dyes, such as the FLIPR Blue, a concept that we and others demonstrated in optical Kir functional assays [46,47]. Changes in membrane voltage alter dye membrane partitioning, and therefore extinction coefficient and fluorescence. Hyperpolarized cells expressing functional Kir2.1 can be separated from more depolarized cells expressing non-functional Kir2.1 by FACS using FLIPR dye fluorescence (**Supplementary Fig. 3**). As with surface expression, phenotype can be linked to genotype by NGS.

A global view of trafficking determinants

To learn how amino acids contribute to and mutations alter Kir2.1 trafficking and folding, we sorted and sequenced the Kir2.1 DMS library based on surface expression by FACS-seq. Surface trafficking fitness was determined for 6,898 Kir2.1 variants (93%). Biological replicates for subpools were highly correlated (Pearson correlations 0.85-0.94, **Supplementary Fig. 4**) and shows read depth is excellent (greater than 30-fold at most positions, **Supplementary Fig. 5**; **Supplementary Table 1A**). Surface expression fitness scores and standard errors were calculated using Enrich2 [48]. Enrich2 calculates log enrichment by fitting a weighted regression based on changes in mutation frequency across samples within an experiment. Median fitness error relative to measurement rang was low (7.5%) in the surface expression assay based on synonymous mutation standard deviations (**Fig. 2A, Supplementary Fig. 6**). Surface fitness

follows a bimodal distribution with one population of mutations centered at wildtype fitness and the other population strongly decreasing surface expression (**Fig. 2A**).

As expected, mutations are highly deleterious within the Flag-tag used for surface labeling and known trafficking signals (**Fig. 2B**). Substituting aromatic residues with charged residues strongly decreases surface expression within the ^{81}WRWMLLLLF^{88} motif that mediate interaction with Caveolin-3 [49]. Glutamates within the di-acidic ER export signal, ^{382}FCYENE^{387} [50], are quite sensitive to mutations with the second glutamate being far more sensitive. Interestingly, negatively charged mutations, N386E or N386D, between the di-acidic motif increase surface expression.

A Golgi export signal comprised of two residues patches at Kir2.1's N- and C-termini interacts with the AP1 adaptin complex to target Kir2.1 to clathrin-coated vesicles for Golgi to plasma membrane trafficking [25]. Others have used alanine mutagenesis screens to identify sequence determinants for Golgi export. First, Ma et al. [25] defined the minimal signal motif comprised of hydrophobic residues (I321, W323, Y316) and a juxtaposed electrostatic interaction between R46 and E327. Later, Li et al. [18] included salt bridges between basic residues in the N-terminus (R44, R46, K50) and C-terminus (E3201, E327), and hydrophobic residues (F203, L239, I240, F300). This structured trafficking signal is formed when the CTD has folded correctly to include a hydrophobic cleft, an adjacent cluster of basic residues, and a network of interactions between termini and adjacent subunits. Ma et al. suggested this structured trafficking signal predisposes Golgi exit on correct protein conformation; our comprehensive mutagenesis suggests this quality control mechanism may extend beyond previously identified sequences. It appears to involve all core beta sheet in the CTD (βD1, βH, βI, βJ, βK, βB2, βC, βG) and helices αG and αF (**Fig. 2B,C**). Across CTD secondary structure elements, we find a distributed network of residues that, when mutated, result in reduced surface expression (**Fig. 2D**). Changes to the packing of the hydrophobic core of the CTD will likely impact the Golgi export motif orientation. We hypothesize that the Golgi export signal is a reporter for folding of the entire CTD. Several lines of evidence support this hypothesis: IgG-like domains are a beta sheet sandwich with conserved hydrophobic residues at sheet interfaces that are crucial for fold stability [51,52], computational mutagenesis in Kir1.1(ROMK1) showed these residues are crucial for fold stability, and experimental mutagenesis found mutations strongly reduces inward rectifier surface expression [15,53]. Residues in this network belong to the same monomer; disrupting interactions between residues belonging

to neighboring monomers (e.g., carbon–ð and ð–ð interactions between F45, L246, Y338; **Fig. 2B,E**) do not uniformly reduce surface expression. Although Kir are presumably already assembled into tetramers [54], our data suggests the conformational checkpoint for Golgi export requires properly folded monomers not correctly assembled tetramers.

Sites enriched for beneficial or deleterious substitutions could point to additional mechanisms for Kir2.1 trafficking control. Along those lines, we observe that substitution of N- and C terminal residues (G2–G31, S377-S381) with polar mutations have neutral trafficking phenotypes, while aromatic or hydrophobic mutations tend to decrease surface expression. While we do not know the underlying mechanism, our data suggests disordered N- and C-termini are important in targeting Kir2.1 to the cell surface.

Mutations along βB2(M211–K215), βDE(S242–P252), βK(R333, P336), βL(F339), βM(Y345), βN(Y366), and αF helix(K372–L376) tend to improve surface-trafficking above WT especially when aromatic residues are replaced with any non-aromatic amino acids (**Fig. 3A**, t test p-value 0.017). These sites form a patch on the outer face of the CTD domain where two subunits interdigitate (βDE from one subunit, the remaining elements from another subunit; **Fig. 3B**). In this region beneficial mutations have no clear physicochemical preferences beyond non-aromatics. While no known trafficking signal matches, aromatic residues are often binding interfaces [49,55]. Perhaps mutations alter trafficking patterns by disrupting protein interactions (e.g., reduce ER retention, reduce forwarding to lysosomal recycling).

The agreement with earlier trafficking studies in Kir2.1 shows that our high-throughput surface expression assay works. This allows us to establish a global view of sequence/trafficking relationships in Kir2.1. Comprehensive mutagenesis allows us to validate and fill in the gaps on existing models of channel trafficking [18,25] while discovering new potential trafficking determinants.

A cotranslationally-folded biogenic unit in Kir2.1

By examining structured regions sensitive to mutations, we identify determinants of Kir2.1 folding. In the pore domain, we find the lower halves of M1 and M2 are surprisingly tolerant to mutation, in particular residues whose sidechains project towards the pore cavity. At the base of the pore domain, mutations are highly deleterious within a cluster of hydrophobic residues (W81, L85, I178, F182, I187, M191) that form inter-monomer interactions between M1 and M2 helices. The top of

the pore domain –a region comprised the upper halves of M1, M2, pore helix, and selectivity filter– is extremely intolerant to substitutions. This includes the M2-pore helix loop (e.g., H110–E133), whose amino acid sidechains contribute to tight packing centered around a hydrophobic pocket formed by F103 (M1), F143 (pore helix), V169 (M2), and V131 M1-pore helix loop (**Fig. 3C**). The same region contains two highly conserved cysteines (C130, C162) that form a disulfide bond which is critical for folding, not function (K^+ conductance) [56,57,57,58]. Others found P156, at M2's apex, is essential for efficient surface trafficking in Kir2.2 [59]. In agreement with folding critical roles, all substitutions in these positions are deleterious to surface expression.

Glycines in the selectivity filter (^{147}TQTTIGYG^{154} in Kir2.1; conserved residues are underlined), which are absolutely conserved in all K^+ channels, are immutable. Because glycine is achiral, it is the only canonical amino acid that can satisfy the unusual conformation of the selectivity filter main chain, which alternates between left-handed and right-handed α-helical dihedral angles [60]. Substitutions of either T150 (which occupies unfavorable backbone torsion angle conformation in the Kir2.2. crystal structure [37,56]) or Y153 (which forms π–π interaction to a neighboring subunit) in the selectivity filter with glycine significantly increase surface expression. This suggests the peculiar conformational requirements of the selectivity filter are a constraint in channel biogenesis.

Based on the extreme mutational sensitivity, high contact density of side chain packing in the Kir2.2 crystal structure, and known disulfide-mediated fold stabilization, we propose that the top halves of M1 & M2, pore helix, and the M2-pore helix loop promote tertiary structure formation within nascent Kir2.1 monomers (perhaps in the ER translocon) to establish correct topology and promote membrane insertion. This may be a general feature of K^+ channel folding, as a similar "cotranslationally folded biogenic unit" was proposed for Kv1.3, in which S5/pore loop/S6 interact to establish a "reentrant pore architecture" and correct topology early in channel biogenesis without requiring tetramerization [61,62]. Interestingly, residues from neighboring subunits interact with this putative biogenic unit in the fully assembled channel (e.g., selectivity filter residues Y153, which forms a ð–ð interaction with F143 and F155, carbon–ð interaction with E133) are relatively tolerant to mutations. This supports the idea that early trafficking-critical folding events involve only intra-monomer interactions.

Regions involved in gating transitions to do not contribute to fold stability

From the perspective of surface-trafficking as the measured phenotype, several regions of Kir2.1 are tolerant to mutations. This includes the interface between pore and CTD (comprised of slide helix αA/αB, inner helix gate (I183–M188), and tether helix αF), the G-loop (βH-βI loop), and the residues lining the CTD cavity (loops between βC-βD and βE-βG) at the interface between different subunits (**Fig. 3D**). Interestingly, these are involved in gating associated conformational changes [37,63] induced by the binding of PIP_2, Kir2.1 allosteric activator (two-sided Fisher's Exact Test, p-value 8.091e-05, odds ratio 2.47). An explanation for high mutational tolerance in gating structural elements is that they have higher conformational flexibility required for interconversion between different gating states. They are therefore unlikely to contain motifs recognized by folding-based quality control mechanisms.

Kir2.1 appears to have an internal organization into contiguous regions involved in fold-stability (biogenic folding unit, IgG-like CTD) and gating transitions (TM/CTD interface, CTD subunit interfaces) with distinct mutational tolerance. To understand the relationship between folding and function, we assayed K^+ conductance as a second phenotype for the DMS library.

Functional phenotype assays map molecular determinants of conduction and PIP_2 sensitization

To assay variant function, we sorted the Kir2.1 DMS library (in duplicate, on separate days) into based on voltage-sensitive dye fluorescence, sequenced, and calculated fitness using the same Enrich2 package. This assay is based on premise that Kir2.1 decreases RMP resulting in decreased fluorescence of the FLIPR dye. Functional fitness was determined for 6,944 Kir2.1 variants (93.4%), with similar replicates (Pearson correlations 0.86-0.93, **Supplementary Fig. 7**) and excellent read depth (greater than 30-fold at most positions, **Supplementary Fig. 8**; **Supplementary Table 1B**). Based on synonymous mutation standard deviations (**Fig. 4A**), median fitness error was low (15.3%). Unlike the bimodal distribution for surface-expression fitness, functional fitness is unimodal, with most mutations neutral (**Fig. 4A**); there is no distinct low function population likely due to lower dynamic range of the voltage sensitive dye compared to fluorescent antibody labelling (**Supplementary Figs. 2-3**). Function fitness is the combination of surface expression (number of channels on surface) and individual channel functional properties (open probability, single channel conductance, K^+ selectivity, etc.). Furthermore, as our assay is measuring steady-state RMP and even partially functional Kir2.1 will eventually

hyperpolarize the cell. This means we must interpret functional fitness in context of surface expression fitness.

Many variants in the pore domain have low functional fitness scores (e.g., pore helix, selectivity filter, **Fig. 4B**). For example, Y153 mutations, which have relatively tolerant surface fitness, strongly reduces function (**Fig. 4C**). Y153 interacts through π-π interactions with F143 and F155 on a neighboring subunit and mutations may preclude correct selectivity filter geometry to conduct K^+ ions. The conservative substitution Y153F has a neutral phenotype, in agreement with earlier electrophysiology studies [64,65]. Many positions along the pore helix that form a hydrogen bond network to support a conductive and K^+ selective state [66] are very sensitive to mutation. Mutations of conserved hydrophobic residues in the CTD core beta sheet (e.g., W220) and the Golgi export signal (e.g., hydrophobic cleft residues Y316, W323, and salt bridge R45, E327) are deleterious as predicted by their effect on surface-expression.

Disordered N and C termini including the ER export signal FCYENE had moderately low surface-expression fitness but their functional fitness is mostly near neutral (**Fig. 4D,F**). This suggests mutations within the disordered regions only impact trafficking of otherwise properly folded and functional channel. Mutations within the unstructured termini they are deleterious to surface-expression and but neutral to individual channel function.

PIP_2 binding at the TM/CTD interface induces a disorder-to-order transition in the tether helix, contracting it and thereby translating the CTD toward the pore domain. The engagement between and CTD and pore domain allows the G-loop to wedge into the pore domain and the inner helix activation gate to open [37]. PIP_2's binding site includes pore domain residues (R80, W81, R82, K190) and CTD residues (K186/193, K188/195, K189/196, R65, R219/226, R197). As expected, surface-expression fitness was neutral and functional fitness was negative (**Fig. 4E,G**). By focusing on mutation-sensitive positions, we can trace secondary structural elements that couple the PIP_2 binding site to the Kir2.1's gate, the G-loop [67]. We find residues that directly interact with PIP_2 in the pore domain (R80, W81, R82) and tether helix (K190, K193, K195, K196). We find additional residues in the tether helix (R197), βB1 (L202), and interfacial helix (R65) interact with the allosteric coupling βC-βD regions. Residues are highly sensitive in the entire βC-βD and its interactions including a hydrophobic interface between βC and βI with each subunit, several

interactions couple to the βCD loop (e.g., H229) and βEG loop (e.g., F270) of one subunit to the βH (I305), βI (R320), and the G-loop gate of another subunit (**Fig. 4H**).

Taken together, deep mutational scanning reinforces a central role of the βCD loop propagating PIP_2 binding at the TM/CTD interface to the G-loop gate. Molecular dynamics simulations uncovered an extended network of interactions between N-terminus, tether helix, CD loop keep the G-loop gate in a closed state [63]. Electrophysiology demonstrated that mutations in R219, which is conserved in the K_{IR} family, attenuate PIP_2 affinity [68] and causes Anderson Tawill Syndrome [69]. Mutating the corresponding residues in GIRK2/Kir3.2 (R201A) constitutively activates channels, presumably by forcing the βCD loop into conformation that mimics the G-protein activated state [70].

In GIRK2, an aspartic acid in βCD (D228) is a key residue in mediating regulation by intracellular sodium (an important physiological role of GIRK2). This Na^+ binding site propagates conformational changes in the CTD's β strands after Gβγ binds to βDE and βLM loops, displacing the βLM loop upward to interact with the N-terminus and βCD loop, ultimately stabilizing the open conformational of the G loop gate [71,72]. The corresponding wildtype amino acid in Kir2.1, which is not regulated by Na^+, is N224 (**Fig. 4B**). Interestingly, substitution with aspartate increases Kir2.1 function, perhaps by recapitulating the Na^+ binding site, which also involves coordination from main chain carbonyls (R226, K227, S228). The function increasing effect of N224K (and the deleterious effect of N224R) could be explained through the Na^+-independent stabilization of the βCD loop through hydrogen bonding between the protonated epsilon-amino group of lysine (mimicking Na^+) and the abovementioned carbonyl oxygens.

Another striking feature revealed by functional assays are function-increasing mutations near the helix bundle crossing gate of Kir2.1 (**Fig. 5A**). Previous studies suggested a kink occurring at G176 in TM2 widens the pore at the helix bundle crossing (HBC) allowing for K^+ to pass [73–75]. As expected, mutating G176 decreased function fitness. Substitution in residues below the kink-inducing G176 and above the actual bundle crossing (V187), increases functional fitness. This effect is strongest in A173, I175, I176, G177 (corresponding to S174, M176, I177, G178 in Kir2.2; **Fig. 5B**). Together, residues form a cuff above the HBC gate coupling TM2 from different subunits. The cuff may stabilize the unkinked conformation of TM2 to decrease open probability. Consistent with this idea, mutating cuff residues to large charged amino acids has the greatest function-

increasing effect (**Fig. 4C**). Perhaps mutating to large, charged residues disrupts nearby hydrophobic interactions networks that stabilize the HBC close state. The HBC gate is also stabilized by hydrophobic contacts to the TM1 of an adjacent subunit [76,77]. Consistent with TM1 interactions forming a gating energy barrier, mutating interacting TM1 residues (F88; F86 in Kir2.2) also increases function fitness.

To identify regions that are important for function and not surface expression, we z-scored and subtracted surface expression from function fitness. We used t-tests with pooled variance estimated from all mutations to test significance of difference in fitness and function scores for each position (**Fig. 5C)**. For many positions, surface scores were significantly lower than function scores (**Fig. 5C, cyan circles**). This subset includes the FLAG tag that is required for surface expression assay, but also Golgi export motifs, transmembrane helices, and CTD core beta sheets. For another subset of positions, function scores were significantly lower than surface-expression scores (**Fig. 5C**, magenta circles). This includes sites involved in gating (PIP_2 binding, G-loop gate), and K^+ conduction (selectivity filter). By making a binary assignment (based on p-value) whether a position belongs to one subset or the other and mapping this assignment onto the Kir2.2 structure, we again find structural organization around elements that are important for fold stability (TM, CTD beta sheets) and function (PIP_2 sensitization, gating, K^+ conduction) (**Fig. 5D**). This distinct organization is clearest in the pore domain, where all interactions within a subunit are driving surface expression score (**Fig. 5E,** cyan sticks), while residues mediating subunit interactions (which is required for stability of the selectivity filter) are driving function score (**Fig. 5E,** magenta sticks). Other residues that drive function scores are distributed along an interaction network that connects the PIP_2 binding site (M2, αF) with the slide helix (αA/B), βCD loop, βEG loop, and the G-loop gate (βHI loop) (**Fig. 5F**). Intriguingly, this network involves interfaces between adjacent subunits (N-terminus<>βLM loop interface, βI<>βCD loop, βD<>βEG loop). Subunit interactions determining gating is consistent with recent crystal structures of a forced-opened Kir2.2 in which inner helix gate opening requires CTD subunits to move relative to each other [77].

Overall, the functional assay allows us to validate and test existing models of Kir2.1 gating while also providing further evidence that inter-subunit interactions serve as an energy barrier to bias Kir2.1's conformational ensemble towards closed states.

Most pathogenic inward rectifier mutations are clustered within functionally important residues

A central goal in molecular genetics is identifying the mechanistic basis by which mutations cause disease. Multiparametric DMS studies that interrogate multiple phenotypes associated with variants are a promising strategy to answer this question. Based on the premise that most mutation affect protein stability, approaches such as Vamp-Seq [78] were developed as generalizable measures of protein abundance. In cases such as Kir2.1, where proper trafficking, localization, and gating are crucial for producing functioning proteins, measuring abundance likely won't work. It is necessary to differentiate between mutations' effects on folding, trafficking, and gating to learn the mechanism for how genotype affects Kir2.1 phenotype. To learn potential pathogenicity and mechanism of action for reported disease-associated mutations, we compared the surface expression and fitness data to clinically observed mutations.

Since the overall domain architecture and structure/function relationships are conserved within the inward rectifier family, we reasoned that the mechanisms underlying variant effects are conserved, as well. We therefore gathered missense variant effects reported in Clinvar and dbSNP for inward rectifiers. By aligning all human Kir, we assigned the corresponding Kir2.1 position to each variant (total variant count: 613) and noted whether wildtype amino acid matches between Kir2.1 and the aligned Kir (**Supplemental Table 2**). To test if variants in Clinvar or dbSNP is related to surface-trafficking or function, we compared the empirical cumulative distribution functions of trafficking and function scores variants in databases vs. those that are not. They differed for trafficking scores but not for function scores (two-sided Kolmogorov-Smirnov test p-values 4.28×10^{-8} and 0.51, respectively; **Fig. 6A**). This means being listed in genetic variation databases is related to Kir2.1 function and less related to trafficking. Variants with low surface scores in our DMS, are underrepresented in databases. A likely explanation is that Kir2.1 is essential for normal physiology and therefore under strong selection. Indeed, Kir2.1 homozygous knockout mice die 8 to 12 hours after birth [79]. Kir2.1's missense constraint score, based on exome and whole-genomes sequencing deposited in gnomAD [80], is 0.5 (i.e., 121 observed vs. 240 expected missense mutations based on background mutation rates). Variants that misregulate surface trafficking likely are more deleterious (e.g., abolishing all K^+ conductance) than variants affecting function (e.g., gating kinetics), which is why they are extremely rare in the living human population. Consistent with this idea, exome and targeted sequencing in products of conception showed a significant enrichment of pathogenic variants

associated with cardiac channelopathies in stillbirths [81]. Furthermore, only one variant (W232C) of the 5 most surface-trafficking impairing positions on Kir2.1's Golgi export motif (R44, S315, E320, W323, G333) is reported in Clinvar.

The correspondence between variant listing and Inward Rectifier function is also apparent when we annotate mean surface-trafficking and function scores with pathogenic variants (**Fig. 6C**). Across the board, hotspots enriched for pathogenic disease-associated mutation have low function scores, whereas their surface-expression scores are more varied. Variants of uncertain significance followed this trend. In addition to regions involved in PIP_2-binding (αA/B slide helix, lower part of M1, αF), and propagating conformational changes to the G-loop gate (βB1, βCD, βHI loop), pore helix and selectivity filter are also hotspots for pathogenic variants. A notable exception to down-trending function in mutational hotspots is a cluster of disease-associated variants near the intracellular end of M2 (D180-A186). Interestingly, many Clinvar-reported variants (e.g., I183L) are associated with Short QT syndrome, a disease that can be caused by gain of function mutations in KNCJ2(Kir2.1) [82]. Consistent with this clinical phenotype, many mutations increase function (compared to wildtype Kir2.1). Based on known structure/function relationship in inward rectifiers, we speculate that substitutions increase function by increasing open probability of Kir2.1 by disrupting the inner helix gate (I183–M188).

We further divided fitness scores by assigned clinical significance to estimate the fitness score bounds of expert-reviewed benign and pathogenic variants (**Fig. 6D,E**). For surface fitness, we find that >97.5% of known benign variant have a fitness score > -0.43. With this lower bound assumption for benign variants, we predict that any 'variant of unknown significance' (VUS) scoring lower will be pathogenic with a loss of surface expression phenotype. Conversely, the upper surface fitness score bound (10^{th} percentile) for expert reviewed benign was 0.95, and VUS with greater surface scores are predicted to have a gain of surface expression pathogenic phenotype. We applied the same reasoning to function fitness scores. Using this estimate, we can assign a predicted pathogenic phenotype (loss/gain of surface expression/function) to 69 of 370 (18%) Kir2.1 VUS **(Supplemental Table 2)**. The primary sequence location of these predicted pathogenic variants is shown in **Fig. 6C**. Many predicted loss of function variants localize to the slide & tether helices, G-loop gate, and selectivity filter/pore helix. Gain of surface expression variants map to the βBC and βK loop near the interface to βDE of a neighboring subunit. The putative biogenic folding unit (top of M1 & M2, pore helix) contains several predicted

loss of surface expression variants. Interestingly, no expert-reviewed pathogenic variants map to this region, which suggests that DMS-based prediction can identify new mutation hotspots.

We can also use estimated bounds of benign variants to predict the mechanism through which 27 out of 144 (18.8%) expert-reviewed pathogenic variants cause Kir2.1 disorders. Of those, eight pathogenic variants have a predicted loss of surface expression while 19 are predicted loss of function. In line with function-impairing variant being overrepresented in ClinVar, the odds ratio between predicted loss of function phenotype of known pathogenic variants vs. all predicted pathogenic variants is significantly different (two-sided Fisher's exact test, p-value = 0.003144).

Taken together, we find variants with deleterious surface-score are underreported in available database, which we propose is due to the essential nature of Kir2.1 in human physiology. Using surface and function scores for expert-assigned variant, we can estimate bounds for benign variants, which then allows us to predict VUS that are above or below these bound to the be gain or loss of surface expression/function, respectively. We can also predict the mechanism of action through which known pathogenic mutations cause Kir2.1 disorders. This suggests that DMS-derived surface-trafficking and function scores can be useful to predict pathogenicity and underlying mechanism of inherited and de-novo mutations. Because of the conserved architecture of the Inward Rectifier family, assignment of mutation hotspots may extend to the entire inward rectifier family. Further corresponding DMS studies in other members of the inward rectifier family are required to separate generalize themes from idiosyncrasies. For example, Kir6.2 requires binding to the ABC-transporter SUR1 to be expressed to the cell surface and function. This means that assay-reported phenotypes for a subset of variation at the Kir6.2/SUR1 interface (involving αA/B slide helix, M1, βLM sheets) have greater bearing in Kir6.2-linked diseases (e.g., diabetes mellitus). The methods described here are a blueprint for these studies.

Discussion

Deep Mutational Scanning (DMS) quantitatively links protein phenotypes to the genetic variation within the protein's coding sequence. This style of systematic amino acid substitution can reveal protein function [83–85], determine protein structure [86], and explain protein behavior in healthy and diseased cellular contexts [87]. Because protein don't exist in isolation –within the context of a cell folding, trafficking, and function states can all be modified through protein interaction (e.g., chaperones) or ligand binding (e.g., allosteric modulators)– the phenotypic outcome of genetic variation can be multi-facetted. To start to explore the numerous impacts of mutations, we

459 measure two phenotypes of Kir2.1 variation: surface-trafficking K^+ conduction. Both assays are
460 based on cell sorting mediated by fluorescent signals (antibody binding to an extracellular loop
461 and voltage sensor dye). By measuring how variants are enriched or depleted, we assign
462 quantitative fitness scores. Many other assay types are compatible with this approach, providing
463 opportunities for even richer phenotypic description of ion channel variation. For example, a
464 recently described approach, HiLITR [88], could provide more granular resolution about trafficking
465 motifs and Kir2.1 localization in living cells. Spontaneous spiking HEK cells [89,90], which co-express
466 Kir2.1, a voltage-dependent Na^+ channel (Nav1.7), the channelrhodopsin CheRiff, and genetically
467 encoded voltage indicator QuasAr2, could be adapted to evaluate how ion channel expression
468 levels and gating properties impact excitability [91]. When assays are conducted with chemical
469 screening, they may aid in the discovery of novel allosteric modulators, state-dependent blockers,
470 and molecular chaperones to precisely treat channelopathies based on genotype. Integration of
471 disparate assays into a common framework of protein variation and its role in structure and
472 function will be challenging but efforts to standardize reporting and unified statistical frameworks
473 for interpretation (e.g., Enrich2[48], the Atlas of Variant Effects [92]) are on the horizon.
474
475 Many of our findings with respect to mutational sensitivity of trafficking motifs, core structural
476 elements, and regions of Kir2.1 involved in gating align with existing knowledge and biophysical
477 intuition. Unlike previous more limited screens and intuition, our data is quantitative and enables
478 data-driven approaches to construct global biophysical models of Kir2.1 structure and function.
479 For example, the Golgi export signal comprised of two patches at the N-terminus and CTD was
480 first described as a minimal set of hydrophobic residues along a CTD cleft and juxtaposed basic
481 residues [25] and later expanded to adjacent sites [18]. Our comprehensive screen shows this
482 trafficking motifs may indirectly probe the correct folding of the entire β-sheet core of the CTD. It
483 reveals scope of what this trafficking motif is reporting to the cellular quality control machinery;
484 not simply the proximity of a few basic and hydrophobic residues, but proper conformation of the
485 entire CTD and assembly into tetramers.
486
487 We observed contiguous regions with neutral expression fitness involved in gating transitions
488 while regions involved in fold-stability were highly sensitive to mutations. Looking at the same
489 regions in functional data, we find the inverse. This suggests two things. First, comprehensive
490 assessment of Kir2.1's phenotypes after perturbation (i.e., mutation) is a high-throughput method
491 to annotate protein sequences into classes linked to specific functions (e.g., putative trafficking

signals, folding units, etc.). Conceptually this is similar to other high-throughput biochemical approaches that probe sequence-function relationships, such as circular permutation profiling [93] or high-throughput enzyme variant kinetics measurements [94]. Second, combining multiple assayed parameters is key to discover general organizational principles in Kir2.1, specifically two distinct structural regions with distinct roles in providing fold stability or dynamics required for gating transitions. Expanding to more measured phenotypes and integrating datasets may be the blueprint for 'sequencing-based' biophysics that probes protein function, folding, and dynamics through steady-state biochemical experiments.

Our DMS studies provide additional context for the mechanistic basis of structure/function relation (e.g., reaffirming the βCD loop's role in propagating PIP_2 binding at the TM/CTD interface to the G-loop gate). We find a biogenic folding unit that represents an early quality control step of reentrant pore architecture and correct topology likely while the monomer is in the translocon. A similar biogenic unit was described in voltage-dependent K^+ channels, where it is stabilized by an extensive network of interactions [61]. Furthermore, many ion channels have structurally homologous reentrant pore loop architectures and earlier studies suggested that the presence of an 'aromatic cuff' is a general feature of their biogenesis [61,95]. DMS studies may provide a path to probe the energetics and biophysics of stabilizing interactions and to test the hypothesis that hydrophobicity is a general stabilizing factor across reentrant pore loop architectures.

DMS may also shed light on how subunit interactions determine inward rectifier gating properties. We find mutations near the interface of subunits strongly increase Kir2.1 function. This is consistent with subunits roles in setting channel gating properties. Single channel patch electrophysiology of Kir2.1/2.2 heterotetramers showed that addition of a Kir2.2 monomer increases single channel conductance and decreases the open dwell time (τ_{open}) [96]. Perhaps this feature contributes to the observed differences in gating between inward rectifier homo- and heterotetramer, which differ in number and nature of subunit interactions.

Our finding that variants with deleterious surface-score are underreported in available database supports the emerging theme that many disease-causing variants are linked to trafficking defects [13–16,16–23]. Other large scale mutational analysis, as undertaken for the voltage-dependent K^+ channel Kv11.1[97,98], has similarly shown that 88% of Long QT-linked variants have trafficking-

deficient mechanisms. They also demonstrate that data-driven approaches outperform smaller, more limited studies that predicted normal trafficking for most mutants [99].

Underrepresentation in variant databases has implications for clinical practice, since standards for the interpretation of sequence variants are heavily focused on null variants (nonsense, frameshift), population frequency (frequent variants are likely benign), predicted functional effect (is the variant in an important domain), and case evidence [100]. In genes under strong purifying selection, such as KCNJ2/Kir2.1, missense mutations cause severe developmental defects (craniofacial structures, limb development [79,101]) likely contribute to or cause spontaneous abortions and pregnancy loss. These variants therefore never enter population- or clinical-associated variant databases. DMS studies are not limited by organismal viability to probe the structural and functional consequences of genetic variation. DMS could be useful to identify drivers of spontaneous abortions and the underlying mechanisms of recurrent pregnancy loss.

By comparing our experimentally determined fitness scores to expert-reviewed assignment of variants effects, which are often based on smaller scale direct biochemical studies, we can estimate the bounds of fitness scores for benign and pathogenic variants. This allows us to make predictions about pathogenicity and mechanisms of action for variants of unknown significance (VUS) and known pathogenic variants, closing the loop between high-throughput assays, biophysical mechanisms underlying fitness scores, and clinical interpretation of human variation in ion channel genes.

These examples demonstrate that deep mutational scanning of Kir2.1 combined with two simple readouts, provides detailed insight into the mechanistic basis of ion channel folding, function under steady state conditions, and how these processes become misregulated in disease.

Materials and Methods

Kir2.1 DMS Library Generation: Into mouse Kir2.1 (Uniprot P35561), we introduced a FLAG tag into an extracellular loop (at position T115) and added a downstream expression marker miRFP670 co-expressed via a P2A sequence. For Kir2.1 residues 2-391, each wildtype amino acid was mutated to all other 19 amino acids weighted by their codon usage frequency in humans. In addition to these missense mutations, mutations synonymous to wildtype were included for 20 positions as a benchmark. We included missense mutation into the FLAG as a negative control. We generated this mouse Kir2.1 DMS library using the SPINE [38], which we briefly summarize as follows: SPINE based libraries employ synthesized pools of DNA oligos with mutations at each position of a gene. Due to high error-rates in oligo synthesis, the current maximum length for

oligos is 230 base pairs. As most genes are longer than 230 base pairs, we break up our gene (8 section in the case of Kir2.1) and replace a subsection of the gene with a pool of mutated oligos. The oligos are designed with unique barcodes for amplifying out a specific subpools library, Golden Gate compatible BsmBI cut sites, and the mutation within a subsection of Kir2.1. OLS oligos were designed using the SPINE scripts on Github (https://github.com/schmidt-lab/spine). These scripts design oligo libraries, primers for amplifying oligo-sublibraries, and inverse PCR primers for adding compatible cut sites to the Kir2.1 plasmid.

All backbone were amplified using a 25 cycle PCR with GXL polymerase and 1 ng of backbone DNA as template. The PCR product was then gel purified. All oligo libraries were amplified using 25 cycles PCR with GXL polymerase and with 1 ul of the OLS library (resuspended in 1 ml TE) as template. To assemble the backbone and library DNA, BsmBI Golden Gate reactions were set up in 20 ul containing 100 ng of amplified backbone DNA, 20 ng of amplified oligo DNA, 0.2 µl BsaI-HFv2 (New England Biolabs), 0.4 µl T4 DNA ligase (New England Biolabs), 2 µl T4 DNA ligase buffer, and 2 µl 10 mg/ml BSA. These reactions were put in a thermocycler overnight using the following program: (1) 5 min at 42°C, (2) 10 min at 16°C, (3) repeat 40 times, (3) 42°C for 20 min, (4) 80°C for 10 min. This reaction was cleaned using a Zymo Research Clean and Concentrate 5 kit and eluted in 6 ul of elution buffer. The entirety of this reaction transformed in E. Cloni 10G electrocompentent cells (Lucigen) according to manufacturer's instructions. Cells were grown overnight with shaking at 30°C to avoid overgrowth in 30 ml of LB with 40ug/ml kanamycin and library DNA was isolated using Zymo Zyppy miniprep kits. A small subset of transformed cells was plated varying dilutions to assess transformation efficiency and validate successful mutations. All libraries at this step yielded >300,000 colonies implying a 100x coverage (assuming 1/3 of the variants were perfect based on our previous analysis of Agilent OLS based libraries). Each sublibrary was combined at an equimolar ratio to make a complete library with all intended mutations included.

Stable Cell Line Generation: To generate cell lines, we used a rapid single-copy mammalian cell line generation pipeline [40]. Briefly, mutational libraries are cloned into a staging plasmid with BxBI-compatible *attB* recombination sites using BsmBI Golden Gate cloning. We amplify the staging plasmid backbone using inverse PCR and the library of interest with primers that add complementary BsmBI cut sites. Golden Gate cloning and subsequent transformation is conducted with BsmbI (NEB), T4 Ligase (NEB) following manufacturer's using the same protocol as previously described for library generation. Completed library landing pad constructs are co-

transfected (1:1) with a BxBI expression construct (pCAG-NLS-Bxb1) into (TetBxB1BFP-iCasp-Blast Clone 12 HEK293T cells) using Turbofect according to the manufacturer's instructions in 6 wells of a 6-well dish. This cell line has a genetically integrated tetracycline induction cassette, followed by a BxBI recombination site, and split rapalog inducible dimerizable Casp-9. Cells were maintained in D10 (DMEM, 10% fetal bovine serum (FBS), 1% sodium pyruvate, and 1% penicillin/streptomycin). Two days after transfection, doxycycline (2 ug/ml, Sigma-Aldrich) is added to induce expression of our genes of interest (successful recombination) or the iCasp-9 selection system (no recombination). Successful recombination shifts the iCasp-9 out of frame, thus only cells that have undergone recombination survive, while those that haven't will die from iCasp-9-induced apoptosis. One day after doxycycline induction, AP1903 (10 nM, MedChemExpress) is added to cause dimerization of Casp9 and selectively kill cells without successful recombination. One day after AP1903-Casp9 selection, media is changed back to D10 + Doxycycline (2 ug/ml, Sigma-Aldrich) for recovery. Two days after cells have recovered, cells are reseeded to enable normal cell growth. Once cells reach confluency, library cells are frozen in 50% FBS and 10% DMSO stocks in aliquots for assays.

Surface Expression cell sorting: Thawed stocks of library cell lines were seeded into a 10 cm dish and media was swapped the following day to D10. Cells were grown and split before confluency to maintain cell health. Media was swapped to D10 + doxycycline (2 ug/ml, Sigma-Aldrich) two days prior to the experiment. Cells were detached with 1 ml Accutase (Sigma-Aldrich), spun down and washed three times with FACS buffer (2% FBS, 0.1% NaN_3, 1X PBS), incubated for 1-hour rocking at 4°C with a BV421 anti-flag antibody (BD Bioscience), washed twice with FACS buffers, filtered with cell strainer 5 ml tubes (Falcon), covered with aluminum foil, and kept on ice for transfer to the flow cytometry core. Before sorting, 5% of cells were for processing and sequencing as a baseline control.

Cells were sorted on a BD FACSAria II P69500132 cell sorter. miRFP670 fluorescence was excited with a 640 nm laser and recorded with a 670/30 nm bandpass filter and 505 nm long-pass filter. BV421 fluorescence was excited using a 405 nm laser. Cells were gated on forward scattering area and side scattering area to find whole cells, forward scattering width, and height to separate single cells, miRFP670 for cells that expressed variants without errors (our library generation results in single base pair deletions that will not have miRFP670 expression because deletions will shift the fluorescent protein out of frame [38]), and label for surface expressed cells. The surface expression label gate boundaries were determined based on unlabeled cells from

the same population because controls tend to have non-representative distributions. Example of the gating strategy for is depicted in **Supplemental Fig. 1**.

Cells were sorted based on surface expression into 4 populations (miRFP^{high}/BV421^{none}, miRFP^{high}/BV421^{low}, miRFP^{high}/BV421^{medium}, miRFP^{high}/BV421^{high}. We collected at least 2.1 million cells in each population to ensure a greater than 100x coverage for each sample in each subpool. The surface expression experiment was done in duplicate on separate days for two entirely independent replicates.

Resting membrane potential cell sorting: Concurrently with preparing samples for surface labeling another sample of the same cells were prepared for sorting based on resting membrane potential. These cells were initially washed with FACS buffer and concentrated in this buffer for cell health prior to sorting. 30 minutes prior to sorting cells were resuspended in Tyrode (125mM NaCl, 2mM KCl, 3mM CaCl2, 1mM MgCl2, 10mM HEPES, 30mM glucose, pH 7.3) that contained FLIPR membrane potential dye with a Blue quencher.

Cells were also sorted based on resting membrane potential on a BD FACSAria II P69500132 cell sorter. miRFP670 fluorescence was excited with a 640 nm laser and recorded with a 670/30 nm bandpass filter and 505 nm long-pass filter. FLIPR fluorescence was excited using a 488 nm laser and recorded on a 525/50 nm bandpass filter. As before the same general sorting scheme was used to identify whole single cells based on forward and side scatter and enriched for good quality library members based on miRFP670 fluorescence. An example of the gating strategy is in **Supplemental Fig. 2** Cells were sorted based on resting membrane potential into 3 populations (miRFP^{high}/FLIPR^{Low}, miRFP^{high}/FLIPR^{medium}, miRFP^{high}/FLIPR^{high}. The resting membrane potential experiment was done in duplicate on separate days for two entirely independent replicates.

Sequencing: For both biological replicates, DNA from pre-sort control and sorted cells was extracted with Microprep DNA kits (Zymo Research) and triple-eluted with water. The elute was diluted such that no more than 1.5ug of DNA was used per PCR reaction and amplified for 20 cycles of PCR using Primestar GXL (Takara Bio), run on a 1% agarose gel, and gel purified. Primers that bind outside the recombination site ensure leftover plasmid DNA from the original cell line construction step is not amplified. Purified DNA was quantified using Picogreen DNA quantification. Equal amounts (by mass) of each domain insertion sample were pooled by cell sorting category (“pre-sort control”, “surface expression”, “no surface expression”). Pooled amplicons were prepared for sequencing using the Nextera XT sample preparation workflow and

sequenced using Illumina Novaseq in 2x150bp mode. Source sequencing data is available in the NCBI Sequence Raw Archive (https://www.ncbi.nlm.nih.gov/sra) under accession code PRJNA791691. Read count statistics are listed in **Supplemental Table 1A.**

Alignment and Enrichment Calculation: Variant frequency for single mutations were determined by joining paired reads with bbmerge, aligning reads to the Kir2.1 reference gene sequence with bbmap, and identifying mutations and filtering to find the OLS programmed mutations with a custom python script. The 150 bp paired-end reads were trimmed to remove standard Illumina adapters (bbmap/resources) using BBDuk with 'mink' at 8 bases. Overlapping reads were corrected without merging using BBMerge with the 'ecco' and 'mix' setting. Reads were aligned to Kir2.1 sequence using BBMap using 'maxindel' at 500 and 'local' alignment. The resulting sam file was analyzed for mutations at each position and filtered to match only mutations that were programmed on the OLS chip. To calculate enrichment of mutations we used Enrich2 [48]. Counts for each mutation were input into the Enrich2 software with weighted least squares scoring and wild type normalization. Scores were output with a standard error in a .csv file. Coverage of mapped reads is listed in **Supplemental Table 1B-C**.

Inward Rectifier Phylogenetic Alignment and Clinvar mutation assignment: We downloaded all human inward rectifiers (KCNJ1(Kir1.1/ROMK; Uniprot P48048), KCNJ10(Kir1.2/Kir4.1; Uniprot P78508), KCNJ15(Kir1.3/Kir4.1; Uniprot Q99712), KCNJ2(Kir2.1; Uniprot P63252), KCNJ12(Kir2.2; Uniprot Q14500), KCNJ4(Kir2.3; Uniprot P48050), KCNJ14(Kir2.4; Uniprot Q9UNX9), KCNJ18(Kir2.6; Uniprot B7U540), KCNJ3(Kir3.1/GIRK1; Uniprot P48549), KCNJ6(Kir3.2/GIRK2; Uniprot P48051), KCNJ9(Kir3.3/GIRK3; Uniprot Q92806), KCNJ5(Kir3.4/GIRK4; Uniprot P48544), KCNJ16(Kir5.1; Uniprot Q9NPI9), KCNJ8(Kir6.1; Uniprot Q15842), KCNJ11(Kir6.2; Uniprot Q14654), KCNJ13(Kir7.1; Uniprot O60928) and aligned these together using MegaX [102]. Based on this alignment, we generated a master list of Inward Rectifier numberings to translate residue numbering between Kir homologues. We assigned mutations observed Clinvar and dbSNP and their pathogenic classification (ClinVar only) to this master alignment (**Supplementary Table 2**).

Figure Legends

Figure 1 Deep Mutational Scanning to improve clinical variant prediction. (A) Clinically observed variation in Kir2.1 and other Kir and their interpretation of pathogenicity. **(B)** Schematic

689 summarizing the various processes that myst work correctly for Kir2.1 to fulfill its role in cellular
690 physiology. **(C)** Schematic summarizing DMS and multiparametric assessment of phenotype.
691 Mutations are introduced into Kir2.1 using SPINE. A stable single-copy insertion library is
692 generated by BxBI-mediated recombination in HEK293T. Cells are sorted based on channel
693 surface expression or function (K^+ conductance) as determined by antibody labeling of an
694 extracellular FLAG tag or voltage-sensitive dye, respectively. Genotypes of each sorted cell
695 population are recovered by NextGen Sequencing (NGS).
696
697 **Figure 2 Surface Expression Fitness. (A)** Distribution of surface expression fitness scores for
698 synonymous mutations (red line) and missense mutations (black line). **(B)** Heatmap of surface
699 expression fitness scores (gradient from blue to red). Wildtype residues are indicated by green
700 boxes. Missing data is indicated by yellow boxes. Synonymous mutations are indicated by red
701 box outline. **(C)** Cartoon of Kir2.2 (PDB 3SPI, 70% identity with Kir2.1). Monomer chains show in
702 different colors. Lipid bilayer boundaries are indicated by dashed lines. **(D)** Close-up of core beta
703 sheet of the CTD with surface expression fitness mapped onto each residue as a gradient from
704 blue to red. Residues that comprise the Golgi export signal are outlined green. **(E)** Interface close-
705 up of neighboring subunits (green and magenta cartoons). Sidechain are colored by surface
706 fitness score. Disrupting carbon–π and π–π interactions interactions between F45, L246, and
707 Y338 does not uniformly decrease fitness.
708
709 **Figure 3 Determinant of improve surface expression and Kir2.1's biogenic folding unit. (A)**
710 Boxplots showing surface fitness in the βDE and βLM loop if the wildtype residues of a specific
711 type (e.g., glutamate, charged) is mutated to another residue of the same type (e.g., Aspartate)
712 or a different type (e.g., Tryptophan). Median is marked with a thick line, the vertical length of the
713 box represents the interquartile range (IQR), upper fence: 75th percentile +1.5 × IQR, lower fence:
714 25th percentile −1.5 × IQR, outlier points are shown as solid black circles. All data points are
715 indicated by transparent dots. Only replacing aromatic residues significantly increase surface
716 expression. Significance is tested using one-sided t-tests; p-values are indicated for each
717 comparison. **(B)** Close-up of surface expression fitness scores (gradient blue to red) in the βDE
718 and βLM loop. **(C)** Close-up of surface expression fitness scores in the pore domain. Residues
719 that are part of the putative biogenic unit of Kir2.1 are show as sticks. **(D)** Surface expression
720 fitness scores mapped onto a single Kir2.1 monomer highlighting the importance of the biogenic
721 folding unit in the pore domain and the core beta sheet of the CTD.

Figure 4 Function Fitness. (A) Distribution of function expression fitness scores for synonymous mutations (red line) and missense mutations (black line). **(B)** Function fitness scores mapped onto a single Kir2.1 monomer highlighting the importance of the pore helix and selectivity filter, and the structural elements are the TM/CTD interface (e.g., interfacial helix, tether helix, G-loop gate) for function. **(C)** Heatmap of function expression fitness scores (gradient from green to magenta). Wildtype residues are indicated by blue boxes. Missing data is indicated by yellow boxes. Synonymous mutations are indicated by red box outline. (**D-G)** Heatmap of fitness score in regions that contain bona-fide trafficking signal (**D,E;** for surface and function scores, respectively) or the PIP_2 binding site (**F,G;** for surface and function scores, respectively). (**H**) Closeup of function fitness at the TM/CTD interface. Allosteric ligand PIP_2 is shown as sticks.

Figure 5 HBC gate mutations and regions with distinct roles stability and function. (A) Function Fitness (gradient from green to magenta) in the pore domain. One subunit is removed for clarity. K+ ions in the selectivity filter a show as purple spheres. Sidechain of residues that are enriched for activating mutations are shown as sticks. **(B)** Detailed view of the HBC gate. **(C)** Difference between z-score normalized mean Function and Surface Fitness scores mapped by position. Filled circles (cyan or magenta) indicated significant differences (two-sided moderated t test p-value < 0.05). Kir2.1 secondary structural element are shown as gray boxes; trafficking signals are colored green. **(D-F)** Residues with significant function/surface fitness score differences are mapped onto the Kir2.2 structure (PBD 3SPI). Backbone cartoons are colored by chain. Residues with mutation that predominantly reduced function are shown in magenta. Residues with mutation that predominantly reduced surface expression are shown in cyan. PIP_2 is shown in blue. Overview **(D)**, close-ups of selectivity filter **(E)** and TM/CTD **(F)**.

Figure 6 Folding and trafficking variants in clinical databases. Cumulative distributions of surface **(A)** or function **(B)** fitness scores for variants that are represented in Clinvar and dbSNP (red line) or that are not (black line). **(C)** Line plot by position of mean function or surface fitness scores (gradient green to magenta and blue to red, respectively). Kir2.1 secondary structural element are shown as gray boxes. Pathogenic variants are mapped as circles with fill color indicating predicted pathogenic mechanism. Mutation hotspots are indicated by gray outlines. Distribution of surface fitness **(D)** and function fitness **(E)** by ClinVar pathogenicity assignment.

Vertical dashed lines represent 2.5th and 97.5th percentiles bounds of expert reviewed pathogenic variants (red) and benign (blue), respectively.

Author contributions

WCM, DN, and DS designed the work presented here. WCM and DN did the experiments with support from YH. DN processed the sequencing data. WCM and DS did the analysis and wrote the manuscript.

Acknowledgement

We are grateful for helpful discussions with Anna Gloyn, James Fraser, Gabbriella Estevam, Eric Greene, the DMS crew, and the rest of the Fraser lab. We also thank you for taking the time to read our manuscript. This work was supported by the National Institutes of Health (1R01GM136851 to D.S.) and a University of Minnesota Genome Center Illumina S2 grant. W.C.-M. is supported by a National Science Foundation Graduate Research Fellowship and a Howard Hughes Medical Institute Gilliam Fellowship for Advanced Study.

Competing Interests

The authors declare no competing interests.

References

1. Hibino, H. et al. Inwardly rectifying potassium channels: their structure, function, and physiological roles. *Physiol Rev* **90**, 291-366 (2010).
2. Bodhinathan, K. & Slesinger, P. A. Molecular mechanism underlying ethanol activation of G-protein-gated inwardly rectifying potassium channels. *Proc Natl Acad Sci U S A* **110**, 18309-18314 (2013).
3. Marron Fernandez de Velasco, E., McCall, N. & Wickman, K. GIRK Channel Plasticity and Implications for Drug Addiction. *Int Rev Neurobiol* **123**, 201-238 (2015).
4. Torrecilla, M. et al. G-protein-gated potassium channels containing Kir3.2 and Kir3.3 subunits mediate the acute inhibitory effects of opioids on locus ceruleus neurons. *J Neurosci* **22**, 4328-4334 (2002).
5. Rachidi, M. & Lopes, C. Mental retardation in Down syndrome: from gene dosage imbalance to molecular and cellular mechanisms. *Neurosci Res* **59**, 349-369 (2007).
6. Köhling, R. & Wolfart, J. Potassium Channels in Epilepsy. *Cold Spring Harb Perspect Med* **6**, (2016).
7. Zhang, L., Zheng, Y., Xie, J. & Shi, L. Potassium channels and their emerging role in parkinson's disease. *Brain Res Bull* **160**, 1-7 (2020).
8. Moss, A. J. & Kass, R. S. Long QT syndrome: from channels to cardiac arrhythmias. *J Clin Invest* **115**, 2018-2024 (2005).

9. Flagg, T. P., Tate, M., Merot, J. & Welling, P. A. A mutation linked with Bartter's syndrome locks Kir 1.1 a (ROMK1) channels in a closed state. *The Journal of general physiology* **114**, 685-700 (1999).
10. Stumvoll, M., Goldstein, B. J. & van Haeften, T. W. Type 2 diabetes: principles of pathogenesis and therapy. *Lancet* **365**, 1333-1346 (2005).
11. Abraham, M. R., Jahangir, A., Alekseev, A. E. & Terzic, A. Channelopathies of inwardly rectifying potassium channels. *FASEB J* **13**, 1901-1910 (1999).
12. Vuong, C. K., Black, D. L. & Zheng, S. The neurogenetics of alternative splicing. *Nat Rev Neurosci* **17**, 265-281 (2016).
13. Peters, M. et al. Classification and rescue of ROMK mutations underlying hyperprostaglandin E syndrome/antenatal Bartter syndrome. *Kidney Int* **64**, 923-932 (2003).
14. O'Donnell, B. M., Mackie, T. D., Subramanya, A. R. & Brodsky, J. L. Endoplasmic reticulum-associated degradation of the renal potassium channel, ROMK, leads to type II Bartter syndrome. *J Biol Chem* **292**, 12813-12827 (2017).
15. Fallen, K. et al. The Kir channel immunoglobulin domain is essential for Kir1.1 (ROMK) thermodynamic stability, trafficking and gating. *Channels (Austin)* **3**, 57-68 (2009).
16. Zangerl-Plessl, E. M., Qile, M., Bloothooft, M., Stary-Weinzinger, A. & van der Heyden, M. A. G. Disease Associated Mutations in K_{IR} Proteins Linked to Aberrant Inward Rectifier Channel Trafficking. *Biomolecules* **9**, (2019).
17. Lin, C. W. et al. Kir6.2 mutations associated with neonatal diabetes reduce expression of ATP-sensitive K+ channels: implications in disease mechanism and sulfonylurea therapy. *Diabetes* **55**, 1738-1746 (2006).
18. Li, X., Ortega, B., Kim, B. & Welling, P. A. A Common Signal Patch Drives AP-1 Protein-dependent Golgi Export of Inwardly Rectifying Potassium Channels. *J Biol Chem* **291**, 14963-14972 (2016).
19. Ma, D. et al. Golgi export of the Kir2.1 channel is driven by a trafficking signal located within its tertiary structure. *Cell* **145**, 1102-1115 (2011).
20. Ma, D. et al. Role of ER export signals in controlling surface potassium channel numbers. *Science* **291**, 316-319 (2001).
21. Ma, D. et al. Diverse trafficking patterns due to multiple traffic motifs in G protein-activated inwardly rectifying potassium channels from brain and heart. *Neuron* **33**, 715-729 (2002).
22. Stockklausner, C., Ludwig, J., Ruppersberg, J. P. & Klöcker, N. A sequence motif responsible for ER export and surface expression of Kir2. 0 inward rectifier K+ channels. *FEBS letters* **493**, 129-133 (2001).
23. Zerangue, N., Schwappach, B., Jan, Y. N. & Jan, L. Y. A new ER trafficking signal regulates the subunit stoichiometry of plasma membrane KATP channels. *Neuron* **22**, 537-548 (1999).
24. Leonoudakis, D. et al. Protein trafficking and anchoring complexes revealed by proteomic analysis of inward rectifier potassium channel (Kir2. x)-associated proteins. *Journal of Biological Chemistry* **279**, 22331-22346 (2004).
25. Ma, D. et al. Golgi export of the Kir2.1 channel is driven by a trafficking signal located within its tertiary structure. *Cell* **145**, 1102-1115 (2011).
26. Landrum, M. J. et al. ClinVar: improving access to variant interpretations and supporting evidence. *Nucleic acids research* **46**, D1062-D1067 (2018).
27. Tennessen, J. A. et al. Evolution and functional impact of rare coding variation from deep sequencing of human exomes. *science* **337**, 64-69 (2012).
28. McClellan, J. & King, M.-C. Genetic heterogeneity in human disease. *Cell* **141**, 210-217 (2010).

29. Adzhubei, I. A. et al. A method and server for predicting damaging missense mutations. *Nat Methods* **7**, 248-249 (2010).
30. Ng, P. C. & Henikoff, S. SIFT: Predicting amino acid changes that affect protein function. *Nucleic Acids Res* **31**, 3812-3814 (2003).
31. Frazer, J. et al. Disease variant prediction with deep generative models of evolutionary data. *Nature* 1-5 (2021).
32. McLaughlin, R. N., Poelwijk, F. J., Raman, A., Gosal, W. S. & Ranganathan, R. The spatial architecture of protein function and adaptation. *Nature* **491**, 138-142 (2012).
33. Atkinson, J. T., Jones, A. M., Zhou, Q. & Silberg, J. J. Circular permutation profiling by deep sequencing libraries created using transposon mutagenesis. *Nucleic Acids Res* **46**, e76 (2018).
34. Coyote-Maestas, W. et al. Probing ion channel functional architecture and domain recombination compatibility by massively parallel domain insertion profiling. *Nat Commun* **12**, 7114 (2021).
35. Schmiedel, J. M. & Lehner, B. Determining protein structures using deep mutagenesis. *Nat Genet* **51**, 1177-1186 (2019).
36. Matreyek, K. A. et al. Multiplex assessment of protein variant abundance by massively parallel sequencing. *Nat Genet* **50**, 874-882 (2018).
37. Hansen, S. B., Tao, X. & MacKinnon, R. Structural basis of PIP2 activation of the classical inward rectifier K+ channel Kir2.2. *Nature* **477**, 495-498 (2011).
38. Coyote-Maestas, W., Nedrud, D., Okorafor, S., He, Y. & Schmidt, D. Targeted insertional mutagenesis libraries for deep domain insertion profiling. *Nucleic Acids Res* (2019).
39. Nedrud, D., Coyote-Maestas, W. & Schmidt, D. A large-scale survey of pairwise epistasis reveals a mechanism for evolutionary expansion and specialization of PDZ domains. *Proteins* (2021).
40. Matreyek, K. A., Stephany, J. J., Chiasson, M. A., Hasle, N. & Fowler, D. M. An improved platform for functional assessment of large protein libraries in mammalian cells. *Nucleic Acids Res* **48**, e1 (2020).
41. Varghese, A., Tenbroek, E. M., Coles, J. & Sigg, D. C. Endogenous channels in HEK cells and potential roles in HCN ionic current measurements. *Prog Biophys Mol Biol* **90**, 26-37 (2006).
42. Bendahhou, S. et al. Defective potassium channel Kir2.1 trafficking underlies Andersen-Tawil syndrome. *J Biol Chem* **278**, 51779-51785 (2003).
43. Pegan, S., Arrabit, C., Slesinger, P. A. & Choe, S. Andersen's syndrome mutation effects on the structure and assembly of the cytoplasmic domains of Kir2.1. *Biochemistry* **45**, 8599-8606 (2006).
44. Tinker, A., Jan, Y. N. & Jan, L. Y. Regions responsible for the assembly of inwardly rectifying potassium channels. *Cell* **87**, 857-868 (1996).
45. Stockklausner, C., Ludwig, J., Ruppersberg, J. P. & Klöcker, N. A sequence motif responsible for ER export and surface expression of Kir2.0 inward rectifier K(+) channels. *FEBS Lett* **493**, 129-133 (2001).
46. Coyote-Maestas, W., He, Y., Myers, C. L. & Schmidt, D. Domain insertion permissibility-guided engineering of allostery in ion channels. *Nat Commun* **10**, 290 (2019).
47. Adams, D. S. & Levin, M. Measuring resting membrane potential using the fluorescent voltage reporters DiBAC4(3) and CC2-DMPE. *Cold Spring Harb Protoc* **2012**, 459-464 (2012).
48. Rubin, A. F. et al. A statistical framework for analyzing deep mutational scanning data. *Genome Biol* **18**, 150 (2017).

49. Vaidyanathan, R. et al. Inward Rectifier Potassium Channels (Kir2.x) and Caveolin-3 Domain-Specific Interaction: Implications for Purkinje Cell-Dependent Ventricular Arrhythmias. *Circ Arrhythm Electrophysiol* **11**, e005800 (2018).
50. Ma, D. et al. Role of ER export signals in controlling surface potassium channel numbers. *Science* **291**, 316-319 (2001).
51. Hamill, S. J., Cota, E., Chothia, C. & Clarke, J. Conservation of folding and stability within a protein family: the tyrosine corner as an evolutionary cul-de-sac. *J Mol Biol* **295**, 641-649 (2000).
52. Cota, E., Steward, A., Fowler, S. B. & Clarke, J. The folding nucleus of a fibronectin type III domain is composed of core residues of the immunoglobulin-like fold. *J Mol Biol* **305**, 1185-1194 (2001).
53. Koster, J. C., Bentle, K. A., Nichols, C. G. & Ho, K. Assembly of ROMK1 (Kir 1.1a) inward rectifier K+ channel subunits involves multiple interaction sites. *Biophys J* **74**, 1821-1829 (1998).
54. Deutsch, C. Potassium channel ontogeny. *Annu Rev Physiol* **64**, 19-46 (2002).
55. Williams, M. A. & Fukuda, M. Accumulation of membrane glycoproteins in lysosomes requires a tyrosine residue at a particular position in the cytoplasmic tail. *J Cell Biol* **111**, 955-966 (1990).
56. Tao, X., Avalos, J. L., Chen, J. & MacKinnon, R. Crystal structure of the eukaryotic strong inward-rectifier K+ channel Kir2. 2 at 3.1 Å resolution. *Science* **326**, 1668-1674 (2009).
57. Cho, H. C., Tsushima, R. G., Nguyen, T. T., Guy, H. R. & Backx, P. H. Two critical cysteine residues implicated in disulfide bond formation and proper folding of Kir2.1. *Biochemistry* **39**, 4649-4657 (2000).
58. Leyland, M. L., Dart, C., Spencer, P. J., Sutcliffe, M. J. & Stanfield, P. R. The possible role of a disulphide bond in forming functional Kir2.1 potassium channels. *Pflugers Arch* **438**, 778-781 (1999).
59. Dassau, L., Conti, L. R., Radeke, C. M., Ptáček, L. J. & Vandenberg, C. A. Kir2. 6 regulates the surface expression of Kir2. x inward rectifier potassium channels. *Journal of Biological Chemistry* **286**, 9526-9541 (2011).
60. Valiyaveetil, F. I., Sekedat, M., Mackinnon, R. & Muir, T. W. Glycine as a D-amino acid surrogate in the K(+)-selectivity filter. *Proc Natl Acad Sci U S A* **101**, 17045-17049 (2004).
61. Delaney, E., Khanna, P., Tu, L., Robinson, J. M. & Deutsch, C. Determinants of pore folding in potassium channel biogenesis. *Proc. Natl. Acad. Sci. U.S.A.* **111**, 4620-4625 (2014).
62. Gajewski, C., Dagcan, A., Roux, B. & Deutsch, C. Biogenesis of the pore architecture of a voltage-gated potassium channel. *Proc Natl Acad Sci U S A* **108**, 3240-3245 (2011).
63. Li, J. et al. Identification of the Conformational transition pathway in PIP 2 Opening Kir Channels. *Scientific reports* **5**, 1-12 (2015).
64. Heginbotham, L., Lu, Z., Abramson, T. & MacKinnon, R. Mutations in the K+ channel signature sequence. *Biophysical journal* **66**, 1061-1067 (1994).
65. Splitt, H., Meuser, D., Borovok, I., Betzler, M. & Schrempf, H. Pore mutations affecting tetrameric assembly and functioning of the potassium channel KcsA from Streptomyces lividans. *FEBS Lett* **472**, 83-87 (2000).
66. Cheng, W. W., McCoy, J. G., Thompson, A. N., Nichols, C. G. & Nimigean, C. M. Mechanism for selectivity-inactivation coupling in KcsA potassium channels. *Proc Natl Acad Sci U S A* **108**, 5272-5277 (2011).
67. Pegan, S. et al. Cytoplasmic domain structures of Kir2.1 and Kir3.1 show sites for modulating gating and rectification. *Nat Neurosci* **8**, 279-287 (2005).

68. Lopes, C. M. B. et al. Alterations in conserved Kir channel-PIP2 interactions underlie channelopathies. *Neuron* **34**, 933-944 (2002).
69. Plaster, N. M. et al. Mutations in Kir2. 1 cause the developmental and episodic electrical phenotypes of Andersen's syndrome. *Cell* **105**, 511-519 (2001).
70. Whorton, M. R. & MacKinnon, R. Crystal structure of the mammalian GIRK2 K+ channel and gating regulation by G proteins, PIP2, and sodium. *Cell* **147**, 199-208 (2011).
71. Mahajan, R. et al. A computational model predicts that Gβγ acts at a cleft between channel subunits to activate GIRK1 channels. *Sci Signal* **6**, ra69 (2013).
72. Whorton, M. R. & MacKinnon, R. X-ray structure of the mammalian GIRK2-βγ G-protein complex. *Nature* **498**, 190-197 (2013).
73. Jin, T. et al. The βγ subunits of G proteins gate a K+ channel by pivoted bending of a transmembrane segment. *Molecular cell* **10**, 469-481 (2002).
74. Sadja, R., Smadja, K., Alagem, N. & Reuveny, E. Coupling Gbetagamma-dependent activation to channel opening via pore elements in inwardly rectifying potassium channels. *Neuron* **29**, 669-680 (2001).
75. Jiang, Y. et al. The open pore conformation of potassium channels. *Nature* **417**, 523-526 (2002).
76. Meng, X. Y., Liu, S., Cui, M., Zhou, R. & Logothetis, D. E. The Molecular Mechanism of Opening the Helix Bundle Crossing (HBC) Gate of a Kir Channel. *Sci Rep* **6**, 29399 (2016).
77. Zangerl-Plessl, E. M. et al. Atomistic basis of opening and conduction in mammalian inward rectifier potassium (Kir2.2) channels. *J Gen Physiol* **152**, e201912422 (2020).
78. Matreyek, K. A. et al. Multiplex assessment of protein variant abundance by massively parallel sequencing. *Nat Genet* **50**, 874-882 (2018).
79. Zaritsky, J. J., Redell, J. B., Tempel, B. L. & Schwarz, T. L. The consequences of disrupting cardiac inwardly rectifying K(+) current (I(K1)) as revealed by the targeted deletion of the murine Kir2.1 and Kir2.2 genes. *J Physiol* **533**, 697-710 (2001).
80. Karczewski, K. J. et al. The mutational constraint spectrum quantified from variation in 141,456 humans. *Nature* **581**, 434-443 (2020).
81. Sahlin, E. et al. Identification of putative pathogenic single nucleotide variants (SNVs) in genes associated with heart disease in 290 cases of stillbirth. *PLoS One* **14**, e0210017 (2019).
82. Priori, S. G. et al. A novel form of short QT syndrome (SQT3) is caused by a mutation in the KCNJ2 gene. *Circ Res* **96**, 800-807 (2005).
83. Araya, C. L. et al. A fundamental protein property, thermodynamic stability, revealed solely from large-scale measurements of protein function. *Proc Natl Acad Sci U S A* **109**, 16858-16863 (2012).
84. Fowler, D. M. et al. High-resolution mapping of protein sequence-function relationships. *Nat Methods* **7**, 741-746 (2010).
85. Starr, T. N. et al. Deep Mutational Scanning of SARS-CoV-2 Receptor Binding Domain Reveals Constraints on Folding and ACE2 Binding. *Cell* **182**, 1295-1310.e20 (2020).
86. Schmiedel, J. M. & Lehner, B. Determining protein structures using deep mutagenesis. *Nat Genet* **51**, 1177-1186 (2019).
87. Matreyek, K. A., Stephany, J. J., Ahler, E. & Fowler, D. M. Integrating thousands of PTEN variant activity and abundance measurements reveals variant subgroups and new dominant negatives in cancers. *Genome Med* **13**, 165 (2021).
88. Coukos, R. et al. An engineered transcriptional reporter of protein localization identifies regulators of mitochondrial and ER membrane protein trafficking in high-throughput CRISPRi screens. *Elife* **10**, e69142 (2021).

89. Hochbaum, D. R. et al. All-optical electrophysiology in mammalian neurons using engineered microbial rhodopsins. *Nat Methods* **11**, 825-833 (2014).
90. Park, J. et al. Screening fluorescent voltage indicators with spontaneously spiking HEK cells. *PLoS One* **8**, e85221 (2013).
91. O'Leary, T., Williams, A. H., Franci, A. & Marder, E. Cell types, network homeostasis, and pathological compensation from a biologically plausible ion channel expression model. *Neuron* **82**, 809-821 (2014).
92. Fowler, D. M. et al. The Atlas of Variant Effects (AVE) Alliance: understanding genetic variation at nucleotide resolution. (2021).
93. Atkinson, J. T., Jones, A. M., Zhou, Q. & Silberg, J. J. Circular permutation profiling by deep sequencing libraries created using transposon mutagenesis. *Nucleic acids research* **46**, e76-e76 (2018).
94. Markin, C. J. et al. Revealing enzyme functional architecture via high-throughput microfluidic enzyme kinetics. *Science* **373**, eabf8761 (2021).
95. Doyle, D. A. et al. The structure of the potassium channel: molecular basis of K+ conduction and selectivity. *Science* **280**, 69-77 (1998).
96. Panama, B. K., McLerie, M. & Lopatin, A. N. Functional consequences of Kir2.1/Kir2.2 subunit heteromerization. *Pflugers Arch* **460**, 839-849 (2010).
97. Anderson, C. L., Kuzmicki, C. E., Childs, R. R. & Hintz…, C. J. Large-scale mutational analysis of Kv11. 1 reveals molecular insights into type 2 long QT syndrome. *Nature …* (2014).
98. Kozek, K. A., Glazer, A. M., Ng, C. A., Blackwell, D. & Egly…, C. L. High-throughput discovery of trafficking-deficient variants in the cardiac potassium channel KV11. 1. *Heart Rhythm* (2020).
99. Harley, C. A., Jesus, C. S. H., Carvalho, R. & Brito…, R. M. M. Changes in channel trafficking and protein stability caused by LQT2 mutations in the PAS domain of the HERG channel. *PLoS …* (2012).
100. Richards, S. et al. Standards and guidelines for the interpretation of sequence variants: a joint consensus recommendation of the American College of Medical Genetics and Genomics and the Association for Molecular Pathology. *Genet Med* **17**, 405-424 (2015).
101. Belus, M. T. et al. Kir2.1 is important for efficient BMP signaling in mammalian face development. *Dev Biol* **444 Suppl 1**, S297-S307 (2018).
102. Kumar, S., Stecher, G., Li, M., Knyaz, C. & Tamura, K. MEGA X: molecular evolutionary genetics analysis across computing platforms. *Molecular biology and evolution* **35**, 1547 (2018).

A

Clinical Interpretation	Kir2.1	other Kir
Benign	1	15
Conflicting interpretations of pathogenicity	12	27
Likely benign	1	10
Likely pathogenic	17	25
not provided	16	2
Pathogenic	27	79
Uncertain significance	89	299

B

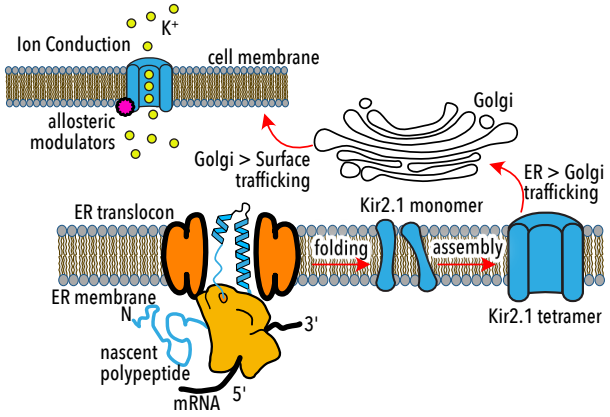

C

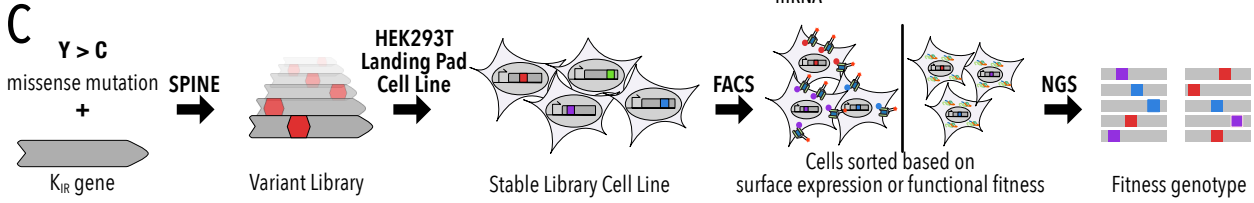

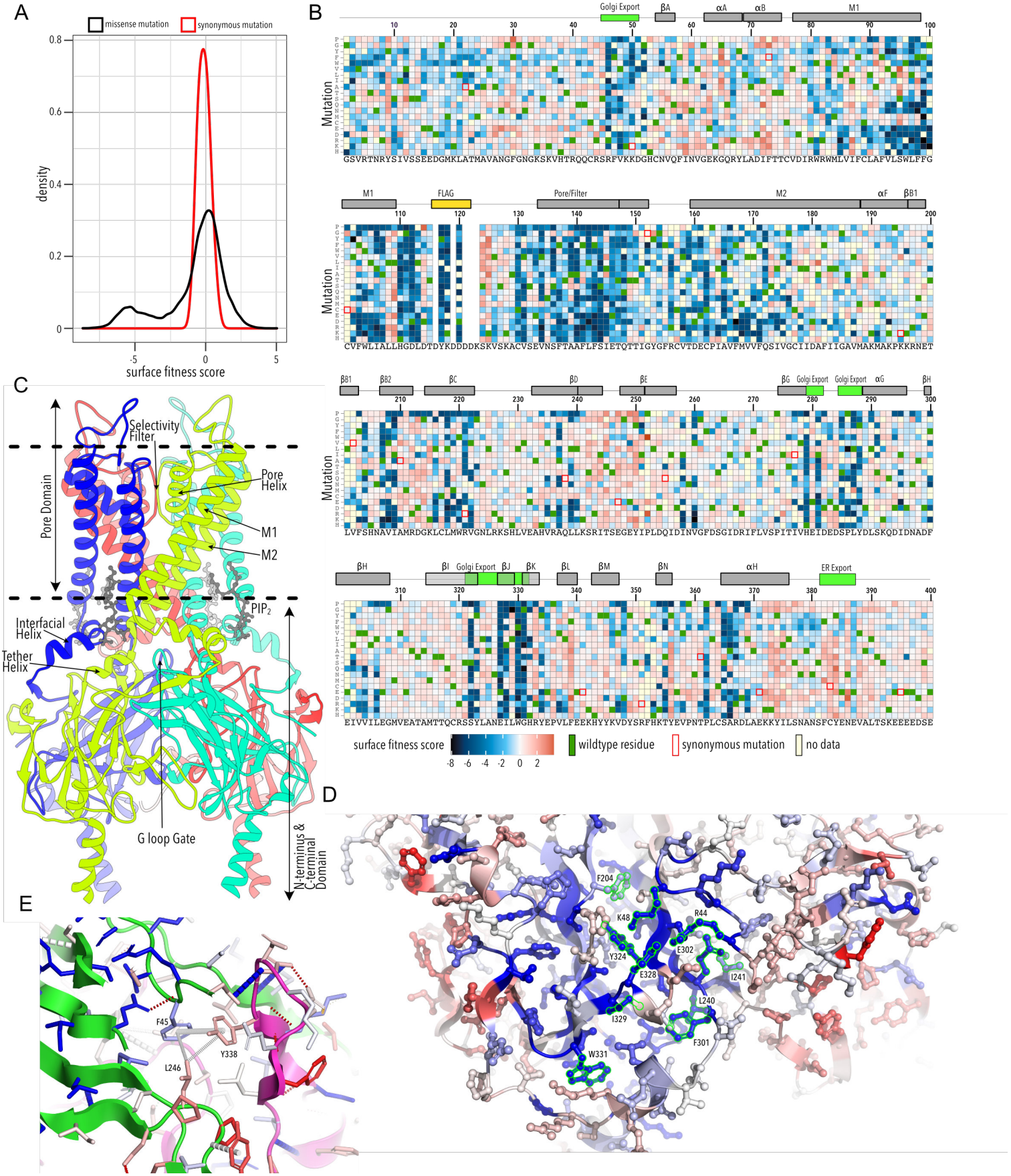

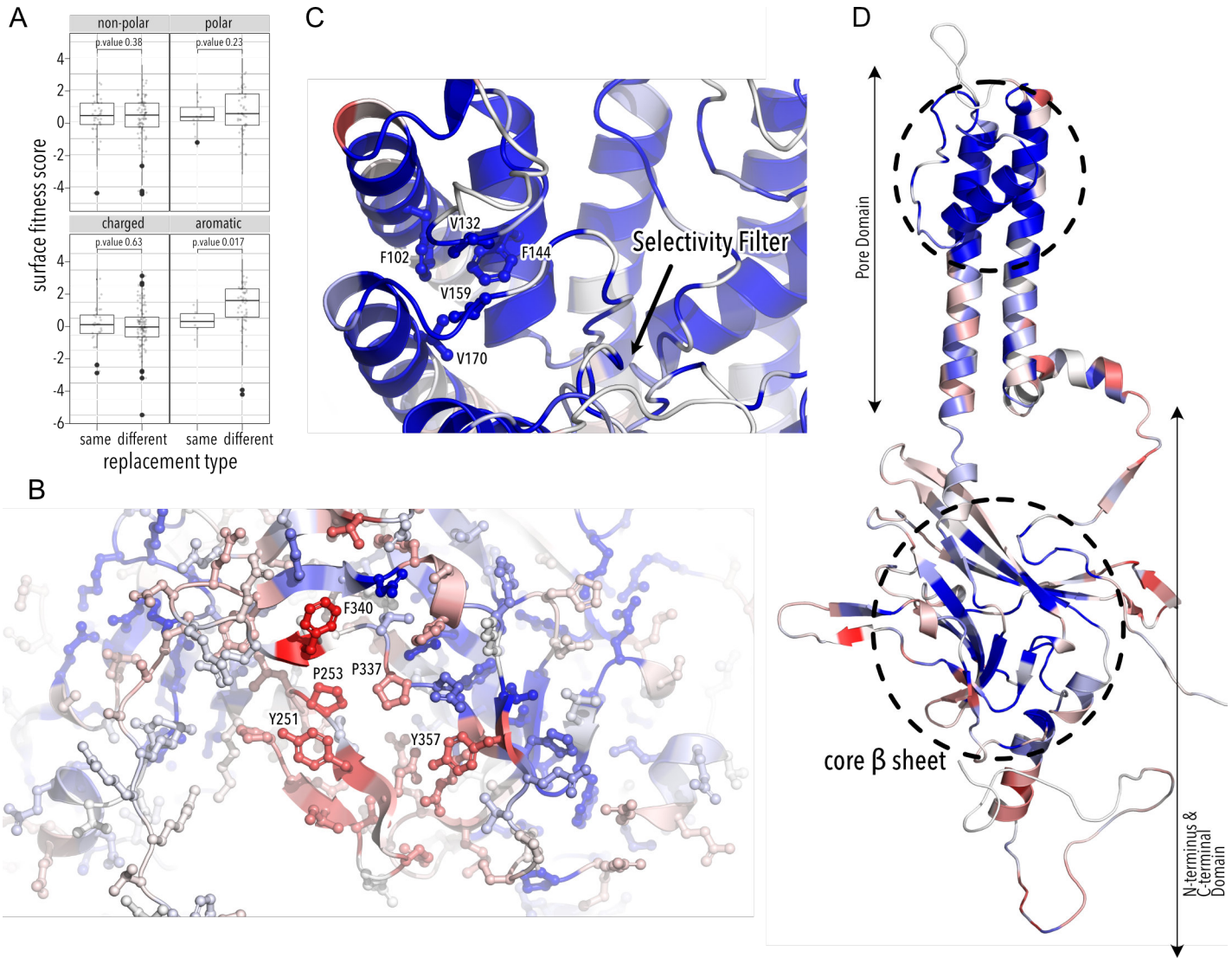

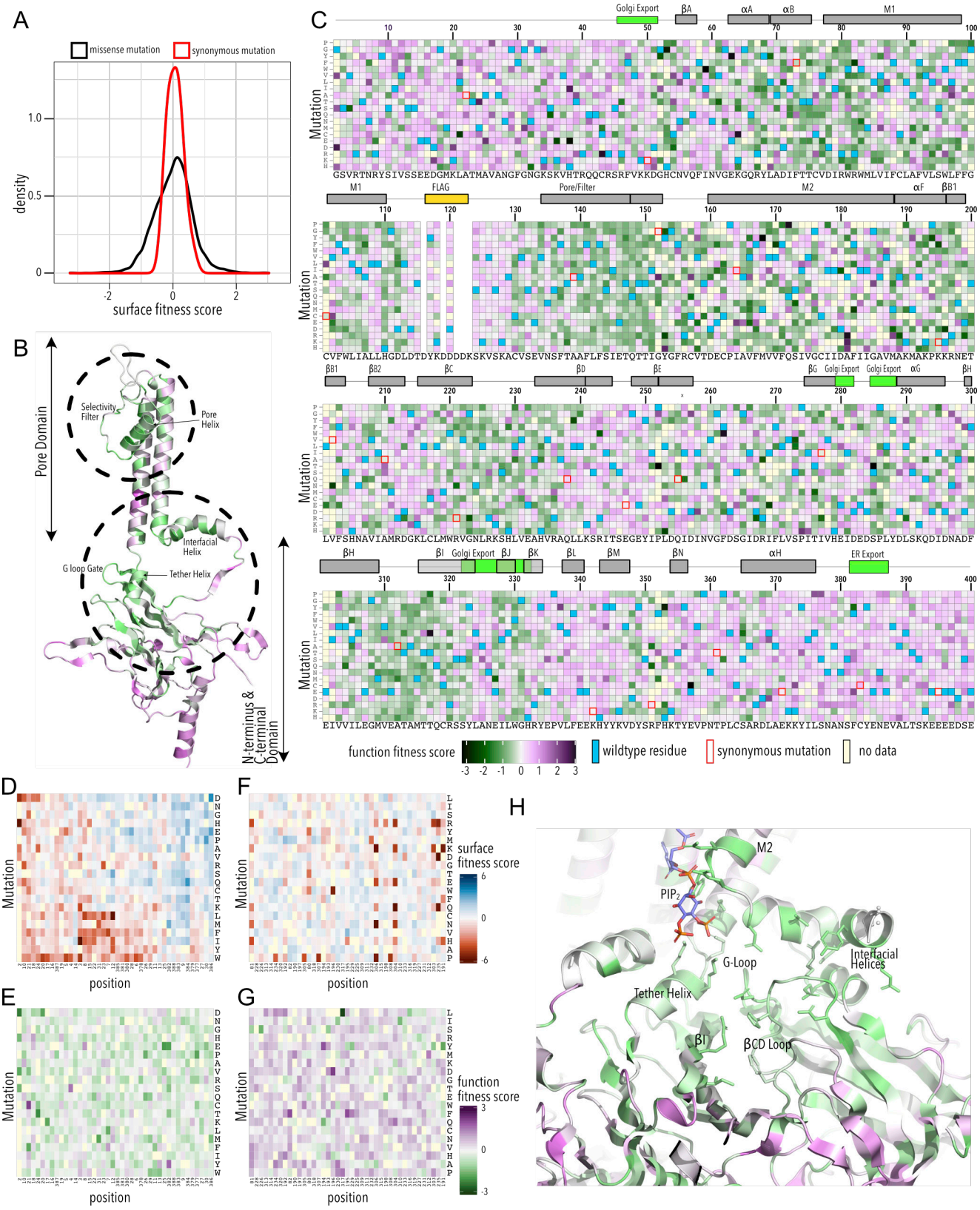

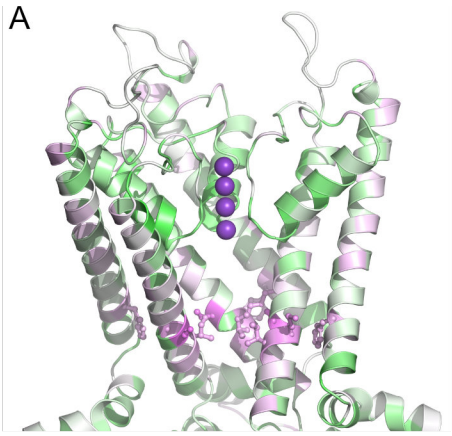

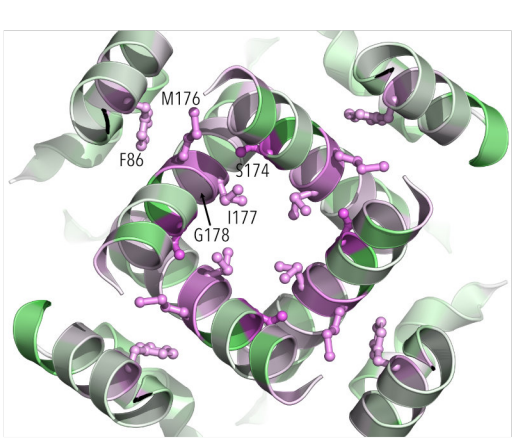

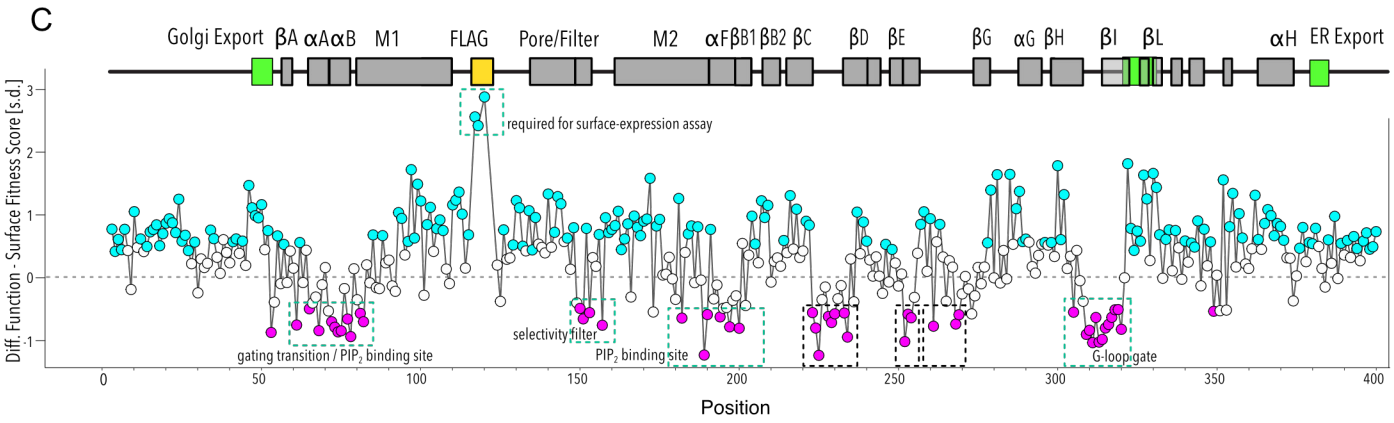

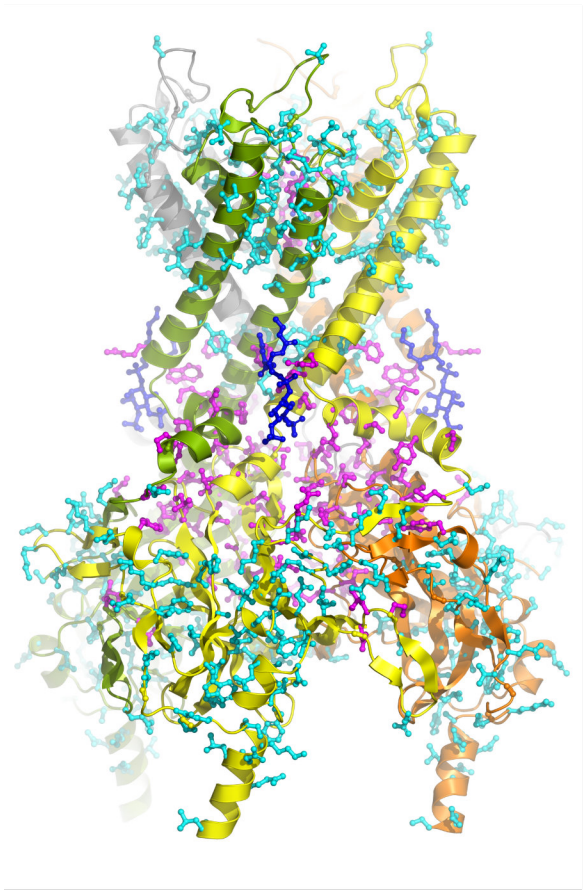

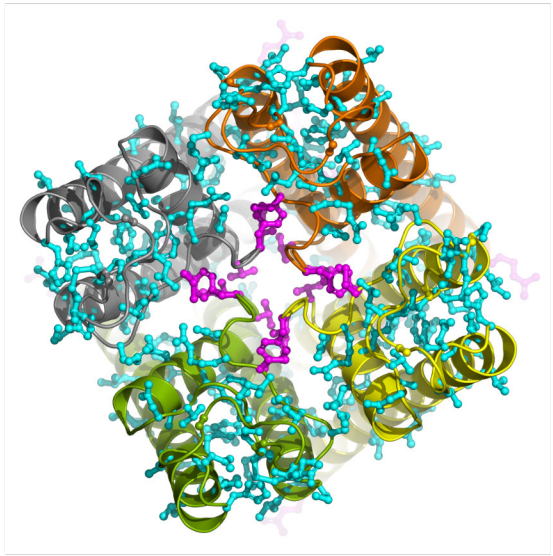

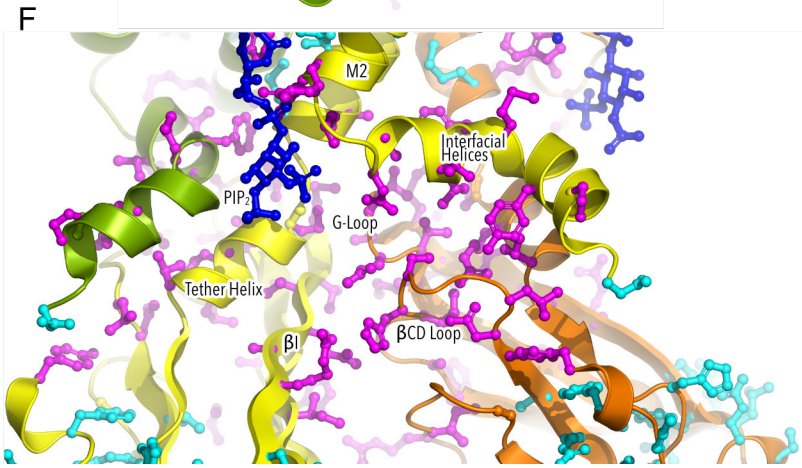

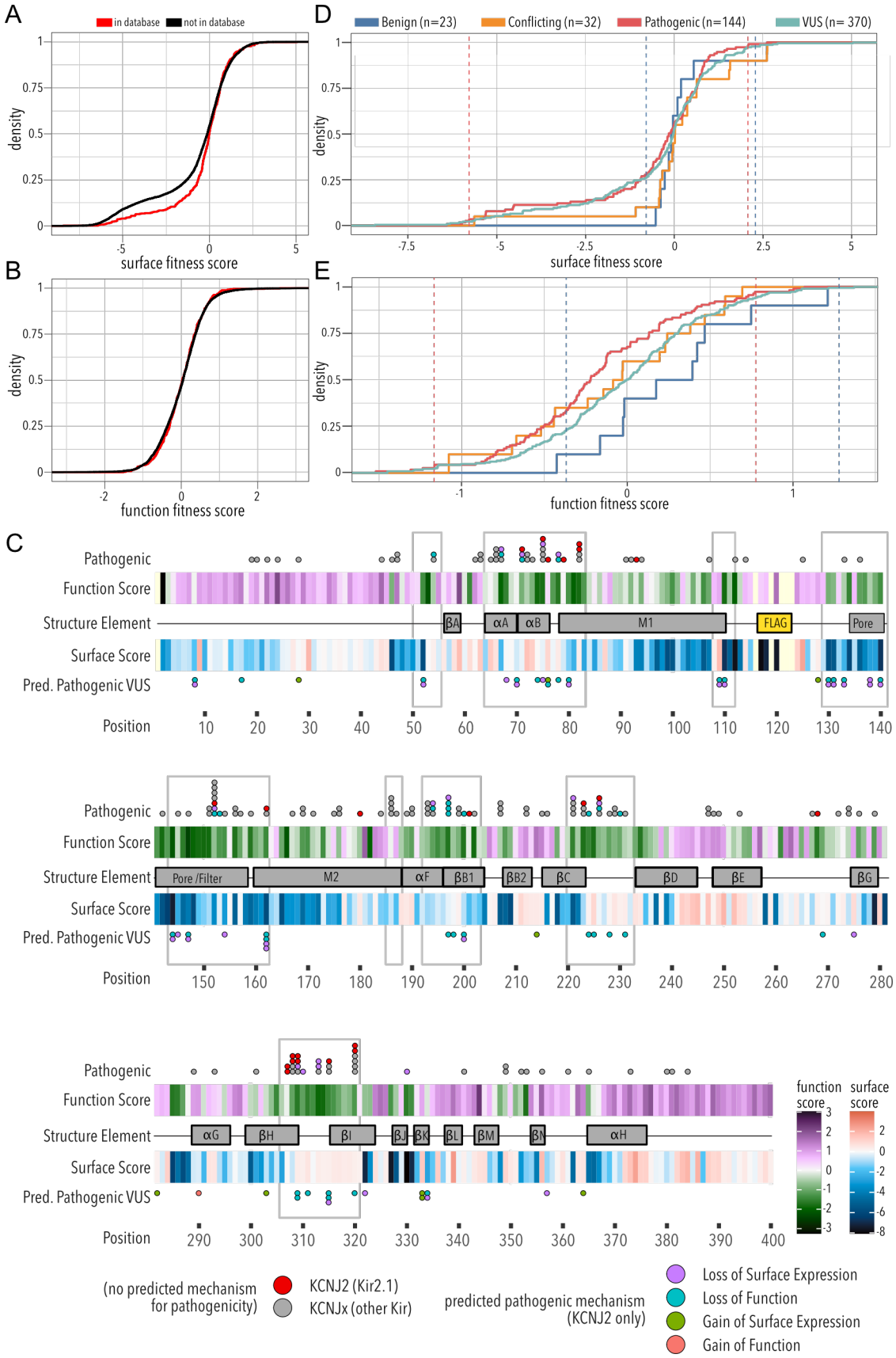

SUPPLEMENTARY MATERIALS FOR:

Determinants of trafficking, conduction, and disease within a K^+ channel revealed through multiparametric deep mutational scanning

Short Title: Multiparametric Deep Mutational Scanning in the Inward Rectifier Kir2.1

Authors:

Willow Coyote-Maestas[1#], David Nedrud[1], Yungui He[2], Daniel Schmidt[2§]

Affiliations:

[1]Department of Biochemistry, Molecular Biology & Biophysics, University of Minnesota, Minneapolis, MN, 55455, USA

[2] Department of Genetics, Cell Biology & Development, University of Minnesota, Minneapolis, MN, 55455, USA

[#]Present address: Department of Bioengineering and Therapeutic Science and Quantitative Biosciences Institute, University of California, San Francisco, San Francisco, CA, 94158

[§]Correspondence and requests for materials should be addressed to D.S. (email: schmida@umn.edu)

This PDF file includes:

Supplemental Figures 1 – 9

Supplemental Tables 1 – 3

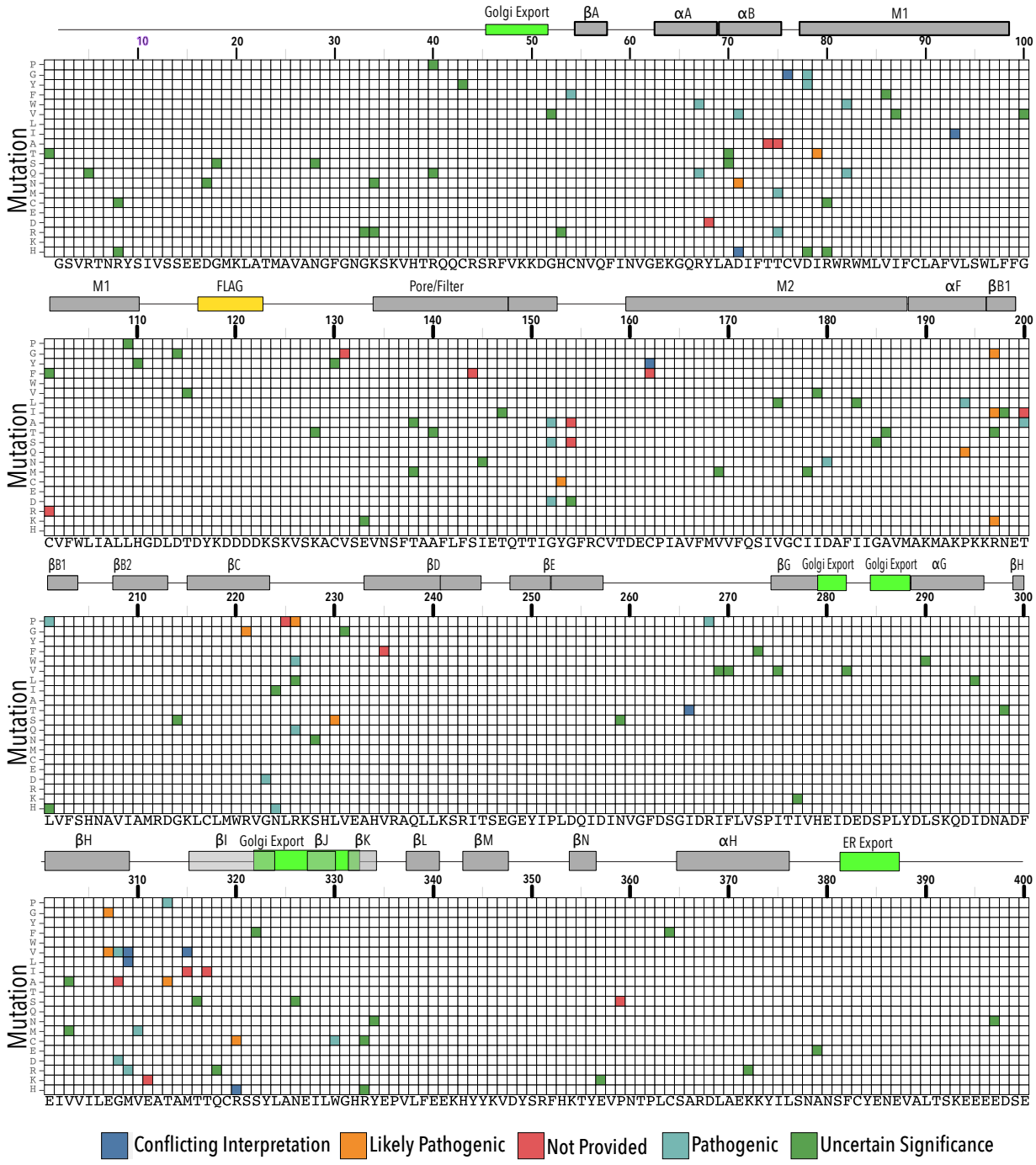

Supplementary Figure 1: Kir2.1 variant effect reported in ClinVar. Heatmap showing clinically observed Kir2.1 variants mapped by position, mutation, and pathogenicity interpretation. Kir2.1 secondary structural element are shown as gray boxes above each panel. Trafficking signals are colored green.

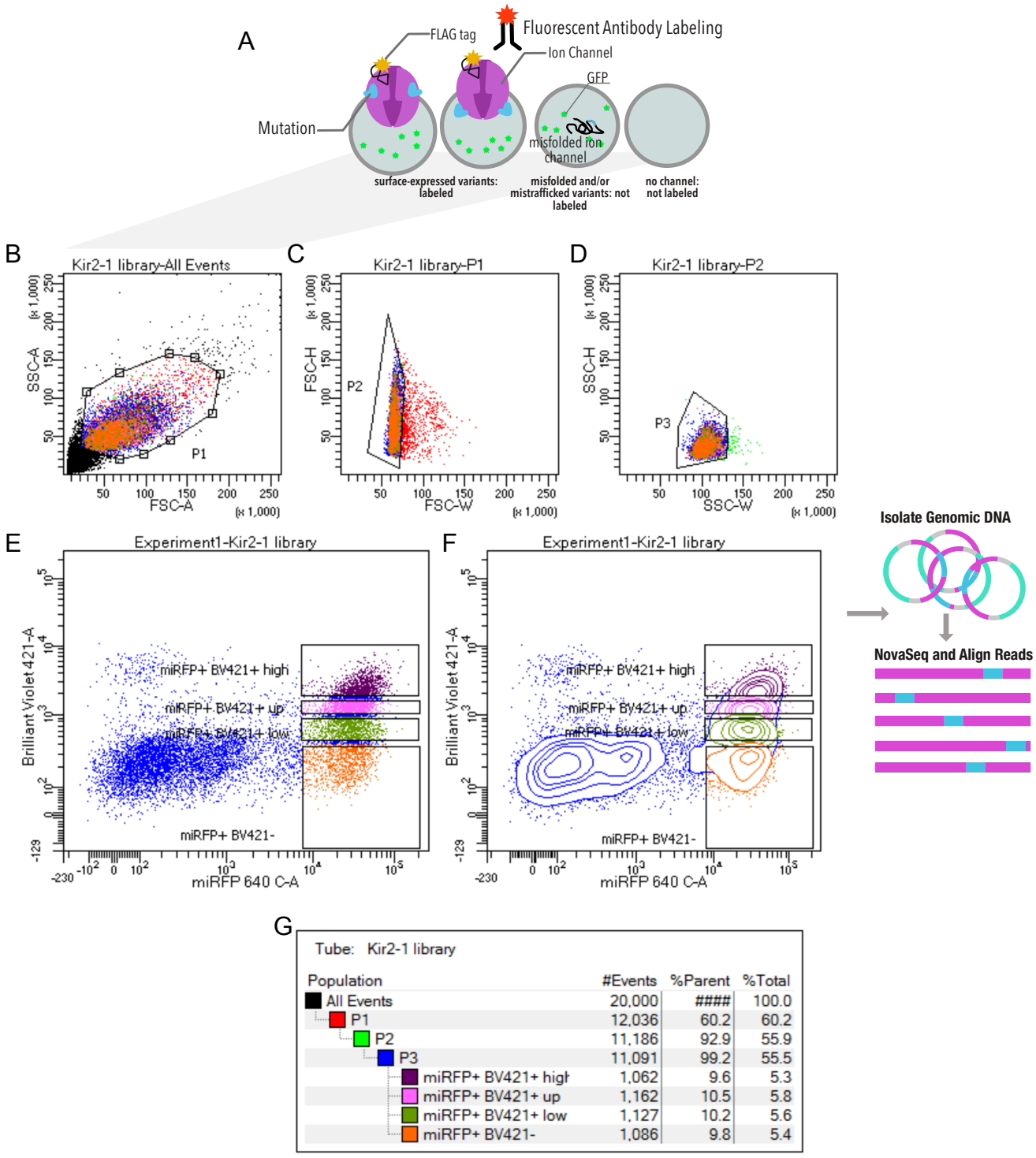

Supplementary Figure 2: Kir2.1 surface expression assay gating scheme. (A) HEK293 cells expressing a single variant are incubated with a fluorescent (Brilliant Violet) antibody that recognizes a FLAG tag inserted into an extracellular loop (Kir2.1 position T115). Cells expressing channel variants that can fold, assemble and traffic to the cell surface are labelled, while those that express variants with impaired folding, assembly, and/or trafficking are not labelled. **(B)** Using FACS, whole HEK293 cells are gated on side (SSC-A) and forward scattering (FSC-A). **(C-D)** Forward scattering height (FSC-H), forward scattering width (FSC-W), and Side scattering width (SSC-W) are used to gate single cells. Non-surface expressed variants ($miRFP_{high}/Label_{low}$) and surface expressed variants ($miRFP_{high}/Label_{high}$) populations are gated into 'negative', 'low', 'up', and 'high' populations based an expression marker (miRFP670) of Anti-Flag Brilliant Violet-421 fluorescence. Scatter plot **(E)** and contour plot **(F)** shown. Contour plots represent 95% confidence intervals with outliers shown as dots. **(G)** Sort statistic for each gated cell population.

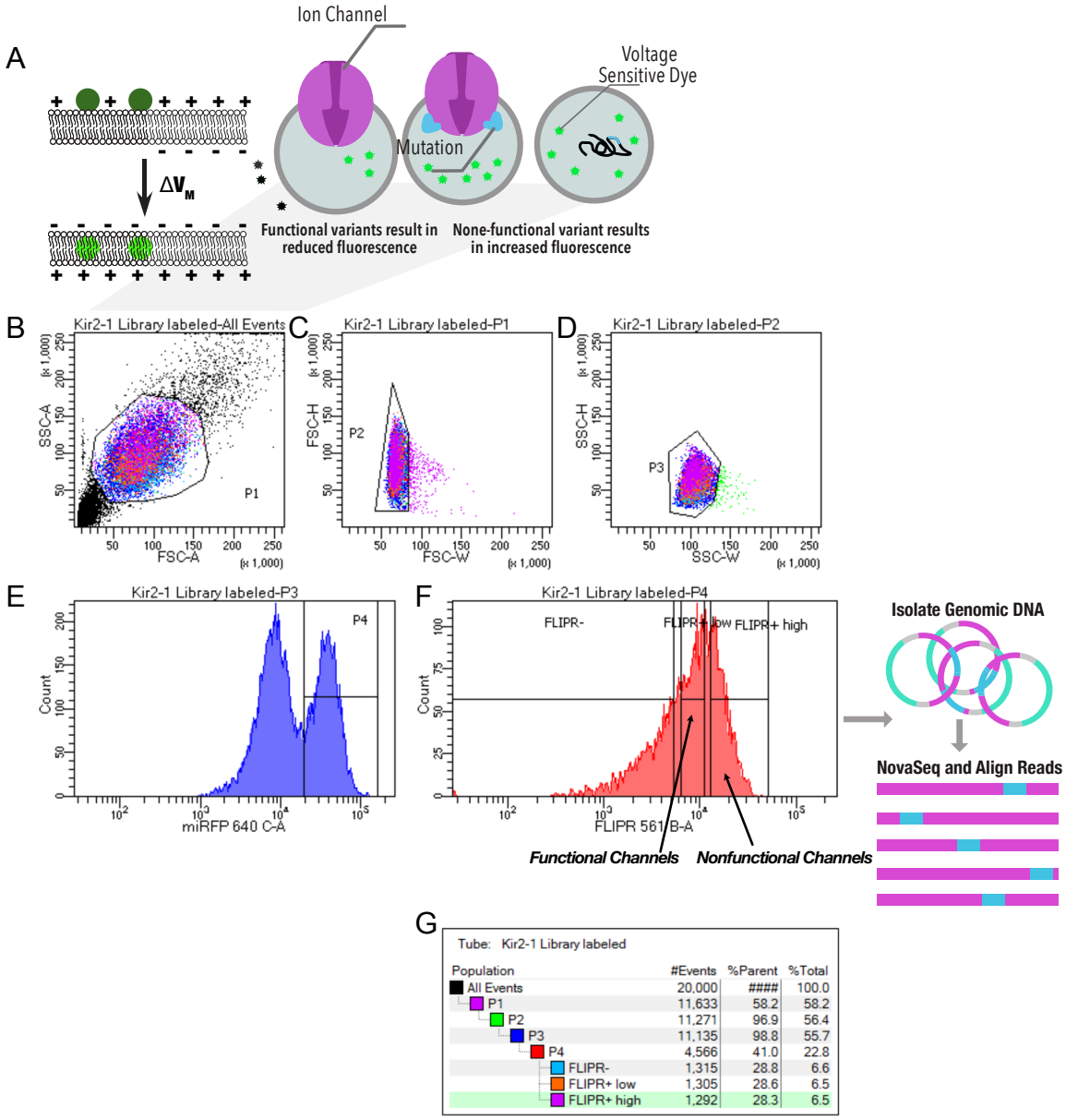

G

Tube: Kir2-1 Library labeled

Population	#Events	%Parent	%Total
All Events	20,000	####	100.0
P1	11,633	58.2	58.2
P2	11,271	96.9	56.4
P3	11,135	98.8	55.7
P4	4,566	41.0	22.8
FLIPR-	1,315	28.8	6.6
FLIPR+ low	1,305	28.6	6.5
FLIPR+ high	1,292	28.3	6.5

Supplementary Figure 3: Kir2.1 functional fitness assay gating scheme. (A) HEK293 cells expressing a single variant are incubated with a voltage-sensitive FLIPR dye. In strongly hyperpolarized cells, this dye partitions out the cell membrane into an aqueous environment, which decreases its extinction coefficient and thus decreases green fluorescence upon excitation with blue light. In depolarized cells, the FLIPR dye fluorescence is brighter because the dye partitions into the membrane, which increases its extinction coefficient. **(B)** Using FACS, whole HEK293 cells are gated on side (SSC-A) and forward scattering (FSC-A). **(C-D)** Forward scattering height (FSC-H), forward scattering width (FSC-W), and Side scattering width (SSC-W) are used to gate single cells. **(E)** Cells are further gated using miRFP670 as an expression marker. **(F)** Non-functional and functional channel population are separated by sorting based on FLIPR fluorescences. **(G)** Sort statistic for each gated cell population.

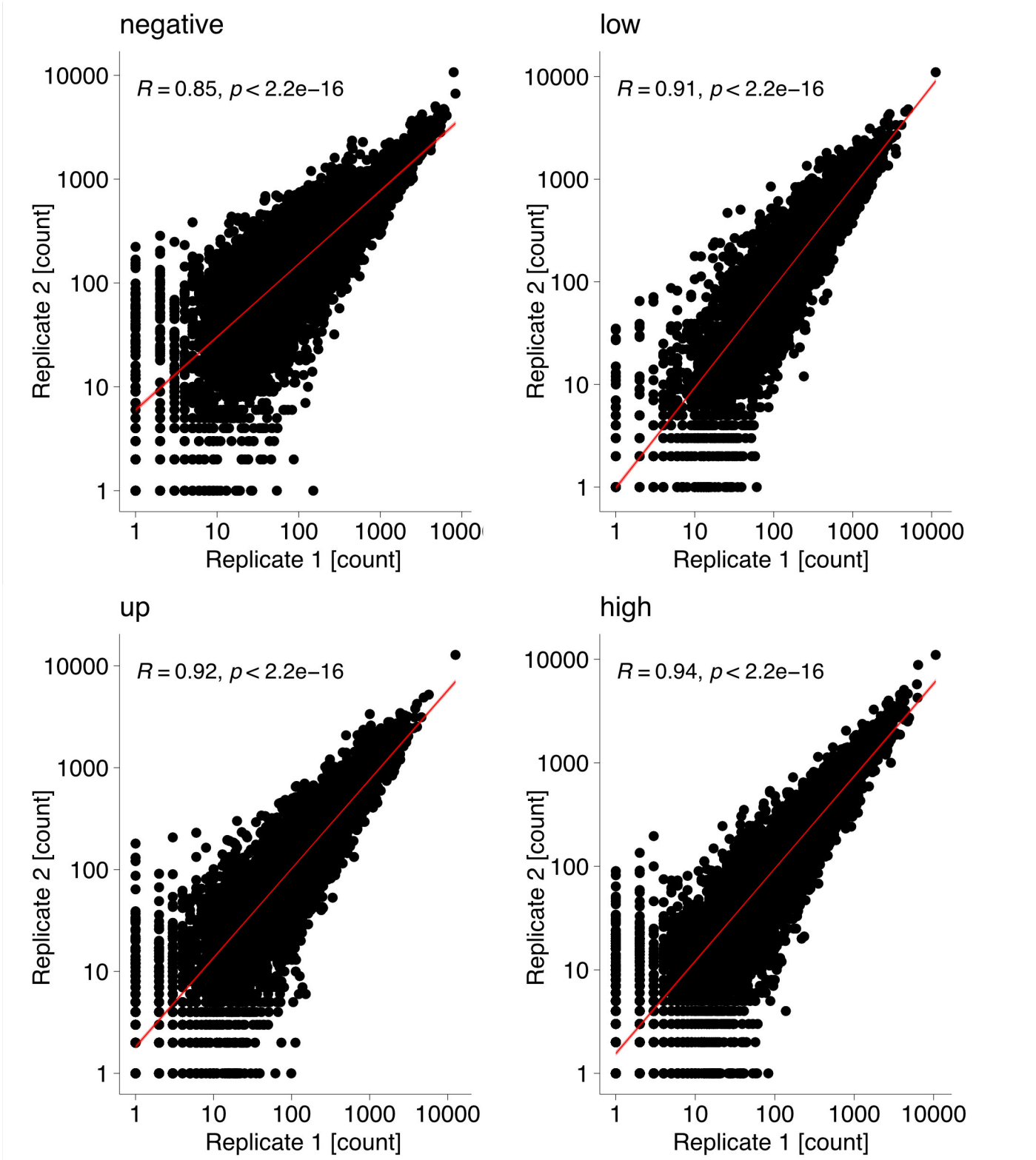

Supplementary Figure 4: Surface fitness assay biological replicates. Scatterplots show mapped read counts for each Kir2.1 variant in each replicate for different assay subpools. Spearman correlation coefficients are inset for each replicate pair. A linear model regression fit is shown as a red line.

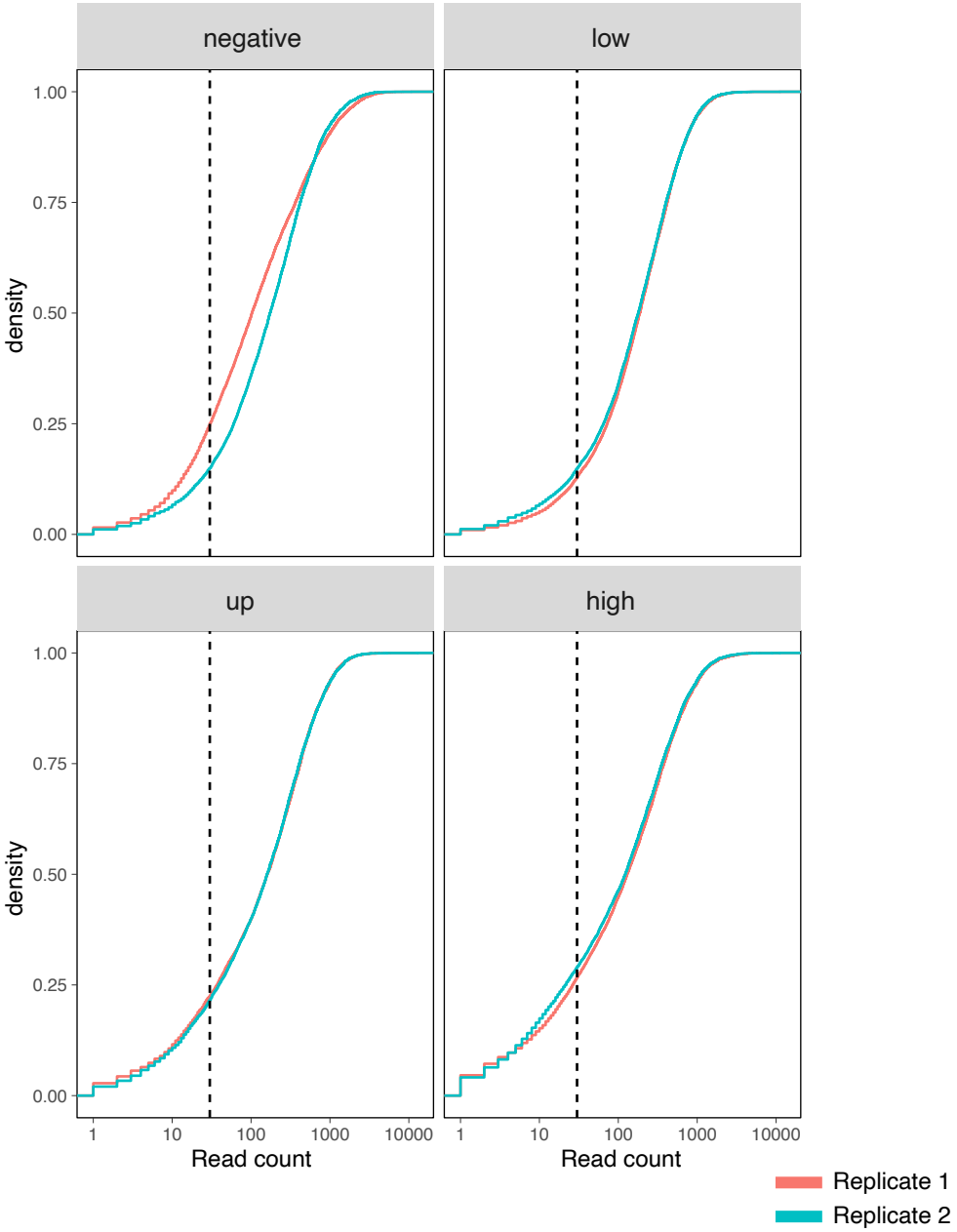

Supplementary Figure 5: Surface fitness assay read count depth. Cumulative density distribution of read counts for each replicate and assay condition subpool. Dashed vertical lines represent 30-fold coverage.

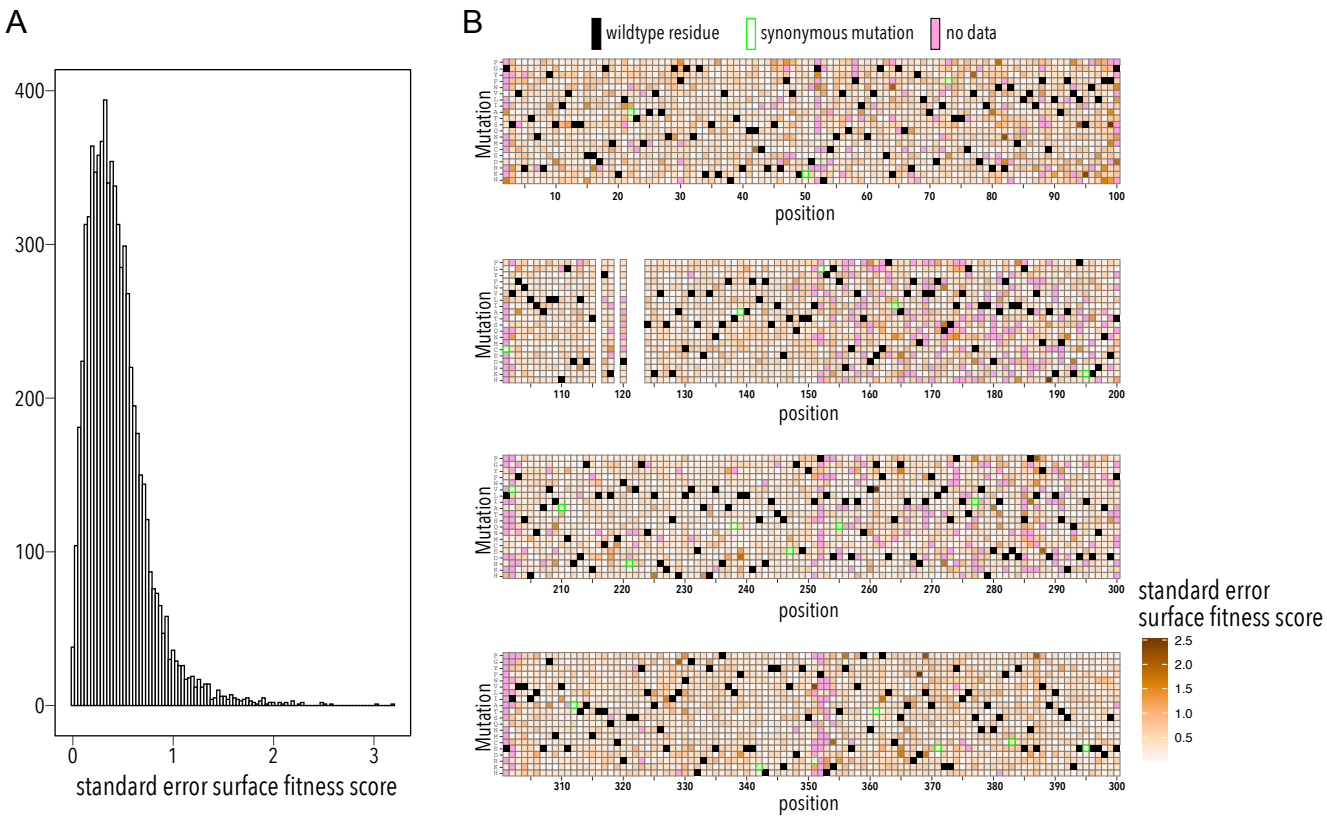

Supplementary Figure 6: Surface fitness assay standard error distribution. (A) Distribution of surface fitness score standard errors. **(B)** Heatmap showing surface fitness standard error (gradient white to brown) mapped to each position and mutation. Wildtype residues are shown as black boxes. Missing data is shown as magenta boxes. Synonymous mutations are indicated by a green outline.

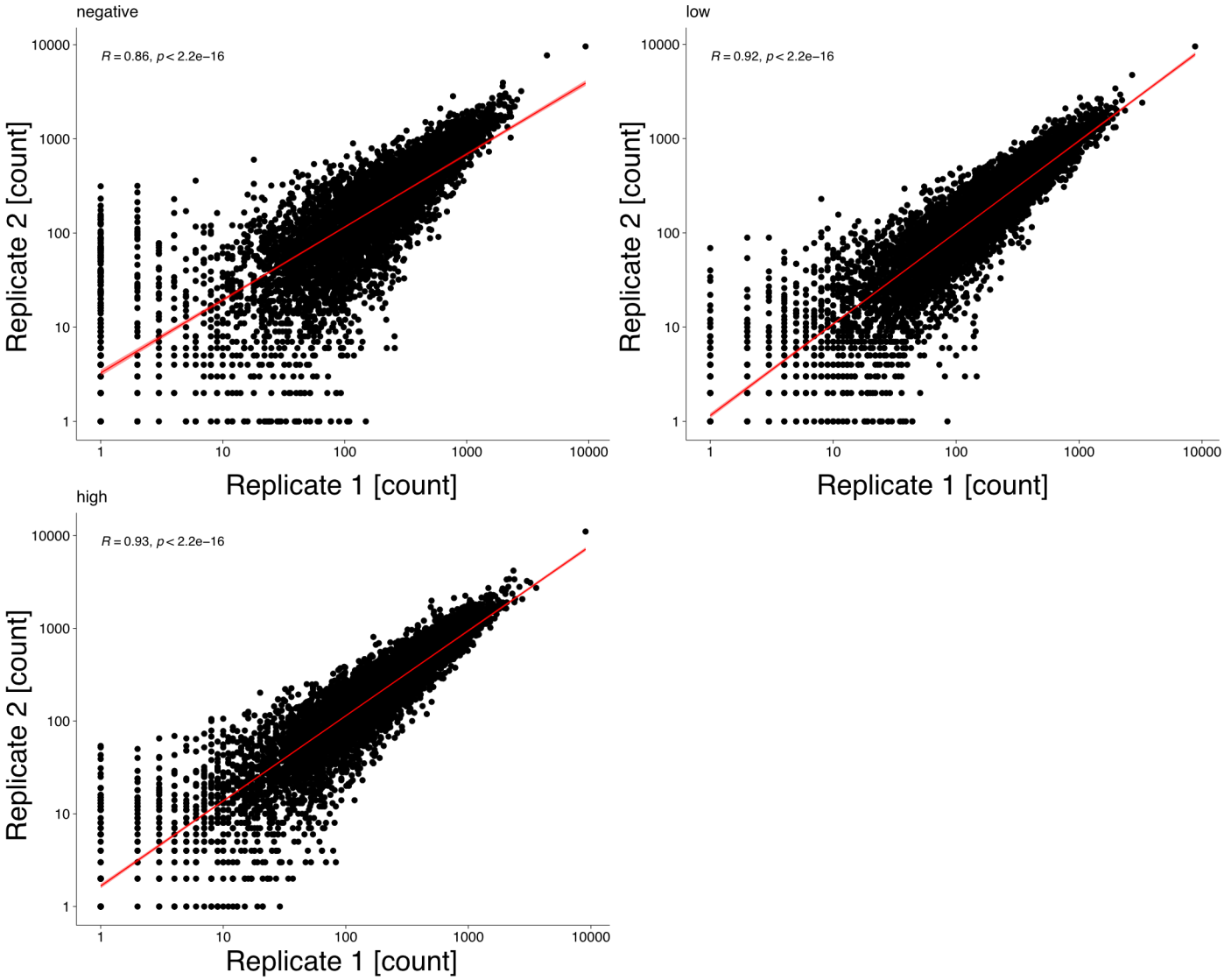

Supplementary Figure 7: Surface fitness assay biological replicates. Scatterplots show mapped read counts for each Kir2.1 variant in each replicate for different assay subpools. Spearman correlation coefficients are inset for each replicate pair. A linear model regression fit is shown as a red line.

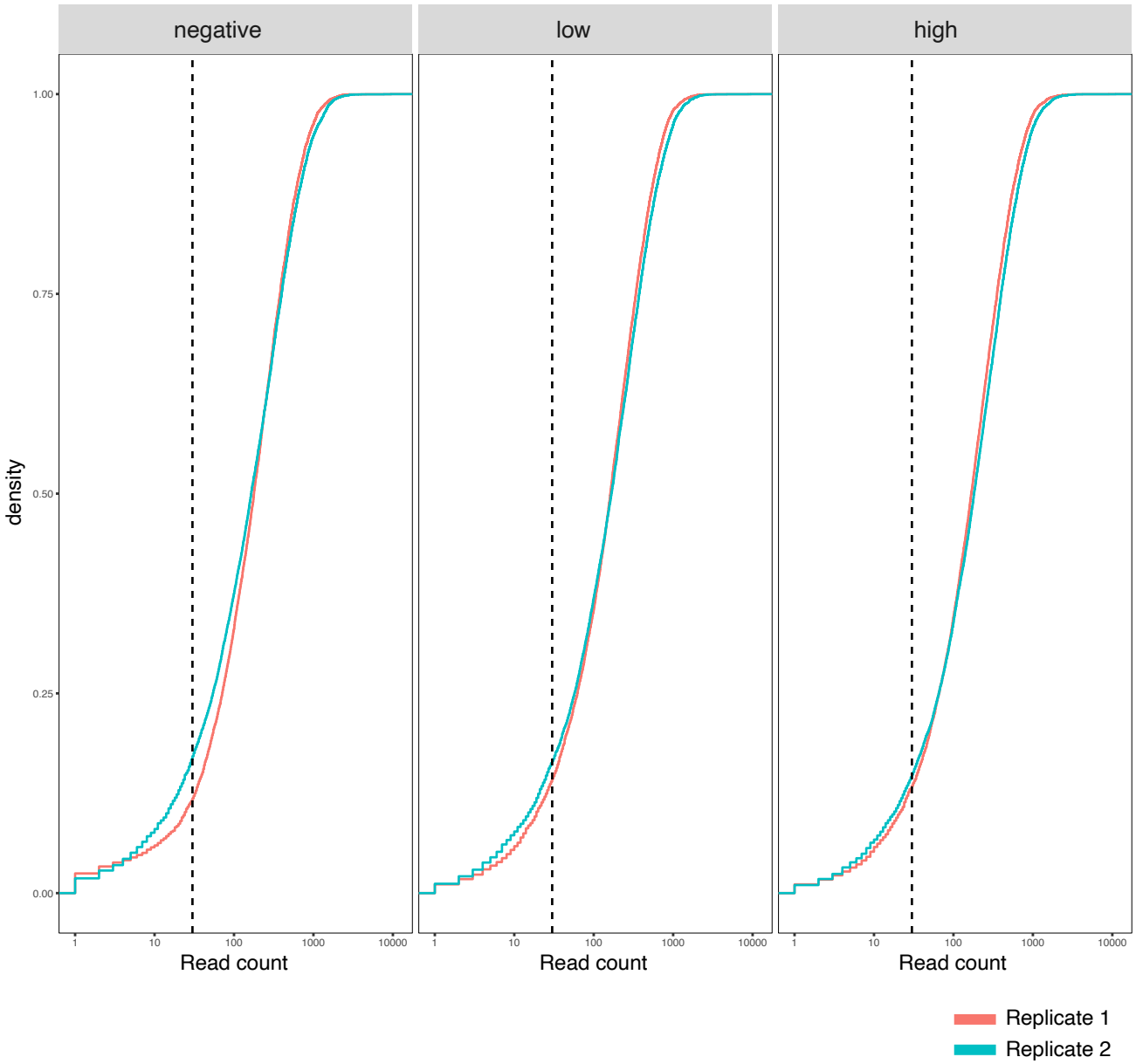

Supplementary Figure 8: Surface fitness assay biological replicates. Cumulative density distribution of read counts for each replicate and assay condition subpool. Dashed vertical lines represent 30-fold coverage.

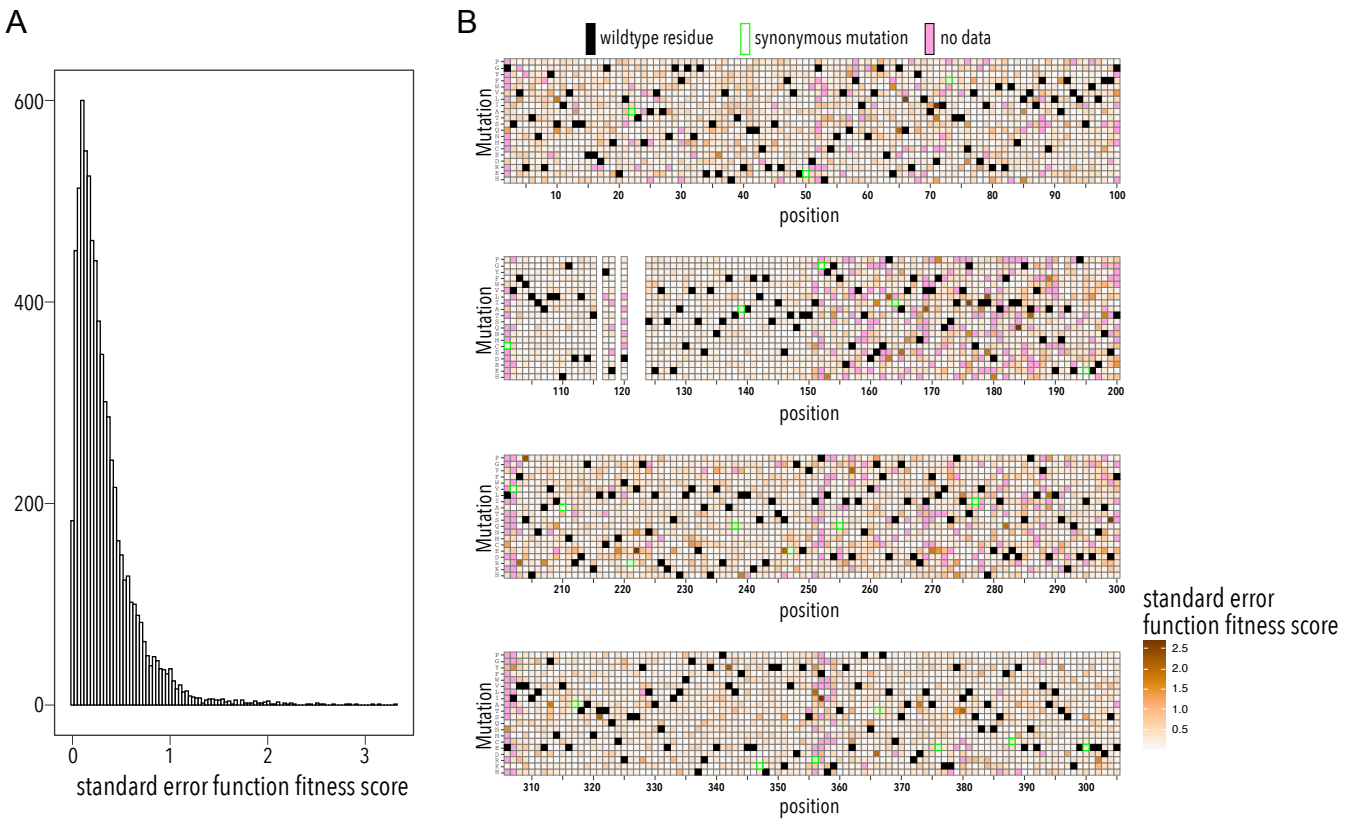

Supplementary Figure 9: Function fitness assay standard error distribution. (A) Distribution of surface fitness score standard errors. **(B)** Heatmap showing surface fitness standard error (gradient white to brown) mapped to each position and mutation. Wildtype residues are shown as black boxes. Missing data is shown as magenta boxes. Synonymous mutations are indicated by a green outline.

A

Sample	Barcode sequence	PF Clusters	% of the lane	% Perfect barcode	% One mismatch barcode	Yield (Mbases)	% PF Clusters	% >=Q30 bases	Mean Quality Score
dms_baseline	CGTACTAG+AGAGGATA	17,942,041	1.78	95.35	4.65	5,418	100	90.5	35.34
dms_function_high1	GTAGAGGA+ATAGAGAG	14,044,823	1.39	95.15	4.85	4,242	100	87.22	34.64
dms_function_high2	TAAGGCGA+AGAGGATA	18,810,378	1.86	96.5	3.5	5,681	100	89.08	35.01
dms_function_low1	CGAGGCTG+ATAGAGAG	14,199,546	1.41	97.46	2.54	4,288	100	88.63	34.99
dms_function_low2	GGAGCTAC+ATAGAGAG	14,903,201	1.48	95.74	4.26	4,501	100	89.28	35.1
dms_function_neg1	TAGGCATG+ATAGAGAG	15,073,953	1.49	97.14	2.86	4,552	100	91.1	35.45
dms_function_neg2	ACTCGCTA+ATAGAGAG	16,560,022	1.64	95.44	4.56	5,001	100	89.56	35.14
dms_surface_high1	TCCTGAGC+ATAGAGAG	15,200,690	1.51	96.22	3.78	4,591	100	90.8	35.37
dms_surface_high2	TAGGCATG+AGAGGATA	14,882,582	1.47	97.33	2.67	4,495	100	90.87	35.4
dms_surface_low1	CGTACTAG+ATAGAGAG	16,320,952	1.62	93.92	6.08	4,929	100	88.75	34.98
dms_surface_low2	TCCTGAGC+AGAGGATA	17,274,356	1.71	97.2	2.8	5,217	100	90.98	35.42
dms_surface_neg1	TAAGGCGA+ATAGAGAG	18,343,213	1.82	94.16	5.84	5,540	100	87.59	34.73
dms_surface_neg2	AGGCAGAA+AGAGGATA	20,844,383	2.07	96.24	3.76	6,295	100	90.49	35.31
dms_surface_up1	AGGCAGAA+ATAGAGAG	16,105,434	1.6	94.92	5.08	4,864	100	89.01	35.01
dms_surface_up2	GGACTCCT+AGAGGATA	16,752,187	1.66	97.54	2.46	5,059	100	90.65	35.36

B

Surface Fitness Assay – Mapped Reads

	Negative		Low		Up		High	
	Rep. 1	Rep. 2	Rep. 1	Rep. 2	Rep. 1	Rep. 2	Rep. 1	Rep. 2
$N_{variants}$	7,282	7,282	7,305	7,305	7,175	7,175	6,975	6,975
median	103	174	187	179	160.5	160	130	123
mean	342.3	344.6	315.5	307.4	310.4	309.5	301.4	285.5
>30-fold [%]	71.7	82.4	85.4	82.2	73.4	73.4	65.7	64.4

C

Function Fitness Assay – Mapped Reads

	Negative		Low		Up	
	Rep. 1	Rep. 2	Rep. 1	Rep. 2	Rep. 1	Rep. 2
N	7,168	7,168	7,284	7,284	7,320	7,320
median	178	165	162	167	168	182
mean	281.6	297.1	248.5	276.5	261.5	295.7
>30-fold [%]	79.4	79.5	82.7	80.9	83.3	83.5

Supplementary Table 1: NGS read statistics and assay repeatability. (A) Read statistics for each sequenced variant pool. Mapped reads for each replicate and surface fitness assay sub-pool **(B)** or function fitness assay **(C)**. $N_{variants}$ represented in each replicate (out of 7,429 total), median read count per variant, mean read count per variant, and percentage of variants that have greater than 30-fold reach coverage.

Supplemental Table 2: Inward Rectifier Missense Variants in ClinVar and dbSNP

Gene	Gene name
AA_pos	mutated residue
AA_pos_Kir2	corresponding residue in Kir2.1 (KCNJ2)
aligned	residues align between reference inward rectifier and Kir2.1; i.e. residue is present in both proteins wildtype amino acid
wt_resid	wildtype amino acid
mut_resid	mutated amino acid
f_wt	physicochemical type of wildtype amino acid
f_mut	physicochemical type of mutated amino acid
clinical_signi	clinical signficance of variant
function_sco	variant function fitness score
function_SE	variant function fitness score standard error
function_eps	variant function fitness score change in standard error after random-effects
surface_scor	model last iteration variant surface fitness score
surface_SE	variant surface fitness score standard error
surface_epsi	variant function fitness score change in standard error after random-effects
VUSpred	model last iteration predicted phenotype

Gene	position	Pos	aligned	wt_resid	mutation	fwt	fmut	function_sco	function_SE	function_eps	surface_scor	surface_SE	surface_epsi	Clinical_Sign	VUSpred
KCNJ5	100	105	TRUE	G	A	NP	NP	0.81379928	0.20469394	2.15E-15	0.49942381	0.31367313	5.95E-40	VUS	NA
KCNJ2	138	130	TRUE	T	A	P	NP	-0.195991	0.07366001	0	-0.7216232	0.15257129	1.10E-29	VUS	NA
KCNJ2	152	144	TRUE	G	A	NP	NP	NA	0.4993218	0	NA	1.13398892	0	Pathog.	NA
KCNJ2	154	146	TRUE	G	A	NP	NP	NA	1.02908233	0	NA	1.03755074	1.73E-48	VUS	NA
KCNJ16	154	135	TRUE	G	A	NP	NP	NA	1.02908233	0	NA	1.03755074	1.73E-48	Pathog.	NA
KCNJ5	159	158	TRUE	T	A	P	NP	-0.6698822	0.03647903	2.41E-118	-2.4926289	0.47133857	6.11E-47	Pathog.	NA
KCNJ2	185	177	TRUE	G	A	NP	NP	0.45419005	0.64934674	0	-0.4033434	0.30475895	2.78E-17	NA	NA
KCNJ11	199	179	TRUE	E	A	C	NP	-0.1415104	0.32803498	1.11E-16	-0.6450818	0.19057407	3.37E-34	Pathog.	NA
KCNJ2	200	192	TRUE	T	A	P	NP	-0.3511751	0.13844753	6.94E-18	-0.2502579	0.09053069	2.94E-55	Pathog.	NA
KCNJ8	250	240	TRUE	Y	A	A	NP	0.85388845	0.31256938	1.31E-51	2.41395965	0.20370115	0	VUS	NA
KCNJ2	260	252	TRUE	V	A	NP	NP	-0.440287	0.19078813	6.94E-18	0.43099892	0.15163039	1.14E-23	NA	NA
KCNJ10	262	240	TRUE	F	A	A	NP	1.01454162	0.38869311	7.80E-08	-0.0074027	0.3568062	3.35E-41	VUS	NA
KCNJ11	272	252	TRUE	V	A	NP	NP	0.13063764	0.16186267	0	-0.2611694	0.17872364	1.34E-40	Pathog.	NA
KCNJ2	274	266	TRUE	P	A	NP	NP	0.51958348	0.2481139	3.28E-33	0.50884055	0.36657689	6.88E-11	NA	NA
KCNJ2	276	268	TRUE	T	A	P	NP	0.73892797	0.73866688	0	-0.6710168	0.13680398	0	NA	NA
KCNJ2	278	270	TRUE	V	A	NP	NP	NA	NA	NA	NA	0.84004943	0	NA	NA
KCNJ2	289	281	TRUE	D	A	C	NP	NA	1.45027593	0	NA	0.28223374	1.89E-73	NA	NA
KCNJ13	303	268	TRUE	V	A	NP	NP	0.03540814	0.48512336	1.06E-56	1.96327758	0.71255152	2.22E-16	VUS	NA
KCNJ2	303	295	TRUE	V	A	NP	NP	0.03540814	0.48512336	1.06E-56	1.96327758	0.71255152	2.22E-16	VUS	NA
KCNJ11	308	289	TRUE	G	A	NP	NP	NA	1.74490369	0	NA	1.38799599	0	Pathog.	NA
KCNJ2	308	300	TRUE	G	A	NP	NP	NA	1.74490369	0	NA	1.38799599	0	VUS	NA
KCNJ13	311	276	TRUE	E	A	C	NP	NA	0.58030396	3.81E-28	NA	NA	NA	Benign	NA
KCNJ2	313	305	TRUE	T	A	P	NP	-0.4981432	0.17439121	0.00014839	0.84058815	0.57908238	1.67E-16	Pathog.	NA
KCNJ8	344	334	TRUE	Y	A	A	NP	0.74708612	0.31973179	6.74E-06	-0.0393025	0.13744429	2.95E-51	Benign	NA
KCNJ10	355	333	TRUE	T	A	P	NP	0.22593992	0.34312936	2.19E-10	-0.5308753	0.46627947	7.29E-11	VUS	NA
KCNJ13	356	322	TRUE	Y	A	A	NP	1.36845724	0.15585434	3.77E-09	2.77353583	0.51543136	1.07E-05	VUS	NA
KCNJ10	361	338	TRUE	T	A	P	NP	0.3241212	0.08222318	8.85E-47	1.42088156	0.32836413	9.66E-12	VUS	NA
KCNJ13	361	327	TRUE	T	A	P	NP	0.3241212	0.08222318	8.85E-47	1.42088156	0.32836413	9.66E-12	VUS	NA
KCNJ2	361	353	TRUE	T	A	P	NP	0.3241212	0.08222318	8.85E-47	1.42088156	0.32836413	9.66E-12	NA	NA
KCNJ10	383	350	FALSE	C	A	P	NP	0.35006372	0.12645806	0	1.25866919	0.20416344	1.39E-38	VUS	NA
KCNJ1	387	362	FALSE	E	A	C	NP	0.26779285	0.41133276	0	-1.37854	0.68718318	1.04E-18	VUS	NA
KCNJ5	388	395	FALSE	V	A	NP	NP	-0.1277329	0.10463024	8.43E-240	0.70863716	0.12122226	1.35E-43	VUS	NA
KCNJ2	56	56	TRUE	V	A	NP	NP	0.03655377	0.06167305	1.95E-59	0.31713065	0.23148171	1.45E-42	NA	NA
KCNJ1	57	52	TRUE	Q	A	P	NP	-0.2115718	0.02271251	1.30E-84	-0.0513936	0.63987301	5.34E-55	VUS	NA
KCNJ2	74	74	TRUE	T	A	P	NP	-0.3229091	0.26441815	2.78E-17	-0.1161493	0.08287003	1.04E-110	VUS	NA
KCNJ2	52	52	TRUE	G	V	NP	NP	-0.6561385	0.41855339	5.55E-17	-5.6237317	0.60967061	1.35E-23	VUS	lof_s
KCNJ10	8	7	FALSE	R	A	C	NP	0.17230596	0.35634447	2.78E-17	0.07582545	0.32924361	3.59E-117	VUS	NA
KCNJ1	90	86	TRUE	L	A	NP	NP	0.17390424	0.05803704	5.79E-22	-0.5254501	0.33093017	4.64E-77	Benign	NA
KCNJ2	93	93	TRUE	V	A	NP	NP	0.68185578	0.00066583	7.28E-35	-0.2166395	0.38640444	9.13E-208	NA	NA
KCNJ1	104	100	TRUE	W	C	A	P	0.2165369	0.20282331	3.47E-17	0.09167085	0.02384098	1.19E-06	VUS	NA
KCNJ2	104	104	TRUE	W	C	A	P	0.2165369	0.20282331	3.47E-17	0.09167085	0.02384098	1.19E-06	NA	NA
KCNJ13	132	102	TRUE	S	C	P	P	-0.5105745	0.14381989	9.29E-11	-1.8147091	0.67212615	6.02E-21	VUS	NA
KCNJ2	153	145	TRUE	Y	C	A	P	-0.3580095	0.21031698	4.11E-11	0.79337902	0.26534972	1.77E-57	Pathog.	NA
KCNJ5	153	152	TRUE	Y	C	A	P	-0.3580095	0.21031698	4.11E-11	0.79337902	0.26534972	1.77E-57	VUS	NA
KCNJ11	156	136	TRUE	R	C	C	P	-1.1635292	0.10055978	3.51E-10	-5.3200824	0.87482383	0	Pathog.	NA
KCNJ16	156	137	TRUE	R	C	C	P	-1.1635292	0.10055978	3.51E-10	-5.3200824	0.87482383	0	Pathog.	NA
KCNJ1	193	186	TRUE	K	C	C	P	0.38011456	0.29107626	9.84E-07	0.62880329	0.83145513	6.65E-07	Conflicting	NA
KCNJ11	196	176	TRUE	K	C	C	P	-0.4618046	0.3431431	0.00025526	-0.6180472	0.28837454	1.85E-42	VUS	NA
KCNJ4	212	196	TRUE	R	C	C	P	0.44795737	0.47066317	0	1.43414597	0.23647147	2.98E-50	VUS	NA
KCNJ11	221	201	TRUE	R	C	C	P	-0.7445034	0.23071532	1.39E-56	-5.3755752	0.38480092	2.78E-17	Pathog.	NA
KCNJ18	226	219	TRUE	R	C	C	P	-0.0973434	0.35794285	5.55E-17	-0.0444598	0.47274289	6.94E-62	VUS	NA
KCNJ1	236	227	TRUE	R	C	C	P	-1.2943545	0.52632233	0	-0.3142736	0.39809579	2.16E-08	VUS	NA
KCNJ11	24	27	FALSE	M	C	NP	P	1.30583705	0.14592196	0	-0.1609631	0.31371149	2.53E-07	Conflicting	NA
KCNJ8	284	274	TRUE	D	C	C	P	0.13197014	0.40674045	2.76E-14	1.68793414	0.26937056	1.29E-20	VUS	NA
KCNJ10	293	271	TRUE	Q	C	P	P	-0.4259897	0.1247458	3.82E-59	-0.2714517	0.40171323	4.87E-46	Benign	NA
KCNJ10	296	273	TRUE	D	C	C	P	NA	NA	NA	NA	NA	NA	VUS	NA
KCNJ10	320	297	TRUE	R	C	C	P	-0.1268682	0.23199411	0	0.24040855	0.35313795	1.05E-118	Pathog.	NA
KCNJ11	320	301	TRUE	R	C	C	P	-0.1268682	0.23199411	0	0.24040855	0.35313795	1.05E-118	Pathog.	NA
KCNJ2	320	312	TRUE	R	C	C	P	-0.1268682	0.23199411	0	0.24040855	0.35313795	1.05E-118	Pathog.	NA
KCNJ2	330	322	TRUE	W	C	A	P	-0.2621312	0.01861152	1.88E-31	-2.9283065	0.56680136	2.66E-85	Pathog.	NA
KCNJ2	333	325	TRUE	R	C	C	P	0.38348744	0.31488635	5.22E-14	2.16633332	0.48675332	1.53E-05	VUS	NA
KCNJ2	344	336	TRUE	Y	C	A	P	0.59714332	0.19627622	2.45E-21	0.35840776	0.16965307	1.47E-32	NA	NA
KCNJ11	349	330	TRUE	Y	C	A	P	0.13017971	0.89312663	2.22E-16	0.84597554	0.40859545	1.11E-16	Pathog.	NA
KCNJ2	350	342	TRUE	S	C	P	P	0.20296962	0.18088686	6.94E-18	0.64928096	0.07230194	3.03E-06	NA	NA
KCNJ5	37	41	FALSE	V	C	NP	P	-0.2911397	0.33590152	0	0.41056417	0.13220065	4.69E-46	Benign	NA
KCNJ2	374	366	TRUE	Y	C	A	P	0.1419044	0.11443585	0	1.0758554	0.24896452	5.55E-17	NA	NA
KCNJ10	376	343	FALSE	L	C	NP	P	0.17764419	0.19654428	1.39E-17	1.56499867	0.21561543	1.08E-26	VUS	NA
KCNJ10	381	348	FALSE	S	C	P	P	0.49882322	0.14385064	0	-0.4706386	0.67186908	5.32E-53	Conflicting	NA
KCNJ10	382	349	FALSE	F	C	A	P	0.33236671	0.10451193	2.72E-19	0.42612159	0.00523588	5.47E-46	VUS	NA
KCNJ2	384	376	TRUE	Y	C	A	P	-0.0075917	0.03642015	3.93E-25	1.21977467	0.40125411	1.61E-06	NA	NA
KCNJ11	385	365	FALSE	E	C	C	P	0.44475678	0.43523647	0	-0.7827948	0.60029454	1.68E-44	VUS	NA
KCNJ11	389	369	FALSE	A	C	NP	P	1.07518128	0.49336054	6.66E-16	0.92070431	0.20394916	5.47E-55	VUS	NA
KCNJ18	44	43	TRUE	R	C	C	P	0.65835074	0.33527128	1.23E-11	-0.0877824	0.05564332	1.93E-129	Pathog.	NA

KCNJ5	44	50	TRUE	R	C	C	P	0.65835074	0.33527128	1.23E-11	-0.0877824	0.05564332	1.93E-129	VUS	NA
KCNJ11	46	34	TRUE	R	C	C	P	-0.4433131	0.16500491	6.94E-18	-1.1029885	0.07876871	3.82E-90	Pathog.	NA
KCNJ2	46	46	TRUE	R	C	C	P	-0.4433131	0.16500491	6.94E-18	-1.1029885	0.07876871	3.82E-90	NA	NA
KCNJ10	53	36	TRUE	H	C	C	P	NA	0.71785089	0	NA	NA	NA	VUS	NA
KCNJ10	65	48	TRUE	G	C	NP	P	0.13578398	0.03455751	4.32E-10	0.034114	0.15129434	1.25E-08	VUS	NA
KCNJ11	67	54	TRUE	R	C	C	P	-0.6455515	0.85521145	9.54E-09	-0.4937374	0.35661966	2.46E-13	Pathog.	NA
KCNJ2	8	8	FALSE	R	C	C	P	-0.301395	0.15176769	5.81E-53	-0.2546448	0.65993922	4.00E-27	VUS	NA
KCNJ2	8	8	TRUE	R	C	C	P	-0.301395	0.15176769	5.81E-53	-0.2546448	0.65993922	4.00E-27	NA	NA
KCNJ2	52	52	TRUE	G	V	NP	NP	-0.6561385	0.41855339	5.55E-17	-5.6237317	0.60967061	1.35E-23	VUS	lof_f
KCNJ10	82	65	TRUE	R	C	C	P	-0.8086745	0.58085307	0	0.77268994	0.33624921	0	Pathog.	NA
KCNJ11	114	101	TRUE	D	D	C	C	NA	NA	NA	NA	NA	NA	VUS	NA
KCNJ2	126	118	TRUE	V	D	NP	C	0.11400258	0.11334002	1.26E-90	-1.3820707	0.71747563	2.46E-37	NA	NA
KCNJ2	152	144	TRUE	G	D	NP	C	-0.4019724	0.54523524	0	-4.5527684	0.54132959	0	Pathog.	NA
KCNJ2	70	70	TRUE	A	S	NP	P	-1.1452141	0.84391008	0	-0.4563385	0.34132524	8.13E-07	VUS	lof_f
KCNJ2	16	16	TRUE	E	D	C	C	-0.0563249	0.05304616	9.72E-52	-0.8682548	0.14350623	6.90E-40	NA	NA
KCNJ13	214	183	TRUE	G	D	NP	C	-0.0695749	0.06482806	5.30E-32	-0.3659988	0.09796553	2.57E-38	VUS	NA
KCNJ2	214	206	TRUE	G	D	NP	C	-0.0695749	0.06482806	5.30E-32	-0.3659988	0.09796553	2.57E-38	NA	NA
KCNJ2	223	215	TRUE	G	D	NP	C	-0.1322202	0.27829654	5.55E-17	0.00798478	0.24588963	7.03E-120	Pathog.	NA
KCNJ5	223	222	TRUE	G	D	NP	C	-0.1322202	0.27829654	5.55E-17	0.00798478	0.24588963	7.03E-120	VUS	NA
KCNJ2	247	239	TRUE	E	D	C	C	0.06797284	0.23905445	8.33E-17	0.12048543	0.31033541	0	NA	NA
KCNJ5	25	29	FALSE	A	D	NP	C	-0.519908	0.2522477	0	-1.4721597	0.35926251	2.98E-151	VUS	NA
KCNJ10	254	232	TRUE	D	D	C	C	NA	NA	NA	NA	NA	NA	VUS	NA
KCNJ10	279	257	TRUE	H	D	C	C	-0.4701277	0.24313397	0	-5.4622296	0.88469283	1.72E-130	VUS	NA
KCNJ10	283	261	TRUE	E	D	C	C	0.5030902	0.26325522	1.82E-33	0.23334417	0.33380385	9.13E-183	VUS	NA
KCNJ5	289	288	TRUE	D	D	C	C	NA	NA	NA	NA	NA	NA	Conflicting	NA
KCNJ5	302	301	TRUE	I	D	NP	C	NA	NA	NA	NA	NA	NA	VUS	NA
KCNJ2	307	299	TRUE	E	D	C	C	-0.170811	0.10837133	4.05E-37	0.05228829	0.12994929	7.42E-20	NA	NA
KCNJ2	308	300	TRUE	G	D	NP	C	0.64851761	0.76670074	0	0.09745429	0.25304202	1.72E-62	Pathog.	NA
KCNJ11	353	334	TRUE	H	D	C	C	0.15155431	0.19452298	1.35E-20	1.4083538	0.47020097	0	Pathog.	NA
KCNJ11	52	40	TRUE	G	D	NP	C	-0.3029205	0.35006207	0	-0.7289752	0.23111833	9.33E-05	VUS	NA
KCNJ10	55	38	TRUE	N	D	P	C	0.0246856	0.13618872	2.30E-43	-0.2488724	0.14297527	7.23E-102	VUS	NA
KCNJ11	66	53	FALSE	Q	D	P	C	-0.5847714	0.2295375	5.69E-11	-0.7753623	0.66110871	3.18E-70	Pathog.	NA
KCNJ2	68	68	TRUE	Y	D	A	C	0.31130465	0.37757411	2.78E-17	-0.7304122	0.23885233	1.04E-15	VUS	NA
KCNJ1	111	107	TRUE	G	E	NP	C	0.09934243	0.57532912	0	-1.4392116	0.75088694	3.32E-39	VUS	NA
KCNJ10	125	100	FALSE	K	E	C	C	-0.2124998	0.01779499	1.33E-05	1.79067289	0.30862893	3.33E-16	Conflicting	NA
KCNJ5	152	151	TRUE	G	E	NP	C	0.12588447	0.0025269	9.38E-56	-0.3069856	0.18721497	5.63E-15	Pathog.	NA
KCNJ2	160	152	TRUE	D	E	C	C	0.27146693	0.25015281	0	-0.3046166	0.00621404	2.91E-110	NA	NA
KCNJ1	176	167	TRUE	G	E	NP	C	-0.6178329	0.17063837	4.78E-62	-1.4245282	0.99936347	1.03E-15	Pathog.	NA
KCNJ11	20	23	FALSE	K	E	C	C	-0.1770849	0.54537255	0	0.3215951	0.22468707	5.38E-08	Pathog.	NA
KCNJ11	20	23	FALSE	K	E	C	C	-0.1770849	0.54537255	0	0.3215951	0.22468707	5.38E-08	Benign	NA
KCNJ2	213	205	TRUE	D	E	C	C	0.58363955	0.47467294	2.78E-16	-0.4112131	0.13343512	1.29E-05	NA	NA
KCNJ1	237	228	TRUE	A	E	NP	C	-0.0914057	0.31690517	0	-2.3961779	0.5105472	8.38E-124	VUS	NA
KCNJ2	255	247	TRUE	Q	E	P	C	NA	NA	NA	NA	NA	NA	NA	NA
KCNJ2	265	257	TRUE	G	E	NP	C	-0.949481	0.25888299	6.96E-06	-0.7321051	0.20786189	1.98E-46	NA	NA
KCNJ10	267	245	TRUE	D	E	C	C	0.19485552	0.29707198	2.78E-17	-0.4329976	0.11377018	9.11E-26	Conflicting	NA
KCNJ5	283	282	TRUE	E	E	C	C	NA	NA	NA	NA	NA	NA	Benign	NA
KCNJ5	283	282	TRUE	E	E	C	C	NA	NA	NA	NA	NA	NA	Benign	NA
KCNJ2	293	285	TRUE	Q	E	P	C	0.96829685	0.28317433	2.65E-12	1.07211795	0.48347776	3.45E-14	NA	NA
KCNJ2	294	286	TRUE	D	E	C	C	-0.5281238	0.26313187	2.78E-17	1.29926957	0.11622671	1.43E-82	NA	NA
KCNJ2	318	310	TRUE	Q	E	P	C	-0.1160145	0.11901938	0.00021687	-0.915957	0.17722522	1.27E-33	NA	NA
KCNJ10	354	332	TRUE	K	E	C	C	-0.0442137	0.16057064	3.07E-23	0.37659786	0.06847808	3.68E-167	VUS	NA
KCNJ2	379	371	TRUE	A	E	NP	C	0.18187466	0.18164391	0	0.06652763	0.12625973	8.74E-38	VUS	NA
KCNJ10	384	351	FALSE	Y	E	A	C	0.5061259	0.22455366	0.00067783	2.66101965	0.72343025	3.33E-15	VUS	NA
KCNJ2	4	4	TRUE	V	E	NP	C	0.3849858	0.88678949	6.18E-14	-1.5654232	0.55587887	1.31E-92	NA	NA
KCNJ2	400	393	TRUE	E	E	C	C	NA	NA	NA	NA	NA	NA	NA	NA
KCNJ11	71	58	TRUE	D	E	C	C	0.32706634	0.40716485	5.55E-17	-0.6614608	0.22057642	5.55E-17	VUS	NA
KCNJ2	101	101	TRUE	C	F	P	A	-0.0350432	0.05564897	2.42E-30	0.59272576	0.18538282	8.94E-32	VUS	NA
KCNJ2	109	109	TRUE	L	F	NP	A	0.23346537	0.01697959	3.05E-19	-1.104082	0.58576989	3.84E-130	NA	NA
KCNJ5	134	133	TRUE	V	F	NP	A	-0.7614036	0.24222388	1.85E-07	-1.9866112	0.65990995	0	VUS	NA
KCNJ2	75	75	TRUE	T	A	P	NP	-0.1961294	0.09724696	5.42E-05	-1.3335851	0.59662842	0	VUS	lof_s
KCNJ2	76	76	TRUE	C	G	P	NP	-0.435815	0.57001367	2.22E-16	1.54288411	0.81153485	4.44E-16	Conflicting	lof_f
KCNJ2	80	80	TRUE	R	C	C	P	-0.3008017	0.15021564	1.63E-98	-1.5635502	0.10965389	8.54E-16	VUS	lof_s
KCNJ2	109	109	TRUE	L	P	NP	NP	-1.0035554	0.11132659	3.12E-21	-2.3151168	0.52993694	6.94E-05	VUS	lof_s
KCNJ10	168	146	TRUE	M	F	NP	A	1.0507945	0.49286944	3.25E-162	1.02895551	0.42039466	3.50E-42	VUS	NA
KCNJ11	184	164	TRUE	I	F	NP	A	-0.2410603	0.07136931	1.06E-10	-0.1878994	0.15018349	6.94E-18	VUS	NA
KCNJ11	186	166	TRUE	A	F	NP	A	NA	0.60987673	0	NA	NA	NA	Pathog.	NA
KCNJ5	186	185	TRUE	A	F	NP	A	NA	0.60987673	0	NA	NA	NA	VUS	NA
KCNJ11	201	181	TRUE	L	F	NP	A	0.31329514	0.01276313	8.68E-57	-0.8308866	0.262226	8.06E-38	VUS	NA
KCNJ1	218	209	TRUE	L	F	NP	A	-0.0178584	0.10993959	0	-0.385115	0.07518002	1.36E-29	Benign	NA
KCNJ1	229	220	TRUE	H	F	C	A	-1.5166506	0.11621838	7.39E-118	0.8379549	0.62099716	2.22E-16	Pathog.	NA
KCNJ10	230	208	TRUE	L	F	NP	A	-0.1860385	0.23146368	1.06E-08	0.47393701	0.5114521	0	VUS	NA
KCNJ2	235	227	TRUE	V	F	NP	A	0.07830082	0.07288967	3.42E-44	0.27300919	0.34058461	1.46E-49	VUS	NA
KCNJ10	240	218	TRUE	L	F	NP	A	0.80694304	0.18122474	0.00050852	0.05415657	0.45748988	2.96E-92	VUS	NA
KCNJ2	240	232	TRUE	L	F	NP	A	0.80694304	0.18122474	0.00050852	0.05415657	0.45748988	2.96E-92	NA	NA
KCNJ10	251	229	TRUE	I	F	NP	A	NA	0.55152638	6.19E-38	NA	1.26764773	3.68E-09	VUS	NA
KCNJ5	251	250	TRUE	I	F	NP	A	NA	0.55152638	6.19E-38	NA	1.26764773	3.68E-09	VUS	NA
KCNJ11	253	233	TRUE	L	F	NP	A	NA	NA	NA	NA	NA	NA	Pathog.	NA
KCNJ2	273	265	TRUE	S	F	P	A	NA	1.25610206	0	NA	0.36622218	9.76E-53	VUS	NA
KCNJ2	287	279	TRUE	L	F	NP	A	0.94198046	0.07892762	8.67E-18	0.67814882	0.43934309	1.97E-08	NA	NA
KCNJ11	288	268	TRUE	Y	F	A	A	NA	NA	NA	NA	0.8445417	0	VUS	NA
KCNJ2	109	109	TRUE	L	P	NP	NP	-1.0035554	0.11132659	3.12E-21	-2.3151168	0.52993694	6.94E-05	VUS	lof_f
KCNJ2	338	330	TRUE	L	F	NP	A	0.16795271	0.09169654	2.28E-32	0.86305369	0.30003576	2.05E-06	NA	NA
KCNJ11	349	330	TRUE	Y	F	A	A	0.31560634	0.30436377	8.83E-80	0.87527195	0.3624119	9.46E-06	VUS	NA
KCNJ2	350	342	TRUE	S	F	P	A	0.3860601	0.22849671	1.64E-30	0.15295919	0.36530923	3.62E-19	NA	NA
KCNJ2	363	355	TRUE	L	F	NP	A	0.27028489	0.31922297	0	-0.6537118	0.23057983	3.69E-101	NA	NA
KCNJ2	364	356	TRUE	C	F	P	A	0.2617204	0.16209431	5.78E-93	1.14118226	0.26738896	1.34E-07	VUS	NA
KCNJ2	369	361	TRUE	L	F	NP	A	0.18145658	0.30442415	2.78E-17	0.61944571	0.28799119	2.15E-42	NA	NA
KCNJ2	390	382	TRUE	L	F	NP	A	-0.0422507	0.15715907	0	0.96070044	0.13366149	1.29E-18	NA	NA
KCNJ2	43	43	TRUE	C	F	P	A	0.00755514	0.02950608	4.46E-08	0.06078058	0.0947131	1.02E-161	NA	NA
KCNJ2	54	54	TRUE	C	F	P	A	-0.5059565	0.15757693	0	-0.4105256	0.06833042	4.34E-60	Pathog.	NA
KCNJ10	67	50	TRUE	R	F	C	A	0.05985188	0.13810596	1.01E-05	-1.9962563	0.80086183	1.10E-98	VUS	NA
KCNJ2	72	72	TRUE	I	F	NP	A	0.81105005	0.56132502	1.24E-08	0.52447509	0.3735688	4.62E-50	NA	NA
KCNJ2	86	86	TRUE	V	F	NP	A	-0.0046024	0.1793771	2.78E-17	-0.4144247	0.19135974	2.17E-81	VUS	NA

KCNJ10	87	70	TRUE	I	F	NP	A	0.11143974	0.29588842	2.78E-17	-0.3538291	0.08752441	1.62E-06	VUS	NA
KCNJ10	98	81	TRUE	F	F	A	A	NA	NA	NA	NA	NA	NA	VUS	NA
KCNJ2	10	10	TRUE	S	G	P	NP	0.77299494	0.190269	5.66E-07	0.30444678	0.88596858	2.22E-16	NA	NA
KCNJ8	100	88	TRUE	G	G	NP	NP	NA	NA	NA	NA	NA	NA	VUS	NA
KCNJ2	114	114	TRUE	D	G	C	NP	0.28262879	0.22701664	1.64E-53	0.71887448	0.1763959	3.08E-24	VUS	NA
KCNJ2	110	110	TRUE	H	Y	C	A	-0.4598419	0.1320753	9.28E-82	-1.7302983	0.36071042	1.20E-29	VUS	lof_s
KCNJ2	110	110	TRUE	H	Y	C	A	-0.4598419	0.1320753	9.28E-82	-1.7302983	0.36071042	1.20E-29	VUS	lof_f
KCNJ10	134	112	TRUE	V	G	NP	NP	-0.5747606	0.24014275	2.87E-99	-5.6075363	0.56058323	0	VUS	NA
KCNJ2	140	132	TRUE	A	G	NP	NP	NA	0.09441655	8.09E-11	NA	1.21673264	4.44E-16	NA	NA
KCNJ2	16	16	TRUE	E	G	C	NP	-0.0108459	0.06370871	1.27E-22	0.49239894	0.11857034	4.51E-25	NA	NA
KCNJ5	160	159	TRUE	D	G	C	NP	NA	NA	NA	NA	NA	NA	VUS	NA
KCNJ2	17	17	TRUE	D	G	C	NP	0.74991648	0.73860041	0	-0.6808698	0.50724033	3.65E-91	NA	NA
KCNJ11	194	174	TRUE	P	G	NP	NP	-0.6226313	0.01538126	8.05E-12	-0.1578201	0.38493283	0	Pathog.	NA
KCNJ2	197	189	TRUE	R	G	C	NP	-1.2341669	0.10158047	3.45E-12	0.71510978	0.22311105	5.35E-08	Pathog.	NA
KCNJ10	199	177	TRUE	E	G	C	NP	-0.0270474	0.86812779	2.22E-16	0.62378117	0.32880307	5.36E-50	Conflicting	NA
KCNJ2	213	205	TRUE	D	G	C	NP	0.7663311	0.13205056	1.88E-183	2.74278616	0.03465425	6.44E-08	NA	NA
KCNJ2	221	213	TRUE	R	G	C	NP	-0.0363706	0.24025459	0	-0.9551471	0.22778754	3.29E-15	Pathog.	NA
KCNJ1	223	214	TRUE	G	G	NP	NP	NA	NA	NA	NA	NA	NA	VUS	NA
KCNJ2	130	122	TRUE	C	Y	P	A	-0.5721161	0.30153904	0	-1.393564	0.30187403	1.92E-34	VUS	lof_s
KCNJ11	241	221	TRUE	K	G	C	NP	0.09566515	0.49578056	4.71E-129	1.3500776	0.47073237	0	VUS	NA
KCNJ2	243	235	TRUE	R	G	C	NP	0.82456574	0.16820238	4.04E-161	1.64489721	0.24880657	7.62E-32	NA	NA
KCNJ13	247	211	TRUE	E	G	C	NP	0.58764494	0.20226234	5.07E-78	1.92551409	0.4502999	1.37E-40	VUS	NA
KCNJ2	284	276	TRUE	D	G	C	NP	0.2596528	0.12679188	9.41E-35	0.71691096	0.1435191	3.67E-06	NA	NA
KCNJ13	294	180	TRUE	D	G	C	NP	0.19245339	0.28343345	0	0.37131952	0.45255221	1.23E-66	VUS	NA
KCNJ2	294	286	TRUE	D	G	C	NP	0.19245339	0.28343345	0	0.37131952	0.45255221	1.23E-66	NA	NA
KCNJ11	296	274	TRUE	D	G	C	NP	NA	NA	NA	NA	0.74162699	4.71E-51	VUS	NA
KCNJ2	303	295	TRUE	V	G	NP	NP	-0.650274	0.91534517	0	-1.2619131	0.84769258	1.47E-58	NA	NA
KCNJ2	307	299	TRUE	E	G	C	NP	-0.1028808	0.13196578	1.39E-17	-0.2936393	0.04434812	6.62E-181	Pathog.	NA
KCNJ2	310	302	TRUE	V	G	NP	NP	-0.6830493	0.1243747	9.53E-07	0.50592117	0.27954123	1.97E-51	NA	NA
KCNJ2	35	35	TRUE	S	G	P	NP	0.53438332	0.2617195	1.85E-58	0.95399457	0.14198809	3.77E-37	NA	NA
KCNJ11	358	339	TRUE	V	G	NP	NP	0.22445441	0.4340141	5.55E-17	-1.6456688	0.24302291	3.11E-46	VUS	NA
KCNJ8	368	357	TRUE	D	G	C	NP	1.02560591	0.3685301	5.13E-15	-0.0119974	0.23990063	1.75E-55	VUS	NA
KCNJ2	370	362	TRUE	A	G	NP	NP	0.39346804	0.34941073	1.67E-16	-0.4343701	0.63363154	1.70E-84	NA	NA
KCNJ2	371	363	TRUE	E	G	C	NP	0.46420949	0.2739702	0.00077148	-0.9751027	0.57939801	4.60E-12	NA	NA
KCNJ10	377	344	FALSE	S	G	P	NP	0.58188581	0.30454128	0	0.79060359	0.14607145	2.11E-30	VUS	NA
KCNJ10	378	345	FALSE	N	G	P	NP	0.58194893	0.11936641	3.82E-17	0.67532652	0.34642269	1.01E-07	VUS	NA
KCNJ1	389	364	FALSE	A	G	NP	NP	0.25259947	0.31221117	2.78E-17	1.90975919	0.75167305	3.33E-16	VUS	NA
KCNJ5	390	397	FALSE	L	G	NP	NP	0.77289587	0.11792867	7.45E-113	1.85549128	0.2051971	1.09E-56	VUS	NA
KCNJ2	396	389	TRUE	E	G	C	NP	0.82607851	0.34814083	1.43E-05	0.56372186	0.47307492	3.42E-05	NA	NA
KCNJ2	398	391	TRUE	D	G	C	NP	0.53747197	0.23244207	7.05E-176	0.54640292	0.24061345	4.35E-23	NA	NA
KCNJ2	5	5	TRUE	R	G	C	NP	0.5170397	0.08424783	3.67E-58	0.59405579	0.35183575	0	NA	NA
KCNJ2	5	5	TRUE	R	G	C	NP	0.5170397	0.08424783	3.67E-58	0.59405579	0.35183575	0	NA	NA
KCNJ2	51	51	TRUE	D	G	C	NP	-0.8666094	0.06175992	1.38E-16	-0.2329427	0.10965853	2.15E-82	NA	NA
KCNJ11	72	59	TRUE	I	G	NP	NP	0.41214946	0.27028432	3.24E-123	2.08878031	0.55808854	1.89E-13	Pathog.	NA
KCNJ2	130	122	TRUE	C	Y	P	A	-0.5721161	0.30153904	0	-1.393564	0.30187403	1.92E-34	VUS	lof_f
KCNJ2	78	78	TRUE	D	G	C	NP	NA	NA	NA	NA	NA	NA	Pathog.	NA
KCNJ1	112	108	TRUE	D	H	C	C	-0.7080561	0.11107699	2.23E-12	-4.5378366	0.5210518	6.57E-10	Pathog.	NA
KCNJ11	13	16	FALSE	S	H	P	C	0.76778586	0.21538065	2.02E-30	-0.5076644	0.52025802	2.25E-50	VUS	NA
KCNJ10	156	134	TRUE	R	H	C	C	NA	NA	NA	NA	NA	NA	VUS	NA
KCNJ11	156	136	TRUE	R	H	C	C	NA	NA	NA	NA	NA	NA	VUS	NA
KCNJ2	17	17	TRUE	D	H	C	C	0.39675214	0.30607095	3.16E-30	-1.0885644	0.3648236	7.04E-52	NA	NA
KCNJ11	196	176	TRUE	K	H	C	C	0.843681	0.23062737	1.45E-05	-0.0723522	0.51476191	0.00193266	VUS	NA
KCNJ2	201	193	TRUE	L	H	NP	C	NA	0.50085312	3.39E-12	NA	1.27134374	0	VUS	NA
KCNJ10	202	180	TRUE	V	H	NP	C	NA	NA	NA	NA	NA	NA	VUS	NA
KCNJ11	212	192	TRUE	R	H	C	C	-0.2270678	0.12343422	0.00021324	-0.9452256	0.62980658	3.07E-61	VUS	NA
KCNJ18	212	205	TRUE	R	H	C	C	-0.2270678	0.12343422	0.00021324	-0.9452256	0.62980658	3.07E-61	Pathog.	NA
KCNJ11	215	195	TRUE	K	H	C	C	0.5909163	0.25974528	4.68E-05	1.57142622	0.50021517	1.11E-16	Conflicting	NA
KCNJ10	216	194	TRUE	L	H	NP	C	1.06820738	0.25055247	0	-0.3991009	0.74616053	4.78E-67	Pathog.	NA
KCNJ11	221	201	TRUE	R	H	C	C	-0.1854487	0.54367692	0	-5.3143855	0.46832533	1.77E-27	Pathog.	NA
KCNJ2	224	216	TRUE	N	H	P	C	-0.7289735	0.25954171	5.42E-48	0.35080021	0.35179429	6.16E-234	Pathog.	NA
KCNJ11	226	206	TRUE	R	H	C	C	-0.3669329	0.43722567	3.72E-37	0.72879583	0.30820324	9.49E-16	Pathog.	NA
KCNJ5	226	225	TRUE	R	H	C	C	-0.3669329	0.43722567	3.72E-37	0.72879583	0.30820324	9.49E-16	VUS	NA
KCNJ11	24	27	FALSE	M	H	NP	C	0.6417158	0.17559353	3.52E-48	0.35516273	0.49933253	2.58E-17	VUS	NA
KCNJ11	241	221	TRUE	K	H	C	C	0.25161509	0.18243214	0	0.03304399	0.15963273	1.43E-65	VUS	NA
KCNJ13	254	218	TRUE	D	H	C	C	-0.1854738	0.12367338	3.49E-34	0.93912852	0.31646327	5.87E-35	VUS	NA
KCNJ5	268	267	TRUE	R	H	C	C	-0.5491185	0.58938255	0	0.64783596	0.48164186	5.55E-17	VUS	NA
KCNJ2	268	260	TRUE	R	H	C	C	-0.5491185	0.58938255	0	0.64783596	0.48164186	5.55E-17	NA	NA
KCNJ1	28	31	FALSE	N	H	P	C	0.37334451	0.22218142	4.16E-17	-0.4315457	0.11399081	1.81E-09	Conflicting	NA
KCNJ8	284	274	TRUE	D	H	C	C	0.40140302	0.71910855	0	2.018957	0.96916758	0	VUS	NA
KCNJ10	293	271	TRUE	Q	H	P	C	0.22901046	0.26938464	0	-0.4064763	0.08926065	6.07E-10	Conflicting	NA
KCNJ13	297	261	TRUE	N	H	P	C	0.52927134	0.20755988	2.08E-17	-0.252291	0.37302964	6.27E-72	VUS	NA
KCNJ11	320	301	TRUE	R	H	C	C	-1.0766496	0.23778485	0	0.36217952	0.28633596	2.79E-05	Conflicting	NA
KCNJ2	131	123	TRUE	V	G	NP	NP	-0.4597477	0.13116723	2.78E-42	-5.1605436	0.60579694	0	VUS	lof_s
KCNJ11	333	314	TRUE	R	H	C	C	0.30749467	0.07619189	3.71E-09	1.0753189	0.25732275	6.77E-49	VUS	NA
KCNJ2	333	325	TRUE	R	H	C	C	0.30749467	0.07619189	3.71E-09	1.0753189	0.25732275	6.77E-49	VUS	NA
KCNJ10	345	323	TRUE	Y	H	A	C	0.28674433	0.52731133	0	1.44463796	0.55552124	1.67E-16	VUS	NA
KCNJ11	349	330	TRUE	Y	H	A	C	-0.1334504	0.18424502	3.14E-57	0.32407988	0.29705136	5.55E-17	Pathog.	NA
KCNJ11	367	347	TRUE	R	H	C	C	0.0641712	0.36867833	5.55E-17	1.04753465	0.37897776	2.28E-15	VUS	NA
KCNJ11	368	348	TRUE	D	H	C	C	-0.3050968	0.16232919	0	-0.3270084	0.32308132	3.47E-06	VUS	NA
KCNJ5	37	41	FALSE	V	H	NP	C	0.08672134	0.73495268	0	-0.0798507	0.23971998	3.51E-151	Benign	NA
KCNJ10	376	343	FALSE	L	H	NP	C	0.62616904	0.37224155	0	1.26756536	0.25116289	1.39E-17	VUS	NA
KCNJ10	381	348	FALSE	S	H	P	C	NA	NA	NA	NA	NA	NA	VUS	NA
KCNJ11	385	365	FALSE	E	H	C	C	0.03976513	0.06346498	1.40E-08	1.24231319	0.32294268	1.16E-49	VUS	NA
KCNJ2	396	389	TRUE	E	H	C	C	0.80754751	0.06211128	5.96E-09	-0.1035554	0.70553903	2.88E-51	NA	NA
KCNJ5	397	404	FALSE	E	H	C	C	-0.0758609	0.52977118	2.00E-09	0.25852343	0.48770142	3.32E-35	VUS	NA
KCNJ5	46	52	TRUE	R	H	C	C	NA	NA	NA	NA	0.69428248	0	VUS	NA
KCNJ2	46	46	TRUE	R	H	C	C	NA	NA	NA	NA	0.69428248	0	NA	NA
KCNJ10	53	36	TRUE	H	H	C	C	NA	NA	NA	NA	NA	NA	VUS	NA
KCNJ2	57	57	TRUE	Q	H	P	C	0.93812919	0.6547823	0	-0.1007234	0.19069919	8.73E-26	NA	NA
KCNJ11	67	54	TRUE	R	H	C	C	-1.23277	0.24018392	9.71E-17	0.03524082	0.55190386	1.55E-40	VUS	NA
KCNJ2	71	71	TRUE	D	H	C	C	NA	1.53545001	0	NA	0.58296031	4.74E-67	Conflicting	NA
KCNJ2	78	78	TRUE	D	H	C	C	-0.2558907	0.13141605	0	0.73936083	0.24170975	5.66E-09	VUS	NA
KCNJ2	8	8	FALSE	R	H	C	C	0.93492039	0.98411663	0	-0.5014422	0.23906903	2.28E-110	VUS	NA

KCNJ2	8	8	TRUE	R	H	C	C	0.93492039	0.98411663	0	-0.5014422	0.23906903	2.28E-110	NA	NA
KCNJ2	80	80	TRUE	R	H	C	C	NA	1.53891264	7.29E-137	NA	0.37309017	0	VUS	NA
KCNJ13	81	54	TRUE	W	H	A	C	-1.2831309	0.57341831	0	-4.0259242	0.90525839	0	VUS	NA
KCNJ5	82	87	TRUE	R	H	C	C	-0.6684356	0.12401969	7.36E-53	0.6719331	0.08234485	3.58E-14	VUS	NA
KCNJ11	101	88	TRUE	C	I	P	NP	NA	NA	NA	NA	NA	NA	VUS	NA
KCNJ2	12	12	TRUE	V	I	NP	NP	0.7117943	0.3988081	5.31E-06	-3.7121245	0.14528291	2.86E-32	NA	NA
KCNJ13	136	105	TRUE	S	I	P	NP	-0.3730782	0.19428182	2.78E-17	-5.7806167	0.15767448	1.32E-48	Pathog.	NA
KCNJ5	14	18	FALSE	S	I	P	NP	-0.254974	0.13239002	2.19E-25	1.47553449	0.17531401	0.0003926	VUS	NA
KCNJ2	142	134	TRUE	L	I	NP	NP	-0.0846043	0.09048194	6.43E-23	-1.1131791	0.12249192	2.79E-05	NA	NA
KCNJ2	131	123	TRUE	V	G	NP	NP	-0.4597477	0.13116723	2.78E-42	-5.1605436	0.60579694	0	VUS	lof_f
KCNJ2	133	125	TRUE	E	K	C	C	-0.2446165	0.01089727	1.12E-12	-1.9410366	0.2682281	3.36E-192	VUS	lof_s
KCNJ2	166	158	TRUE	V	I	NP	NP	-0.8294688	0.44724057	0	0.63658997	0.32193228	4.64E-43	NA	NA
KCNJ5	178	178	TRUE	I	I	NP	NP	NA	NA	NA	NA	NA	NA	VUS	NA
KCNJ13	184	153	TRUE	I	I	NP	NP	NA	NA	NA	NA	NA	NA	Pathog.	NA
KCNJ10	186	164	TRUE	A	I	NP	NP	0.97775182	0.5543067	0	-1.0874341	0.41908639	0	Pathog.	NA
KCNJ2	187	179	TRUE	V	I	NP	NP	0.02914302	0.2585797	1.82E-88	-0.0272522	0.3253605	1.27E-76	NA	NA
KCNJ2	197	189	TRUE	R	I	C	NP	-0.2901507	0.07447715	0	-0.1553375	0.02288361	9.06E-49	Pathog.	NA
KCNJ2	138	130	TRUE	T	M	P	NP	-0.051422	0.35199512	0	-1.3558388	0.62477312	5.74E-55	VUS	lof_s
KCNJ2	140	132	TRUE	A	T	NP	P	-0.6449412	0.1622505	0	-4.8234192	0.63794591	4.00E-08	VUS	lof_s
KCNJ2	140	132	TRUE	A	T	NP	P	-0.6449412	0.1622505	0	-4.8234192	0.63794591	4.00E-08	VUS	lof_f
KCNJ13	206	175	TRUE	N	I	P	NP	-0.1642912	0.15696492	1.79E-57	-0.1573526	0.64657407	9.82E-31	Benign	NA
KCNJ5	211	210	TRUE	M	I	NP	NP	-0.0257181	0.1592545	0	-0.0895183	0.30025758	8.11E-12	Benign	NA
KCNJ8	211	201	TRUE	M	I	NP	NP	-0.0257181	0.1592545	0	-0.0895183	0.30025758	8.11E-12	VUS	NA
KCNJ2	144	136	TRUE	S	F	P	A	-0.4344781	0.24175847	8.03E-17	-2.9848271	0.52951614	4.59E-34	VUS	lof_s
KCNJ2	225	217	TRUE	L	I	NP	NP	-0.1939068	0.34425751	1.30E-68	1.039706	0.39564811	1.51E-61	NA	NA
KCNJ2	239	231	TRUE	L	I	NP	NP	0.16976432	0.41265134	3.20E-40	0.7637182	0.2905328	3.26E-62	NA	NA
KCNJ8	244	234	TRUE	I	I	NP	NP	NA	NA	NA	NA	NA	NA	VUS	NA
KCNJ2	245	237	TRUE	T	I	P	NP	-0.6024053	0.37798213	0	-1.8379337	0.3879486	4.71E-97	NA	NA
KCNJ2	26	26	TRUE	V	I	NP	NP	0.3187193	0.11046323	2.09E-109	-0.1036036	0.22981555	1.19E-79	NA	NA
KCNJ10	264	242	TRUE	S	I	P	NP	-0.0091588	0.1899588	0	-0.1487294	0.07261986	9.17E-39	VUS	NA
KCNJ11	285	265	TRUE	S	I	P	NP	NA	NA	NA	NA	NA	NA	VUS	NA
KCNJ11	304	285	TRUE	V	I	NP	NP	-0.2854464	0.06862132	3.11E-34	-0.0249485	0.04319423	8.81E-18	VUS	NA
KCNJ1	309	300	TRUE	M	I	NP	NP	-0.6017221	0.06569121	4.86E-47	-0.0197267	0.14551576	5.40E-105	VUS	NA
KCNJ2	144	136	TRUE	S	F	P	A	-0.4344781	0.24175847	8.03E-17	-2.9848271	0.52951614	4.59E-34	VUS	lof_f
KCNJ10	316	293	TRUE	T	I	P	NP	-0.298403	0.10720142	8.08E-09	0.12497717	0.42061166	4.88E-56	VUS	NA
KCNJ2	317	309	TRUE	T	I	P	NP	-0.1319557	0.02930943	4.85E-22	0.24613295	0.11957045	3.47E-18	VUS	NA
KCNJ11	321	302	TRUE	S	I	P	NP	-0.0536048	0.05082171	2.80E-19	0.29515752	0.20582738	7.44E-35	VUS	NA
KCNJ11	352	333	TRUE	F	I	A	NP	NA	2.67484675	0	NA	NA	NA	Pathog.	NA
KCNJ11	356	337	TRUE	Y	I	A	NP	0.46680221	0.05551194	1.02E-33	2.60692479	0.60728187	2.30E-12	Benign	NA
KCNJ8	356	346	TRUE	Y	I	A	NP	0.46680221	0.05551194	1.02E-33	2.60692479	0.60728187	2.30E-12	Conflicting	NA
KCNJ2	361	353	TRUE	T	I	P	NP	0.67893491	0.49478693	0	0.72740608	0.3764986	2.70E-31	NA	NA
KCNJ2	373	365	TRUE	K	I	C	NP	0.52793727	0.18017155	0	2.43313055	0.89488864	0	NA	NA
KCNJ2	39	39	TRUE	T	I	P	NP	NA	1.073612	0	NA	0.4255607	4.04E-76	NA	NA
KCNJ8	394	392	FALSE	E	I	C	NP	0.33917826	0.21762284	6.07E-27	-0.1713313	0.7302885	3.97E-95	VUS	NA
KCNJ13	395	337	FALSE	E	I	C	NP	0.04762736	0.13720426	2.50E-36	0.68449094	0.5317503	2.98E-62	VUS	NA
KCNJ1	397	372	FALSE	E	I	C	NP	1.2791393	0.60486894	5.02E-10	-0.8750433	0.55323828	2.22E-16	VUS	NA
KCNJ2	397	390	TRUE	E	I	C	NP	1.2791393	0.60486894	5.02E-10	-0.8750433	0.55323828	2.22E-16	NA	NA
KCNJ10	5	4	FALSE	R	I	C	NP	-0.0757442	0.07200367	2.02E-39	-0.1175431	0.38822494	1.14E-65	VUS	NA
KCNJ2	55	55	TRUE	N	I	P	NP	0.37629117	0.72835388	3.69E-11	0.47864944	0.63767393	4.22E-47	NA	NA
KCNJ2	56	56	TRUE	V	I	NP	NP	0.36443462	0.39033215	5.55E-17	0.88034322	0.2756218	1.10E-12	NA	NA
KCNJ2	58	58	TRUE	F	I	A	NP	0.2302305	0.0390329	2.12E-19	0.77077259	0.26480583	4.67E-47	NA	NA
KCNJ2	6	6	TRUE	T	I	P	NP	0.36355579	0.06862596	1.73E-18	-0.6633272	0.19683983	1.39E-17	NA	NA
KCNJ16	75	64	TRUE	T	I	P	NP	-0.1670485	0.019292	4.81E-72	-0.8262032	0.07498411	0	Pathog.	NA
KCNJ5	86	92	TRUE	V	I	NP	NP	-1.1603225	0.51653103	5.58E-71	0.95843338	0.29015653	1.55E-78	VUS	NA
KCNJ10	91	74	TRUE	A	I	NP	NP	-0.4432175	0.14344457	8.50E-05	-0.0371065	0.66978279	4.93E-94	Conflicting	NA
KCNJ2	93	93	TRUE	V	I	NP	NP	0.69361956	0.66443663	0	-0.3399999	0.16199685	1.62E-23	Conflicting	NA
KCNJ5	93	99	TRUE	V	I	NP	NP	0.69361956	0.66443663	0	-0.3399999	0.16199685	1.62E-23	VUS	NA
KCNJ2	98	98	TRUE	F	I	A	NP	0.21537059	0.46516103	5.55E-17	2.79449487	0.55745532	1.23E-14	NA	NA
KCNJ13	107	80	FALSE	A	K	NP	C	-0.8905819	0.11985504	3.01E-30	-6.0351013	0.26826644	1.65E-10	Conflicting	NA
KCNJ10	115	98	TRUE	T	K	P	C	0.4120712	0.23364239	1.76E-06	-0.6512259	0.33095608	7.92E-23	VUS	NA
KCNJ1	133	124	TRUE	E	K	C	C	-0.2446165	0.01089727	1.12E-12	-1.9410366	0.2682281	3.36E-192	Pathog.	NA
KCNJ2	145	137	TRUE	I	N	NP	P	-0.1261051	0.01132965	3.18E-56	-6.4093326	0.92235103	5.95E-07	VUS	lof_s
KCNJ5	148	147	TRUE	Q	K	P	C	-0.7346284	0.45795935	5.55E-17	-4.2483697	0.04326698	0	VUS	NA
KCNJ2	197	189	TRUE	R	K	C	C	-0.5539186	0.17248867	0	-1.5149408	0.33481172	3.65E-94	Pathog.	NA
KCNJ13	216	186	TRUE	L	K	NP	C	-0.1745829	0.31864486	1.08E-96	-6.31805	0.382217	1.40E-134	VUS	NA
KCNJ11	247	227	TRUE	E	K	C	C	0.19154869	0.16342938	2.66E-06	0.96197568	0.32432866	3.47E-48	Pathog.	NA
KCNJ5	247	246	TRUE	E	K	C	C	0.19154869	0.16342938	2.66E-06	0.96197568	0.32432866	3.47E-48	Pathog.	NA
KCNJ11	249	229	TRUE	E	K	C	C	0.52705767	0.16729435	7.84E-51	2.61196621	0.44306562	0.00012066	Pathog.	NA
KCNJ2	277	269	TRUE	I	K	NP	C	NA	0.65840974	0	NA	NA	NA	VUS	NA
KCNJ11	301	282	TRUE	E	K	C	C	-0.1982134	0.06562131	1.15E-59	-1.606541	0.32822265	3.92E-20	Pathog.	NA
KCNJ11	311	292	TRUE	E	K	C	C	-0.2807494	0.08610639	1.73E-18	-0.3675051	0.14063385	1.39E-17	VUS	NA
KCNJ2	311	303	TRUE	E	K	C	C	-0.2807494	0.08610639	1.73E-18	-0.3675051	0.14063385	1.39E-17	VUS	NA
KCNJ2	326	318	TRUE	N	K	P	C	0.16293125	0.16629452	1.39E-17	-0.4193207	0.27249133	5.55E-17	NA	NA
KCNJ2	335	327	TRUE	E	K	C	C	-0.1681987	0.04950005	1.52E-41	-0.7272217	0.13007746	0.00019507	NA	NA
KCNJ11	341	322	TRUE	E	K	C	C	0.35226826	0.20075323	1.57E-19	0.65722688	0.20568913	2.08E-17	Pathog.	NA
KCNJ11	354	335	TRUE	K	K	C	C	NA	NA	NA	NA	NA	NA	VUS	NA
KCNJ2	147	139	TRUE	T	I	P	NP	-0.5014287	0.21571924	0	-1.8465052	0.22060515	2.23E-91	VUS	lof_s
KCNJ2	378	370	TRUE	N	K	P	C	0.09282313	0.29177387	0	0.33130602	0.30925026	5.41E-105	NA	NA
KCNJ1	387	362	FALSE	E	K	C	C	0.37820482	0.49986402	0	-1.6781921	0.53465754	5.48E-10	VUS	NA
KCNJ2	394	387	TRUE	E	K	C	C	0.17860232	0.00066668	3.27E-24	0.03754586	0.21105298	6.88E-34	NA	NA
KCNJ10	59	42	TRUE	I	K	NP	C	0.55824424	0.19475043	1.71E-23	2.90838981	0.34496538	6.22E-09	VUS	NA
KCNJ11	7	10	FALSE	N	K	P	C	0.41661551	0.26958202	2.78E-17	-0.3937059	0.21873573	1.19E-15	Benign	NA
KCNJ5	101	106	TRUE	C	L	P	NP	NA	0.08977184	4.41E-08	NA	1.34912955	0	VUS	NA
KCNJ10	110	93	TRUE	H	L	C	NP	0.12717242	0.40089533	5.02E-08	-4.6205839	0.84643568	0	VUS	NA
KCNJ1	114	110	FALSE	D	L	C	NP	0.45294575	0.2596257	2.78E-17	1.65104365	0.31420569	2.26E-07	Pathog.	NA
KCNJ10	126	101	FALSE	V	L	NP	NP	0.28731006	0.44281692	1.75E-73	0.70086773	0.14174968	1.86E-60	VUS	NA
KCNJ10	127	102	FALSE	S	L	P	NP	-0.0603952	0.57297232	0	1.26580686	0.20185445	8.36E-77	VUS	NA
KCNJ10	134	112	TRUE	V	L	NP	NP	-0.2014499	0.16664432	1.21E-15	-0.6737369	0.0680953	1.64E-13	VUS	NA
KCNJ2	167	159	TRUE	F	L	A	NP	-0.2818367	0.29014686	2.08E-72	-2.9112195	0.84031086	0	NA	NA
KCNJ2	168	160	TRUE	M	L	NP	NP	0.09737738	0.02818671	1.07E-37	-0.3655113	0.55822887	2.05E-105	NA	NA
KCNJ2	175	167	TRUE	V	L	NP	NP	NA	1.03420361	0	NA	0.18788451	3.33E-45	VUS	NA
KCNJ11	178	158	TRUE	I	L	NP	NP	0.72829378	0.33524374	5.55E-17	1.40682567	0.13324786	1.47E-85	VUS	NA
KCNJ2	183	175	TRUE	I	L	NP	NP	0.72875385	0.09194162	3.51E-24	0.58623388	0.11594865	4.45E-76	VUS	NA

KCNJ11	187	167	TRUE	V	L	NP	NP	-0.1212337	0.12348462	5.58E-75	-0.7126831	0.31336366	1.04E-19	Pathog.	NA
KCNJ2	194	186	TRUE	P	L	NP	NP	-0.2216901	0.2251755	6.49E-10	-0.9266407	0.19419232	6.94E-18	Pathog.	NA
KCNJ10	203	181	TRUE	F	L	A	NP	0.13585524	0.13228684	2.92E-42	-0.2834684	0.20828731	2.53E-80	VUS	NA
KCNJ11	221	201	TRUE	R	L	C	NP	-0.2918803	0.20590776	1.39E-17	-3.3015328	0.40965327	1.22E-71	Pathog.	NA
KCNJ5	221	220	TRUE	R	L	C	NP	-0.2918803	0.20590776	1.39E-17	-3.3015328	0.40965327	1.22E-71	VUS	NA
KCNJ11	226	206	TRUE	R	L	C	NP	0.07231522	0.30444707	5.55E-63	-0.1558183	0.25831463	5.80E-22	VUS	NA
KCNJ2	226	218	TRUE	R	L	C	NP	0.07231522	0.30444707	5.55E-63	-0.1558183	0.25831463	5.80E-22	VUS	NA
KCNJ8	270	260	TRUE	F	L	A	NP	NA	1.00696405	0	NA	0.51505759	1.10E-24	VUS	NA
KCNJ13	271	237	TRUE	L	L	NP	NP	NA	NA	NA	NA	NA	NA	VUS	NA
KCNJ11	274	254	TRUE	P	L	NP	NP	0.19218465	0.42594084	1.70E-26	0.29852504	0.23342981	3.56E-167	Pathog.	NA
KCNJ16	274	250	TRUE	P	L	NP	NP	0.19218465	0.42594084	1.70E-26	0.29852504	0.23342981	3.56E-167	Pathog.	NA
KCNJ11	286	266	TRUE	P	L	NP	NP	-1.1442138	0.17549827	3.44E-43	-8.4305049	0.44244691	0	VUS	NA
KCNJ2	295	287	TRUE	I	L	NP	NP	0.2173888	0.23578226	4.98E-12	0.07415417	0.30233851	0	VUS	NA
KCNJ2	305	297	TRUE	I	L	NP	NP	0.06446224	0.15556473	2.25E-10	-0.1373077	0.07646681	4.61E-119	NA	NA
KCNJ2	147	139	TRUE	T	I	P	NP	-0.5014287	0.21571924	0	-1.8465052	0.22060515	2.23E-91	VUS	lof_f
KCNJ11	315	296	TRUE	M	L	NP	NP	-0.1176397	0.46667952	6.21E-108	1.00044586	0.31448903	4.35E-31	Pathog.	NA
KCNJ10	335	312	TRUE	E	L	C	NP	-0.2278635	0.21909012	1.39E-17	-1.1397052	0.35795073	5.86E-23	VUS	NA
KCNJ1	336	327	TRUE	P	L	NP	NP	0.01804828	0.42396307	6.15E-07	-1.1643381	0.63270297	0	VUS	NA
KCNJ2	337	329	TRUE	V	L	NP	NP	0.26361588	0.05542409	2.12E-64	0.5557232	0.28070346	1.34E-113	NA	NA
KCNJ10	358	336	TRUE	V	L	NP	NP	0.78514618	0.05198701	1.12E-18	-1.5853827	0.1507058	3.63E-41	VUS	NA
KCNJ1	384	359	FALSE	Y	L	A	NP	0.5534912	0.2315854	1.85E-42	1.84670696	0.39993082	0	VUS	NA
KCNJ11	47	35	TRUE	F	L	A	NP	0.77027742	0.33091417	0	0.19706984	0.09169366	2.01E-22	Pathog.	NA
KCNJ13	5	8	FALSE	R	L	C	NP	0.12022329	0.21823008	0	-1.7648754	0.62341941	2.57E-12	VUS	NA
KCNJ2	8	8	TRUE	R	L	C	NP	-0.1418519	0.82638057	0	-4.2864672	0.29328574	0	NA	NA
KCNJ10	92	75	TRUE	F	L	A	NP	NA	0.87679461	0	NA	NA	NA	Pathog.	NA
KCNJ10	101	84	TRUE	C	M	P	NP	NA	NA	NA	NA	NA	NA	VUS	NA
KCNJ2	102	102	TRUE	V	M	NP	NP	0.61679863	0.32513302	0	0.57001567	0.12508356	1.96E-07	NA	NA
KCNJ2	105	105	TRUE	L	M	NP	NP	0.33705443	0.36011272	5.55E-17	-0.0267749	0.16773161	1.60E-15	NA	NA
KCNJ2	154	146	TRUE	G	D	NP	C	0.09586556	0.41102704	8.94E-39	-2.4249064	0.68681546	5.08E-18	VUS	lof_s
KCNJ18	147	140	TRUE	T	M	P	NP	-0.6138701	0.02204406	3.93E-64	-0.4225078	0.51024038	1.30E-67	Pathog.	NA
KCNJ2	159	151	TRUE	T	M	P	NP	NA	NA	NA	NA	0.35911106	0	NA	NA
KCNJ2	169	161	TRUE	V	M	NP	NP	NA	NA	NA	NA	NA	NA	VUS	NA
KCNJ11	171	151	TRUE	F	M	A	NP	-0.0299242	0.00275384	7.75E-11	0.01952383	0.63142016	2.27E-34	Conflicting	NA
KCNJ10	173	151	TRUE	S	M	P	NP	-0.6450414	0.76004568	0	1.96674399	0.09281178	4.32E-49	VUS	NA
KCNJ11	175	155	TRUE	V	M	NP	NP	0.21973624	0.4902417	0	0.80352984	0.15170364	3.23E-55	VUS	NA
KCNJ18	175	168	TRUE	V	M	NP	NP	0.21973624	0.4902417	0	0.80352984	0.15170364	3.23E-55	Pathog.	NA
KCNJ5	175	174	TRUE	V	M	NP	NP	0.21973624	0.4902417	0	0.80352984	0.15170364	3.23E-55	VUS	NA
KCNJ2	175	167	TRUE	V	M	NP	NP	0.21973624	0.4902417	0	0.80352984	0.15170364	3.23E-55	NA	NA
KCNJ2	178	170	TRUE	I	M	NP	NP	0.04029794	0.07070968	6.63E-135	0.75094064	0.15503685	8.43E-25	VUS	NA
KCNJ1	200	193	TRUE	T	M	P	NP	NA	NA	NA	NA	0.9521989	2.22E-16	Benign	NA
KCNJ13	206	175	TRUE	N	M	P	NP	0.13360505	0.17032877	0	0.0252715	0.25299884	1.02E-106	VUS	NA
KCNJ2	216	208	TRUE	L	M	NP	NP	0.33616329	0.33060923	0	-0.4063305	0.05550145	1.93E-08	NA	NA
KCNJ5	230	229	TRUE	L	M	NP	NP	0.53756118	0.74709353	0	-0.3778821	0.65372829	3.88E-34	VUS	NA
KCNJ2	256	248	TRUE	I	M	NP	NP	-0.0739914	0.04619575	4.34E-19	-0.4136566	0.01150199	6.84E-33	NA	NA
KCNJ2	266	258	TRUE	I	M	NP	NP	0.60369277	0.37556234	0	-0.0672841	0.33435095	0	NA	NA
KCNJ5	272	271	TRUE	V	M	NP	NP	-0.593374	0.10065098	2.30E-23	-0.0151502	0.38966588	1.78E-34	VUS	NA
KCNJ2	275	267	TRUE	I	M	NP	NP	0.37448283	0.4583366	2.38E-39	0.48236989	0.22163421	9.26E-08	NA	NA
KCNJ2	281	273	TRUE	I	M	NP	NP	0.43824131	0.30933843	8.33E-17	-0.7106228	0.25730068	1.96E-56	NA	NA
KCNJ2	303	295	TRUE	V	M	NP	NP	-0.1401705	0.14327139	0	0.52695609	0.30770884	2.43E-170	VUS	NA
KCNJ11	309	290	TRUE	M	M	NP	NP	NA	NA	NA	NA	NA	NA	Pathog.	NA
KCNJ2	310	302	TRUE	V	M	NP	NP	-0.4698928	0.15609388	0	0.44648589	0.23573544	2.11E-07	Pathog.	NA
KCNJ11	313	294	TRUE	T	M	P	NP	-0.7827048	0.33111049	1.11E-16	0.46440249	0.31057045	1.71E-10	Pathog.	NA
KCNJ2	316	308	TRUE	T	M	P	NP	-0.4959804	0.15442148	0.00037614	-0.0413611	0.47992634	1.34E-66	NA	NA
KCNJ10	358	336	TRUE	V	M	NP	NP	-0.1862123	0.40628418	0	0.25645768	0.36604162	5.12E-46	VUS	NA
KCNJ5	36	40	FALSE	K	M	C	NP	0.43689051	0.21681917	2.78E-17	-0.3088274	0.38369266	0	VUS	NA
KCNJ18	361	354	TRUE	T	M	P	NP	-0.3426895	0.29129296	8.33E-17	-0.1002096	0.23127021	1.13E-56	Pathog.	NA
KCNJ11	365	345	TRUE	S	M	P	NP	-0.1443702	0.31095924	2.78E-17	-5.6360751	0.97858424	0	Conflicting	NA
KCNJ2	4	4	TRUE	V	M	NP	NP	-0.2234923	0.21212763	0	-1.0246699	0.2595678	1.68E-53	NA	NA
KCNJ8	400	398	FALSE	E	M	C	NP	0.10812566	0.09988851	1.56E-22	0.56995537	0.31181778	8.69E-74	Benign	NA
KCNJ5	56	62	TRUE	V	M	NP	NP	0.08652403	0.26209236	6.33E-40	0.1857254	0.13788571	6.76E-08	VUS	NA
KCNJ13	6	9	FALSE	T	M	P	NP	-0.3572783	0.35316362	1.11E-16	-1.2458506	0.0719615	4.81E-08	VUS	NA
KCNJ11	72	59	TRUE	I	M	NP	NP	0.32387726	0.40367455	1.11E-16	-0.5224627	0.25140753	2.78E-17	Pathog.	NA
KCNJ2	72	72	TRUE	I	M	NP	NP	0.32387726	0.40367455	1.11E-16	-0.5224627	0.25140753	2.78E-17	NA	NA
KCNJ1	75	71	TRUE	T	M	P	NP	-0.3070465	0.19867198	0.00118776	0.45179334	0.04869934	7.12E-30	VUS	NA
KCNJ11	75	62	TRUE	T	M	P	NP	-0.3070465	0.19867198	0.00118776	0.45179334	0.04869934	7.12E-30	Pathog.	NA
KCNJ2	75	75	TRUE	T	M	P	NP	-0.3070465	0.19867198	0.00118776	0.45179334	0.04869934	7.12E-30	Pathog.	NA
KCNJ8	77	65	TRUE	V	M	NP	NP	-0.1207511	0.12158047	0	0.18082482	0.25324142	1.27E-78	VUS	NA
KCNJ2	10	10	TRUE	S	N	P	P	0.69185744	0.41101708	1.31E-27	-0.4420171	0.36500358	1.15E-104	NA	NA
KCNJ5	125	123	FALSE	K	N	C	P	0.1224369	0.32383391	0	-0.0719367	0.10011987	1.40E-117	VUS	NA
KCNJ10	13	12	FALSE	S	N	P	P	-0.1714686	0.34768114	0	-0.260409	0.18757945	5.73E-09	VUS	NA
KCNJ2	162	154	TRUE	C	F	P	A	-0.6840665	0.12534076	5.68E-14	-1.7984946	0.50400288	1.78E-126	VUS	lof_s
KCNJ2	17	17	FALSE	D	N	C	P	-0.286389	0.59687866	1.11E-16	0.00344239	0.11214169	5.58E-82	VUS	NA
KCNJ2	17	17	TRUE	D	N	C	P	-0.286389	0.59687866	1.11E-16	0.00344239	0.11214169	5.58E-82	NA	NA
KCNJ2	180	172	TRUE	D	N	C	P	NA	1.26862009	0	NA	NA	NA	Pathog.	NA
KCNJ11	190	170	TRUE	K	N	C	P	-0.001461	0.35988682	7.51E-08	-0.3515505	0.14545642	0	Pathog.	NA
KCNJ11	200	180	TRUE	T	N	P	P	NA	1.06108388	4.44E-16	NA	0.59188493	1.38E-07	VUS	NA
KCNJ10	201	179	TRUE	L	N	NP	P	NA	NA	NA	NA	NA	NA	VUS	NA
KCNJ5	224	223	TRUE	N	N	P	P	NA	NA	NA	NA	NA	NA	VUS	NA
KCNJ2	228	220	TRUE	S	N	P	P	-0.2936499	0.39088173	1.39E-16	0.11960759	0.49194489	3.28E-187	VUS	NA
KCNJ2	257	249	TRUE	D	N	C	P	-0.1457018	0.0667131	0	-0.568321	0.1208026	1.14E-109	NA	NA
KCNJ2	263	255	TRUE	D	N	C	P	0.36596737	0.14169218	2.08E-47	1.08750075	0.41514845	4.57E-07	NA	NA
KCNJ2	267	259	TRUE	D	N	C	P	-0.0145892	0.18242597	0	-0.3796699	0.31247044	2.92E-75	NA	NA
KCNJ2	291	283	TRUE	S	N	P	P	0.61733192	0.15591346	2.35E-58	0.82277736	0.23115071	4.08E-42	NA	NA
KCNJ2	299	291	TRUE	D	N	C	P	0.24979768	0.05492905	1.05E-48	-0.513045	0.20263587	9.05E-11	NA	NA
KCNJ10	305	282	TRUE	I	N	NP	P	-0.5268437	0.08145155	5.73E-15	0.20613874	0.44879041	3.46E-174	VUS	NA
KCNJ2	321	313	TRUE	S	N	P	P	0.57927089	0.07381335	9.53E-10	1.18861925	0.2349342	4.89E-33	NA	NA
KCNJ2	162	154	TRUE	C	F	P	A	-0.6840665	0.12534076	5.68E-14	-1.7984946	0.50400288	1.78E-126	VUS	lof_f
KCNJ2	34	34	FALSE	K	N	C	P	0.20609051	0.01051402	2.33E-09	-0.3091277	0.15073744	3.85E-13	VUS	NA
KCNJ2	34	34	TRUE	K	N	C	P	0.20609051	0.01051402	2.33E-09	-0.3091277	0.15073744	3.85E-13	NA	NA
KCNJ2	34	34	TRUE	K	N	C	P	0.20609051	0.01051402	2.33E-09	-0.3091277	0.15073744	3.85E-13	NA	NA
KCNJ2	372	364	TRUE	K	N	C	P	0.41804984	0.25635929	0	1.76796144	0.10374317	6.39E-42	NA	NA
KCNJ10	384	351	FALSE	Y	N	A	P	0.9034885	0.14483242	6.78E-05	2.43116722	0.11014233	9.47E-05	Conflicting	NA
KCNJ2	396	389	TRUE	E	N	C	P	0.24135362	0.16464453	6.94E-18	0.63634055	0.21579512	4.67E-24	NA	NA

KCNJ2	397	389	FALSE	E	N	C	P	0.54611832	0.48411924	2.22E-16	0.42611044	0.42973171	1.91E-159	VUS	NA
KCNJ13	50	23	TRUE	K	N	C	P	0.31662596	0.29911983	4.00E-07	-0.4685752	0.22763825	1.39E-17	VUS	NA
KCNJ10	62	46	TRUE	G	N	NP	P	NA	1.00169704	0	NA	0.50680503	3.42E-77	Conflicting	NA
KCNJ2	71	71	TRUE	D	N	C	P	-0.1733876	0.30307368	8.33E-17	0.71382525	0.06833163	4.15E-49	Pathog.	NA
KCNJ11	95	82	TRUE	S	N	P	P	0.074296	0.1868002	6.63E-19	-1.7606976	0.7213552	1.45E-87	VUS	NA
KCNJ2	162	154	TRUE	C	Y	P	A	-0.2389272	0.02706514	2.90E-57	-1.0908619	0.237178	5.46E-132	Conflicting	lof_s
KCNJ2	197	189	TRUE	R	T	C	P	-1.1450997	0.12714229	8.61E-12	0.57566815	0.2337906	4.12E-18	VUS	lof_f
KCNJ10	124	99	FALSE	S	P	P	NP	0.51533605	0.17029126	0	-1.5462745	0.33577977	4.60E-182	VUS	NA
KCNJ11	136	116	TRUE	S	P	P	NP	-0.4499217	0.04467467	1.91E-78	-6.0675126	0.55351694	3.70E-169	VUS	NA
KCNJ11	142	122	TRUE	L	P	NP	NP	-0.148915	0.17299595	8.20E-12	-5.9790891	0.11095878	1.63E-64	Pathog.	NA
KCNJ13	145	114	TRUE	I	P	NP	NP	-0.7061676	0.15045199	2.05E-18	-5.9593555	0.66293636	0	VUS	NA
KCNJ11	167	147	TRUE	F	P	A	NP	NA	0.5823058	0	NA	NA	NA	Pathog.	NA
KCNJ13	175	144	TRUE	V	P	NP	NP	NA	NA	NA	NA	NA	NA	VUS	NA
KCNJ2	201	193	TRUE	L	P	NP	NP	NA	NA	NA	NA	NA	NA	Pathog.	NA
KCNJ18	207	200	TRUE	A	P	NP	NP	0.38926743	0.34111238	0	1.1257504	0.36731717	8.44E-16	Pathog.	NA
KCNJ1	221	212	TRUE	R	P	C	NP	-0.3877531	0.24859183	1.53E-05	-5.0649577	0.39393003	1.28E-06	VUS	NA
KCNJ2	198	190	TRUE	N	I	P	NP	-0.550841	0.60824066	0	0.48697007	0.33256938	2.55E-48	VUS	lof_f
KCNJ2	226	218	TRUE	R	P	C	NP	-0.2179809	0.95805365	0	-1.1941792	0.35842451	0	Pathog.	NA
KCNJ8	25	28	FALSE	A	P	NP	NP	0.39640355	0.02335592	1.15E-83	0.38269724	0.33388447	0	VUS	NA
KCNJ2	25	25	TRUE	A	P	NP	NP	0.39640355	0.02335592	1.15E-83	0.38269724	0.33388447	0	NA	NA
KCNJ2	268	260	TRUE	R	P	C	NP	-0.4581835	0.67753681	6.66E-16	0.77404667	0.50422469	1.87E-17	Pathog.	NA
KCNJ13	276	241	TRUE	T	P	P	NP	-0.3156926	0.50418577	1.67E-16	-1.0953166	0.69347023	1.08E-33	Pathog.	NA
KCNJ2	313	305	TRUE	T	P	P	NP	-0.3022349	0.14902165	3.19E-49	-0.3603093	0.41189316	1.82E-89	Pathog.	NA
KCNJ11	320	301	TRUE	R	P	C	NP	-0.085849	0.11349844	6.47E-12	-0.3967804	0.60734474	9.30E-224	Conflicting	NA
KCNJ13	324	289	TRUE	L	P	NP	NP	0.23251612	0.22730006	1.73E-76	-1.1498977	0.38553571	3.77E-07	VUS	NA
KCNJ1	329	301	TRUE	L	P	NP	NP	-0.3279855	0.18240395	2.13E-74	-5.3137211	0.65058704	0.00051825	VUS	NA
KCNJ13	337	302	TRUE	V	P	NP	NP	0.34008129	0.24557281	0	-2.2700407	0.56713841	3.40E-37	VUS	NA
KCNJ11	375	355	FALSE	I	P	NP	NP	-0.0149996	0.24895746	1.46E-13	1.38325817	0.58754565	3.89E-16	VUS	NA
KCNJ2	39	39	TRUE	T	P	P	NP	-0.0557057	0.15700515	1.87E-12	0.67993932	0.33265118	5.13E-47	NA	NA
KCNJ2	391	383	TRUE	T	P	P	NP	-0.1498527	0.25879987	2.41E-05	0.59734806	0.22464491	1.01E-37	NA	NA
KCNJ2	40	40	TRUE	R	P	C	NP	0.19531785	0.16232308	7.56E-05	-0.403249	0.21644627	8.93E-117	VUS	NA
KCNJ2	6	6	TRUE	T	P	P	NP	0.06422577	0.43163943	1.11E-16	0.77535928	0.16012158	1.47E-56	NA	NA
KCNJ11	63	50	TRUE	E	P	C	NP	NA	0.45387317	2.52E-05	NA	1.03723035	0	Pathog.	NA
KCNJ10	65	48	TRUE	G	P	NP	NP	0.12258965	0.10344839	1.74E-46	0.27221857	0.30548284	0.00015561	VUS	NA
KCNJ13	69	42	TRUE	L	P	NP	NP	0.42781756	0.67497991	1.96E-98	-0.5107045	0.71251235	1.33E-15	VUS	NA
KCNJ2	70	70	TRUE	A	P	NP	NP	-0.1877762	0.25300815	0	-0.3867626	0.22733274	1.09E-43	NA	NA
KCNJ10	82	65	TRUE	R	P	C	NP	0.49584	0.92447792	4.44E-16	1.48069054	0.45136594	7.09E-88	Pathog.	NA
KCNJ5	110	115	TRUE	H	Q	C	P	-0.7885147	0.13516796	0	-3.2076772	0.48363742	1.26E-14	VUS	NA
KCNJ10	114	97	TRUE	D	Q	C	P	0.2453186	0.42030739	0	1.71702862	0.54909852	0	VUS	NA
KCNJ2	16	16	TRUE	E	Q	C	P	0.14365255	0.07792135	2.13E-09	-0.4223595	0.20000718	3.63E-05	NA	NA
KCNJ10	19	18	FALSE	M	Q	NP	P	NA	1.17296925	0	NA	0.50066697	0	Conflicting	NA
KCNJ10	193	171	TRUE	K	Q	C	P	0.44827543	0.448121	0	-0.7867159	0.19207483	8.13E-35	Pathog.	NA
KCNJ13	193	162	TRUE	K	Q	C	P	0.44827543	0.448121	0	-0.7867159	0.19207483	8.13E-35	VUS	NA
KCNJ2	194	186	TRUE	P	Q	NP	P	NA	0.60439921	0	NA	NA	NA	Pathog.	NA
KCNJ11	195	175	TRUE	K	Q	C	P	-0.3952658	0.11612798	3.41E-47	-0.0876982	0.06591348	2.42E-97	VUS	NA
KCNJ10	197	175	TRUE	R	Q	C	P	NA	1.23718672	0	NA	0.7047267	3.40E-32	VUS	NA
KCNJ1	212	203	TRUE	R	Q	C	P	0.7609417	0.03194914	1.81E-19	1.19693932	0.41536539	1.16E-30	Pathog.	NA
KCNJ1	22	25	FALSE	A	Q	NP	P	1.30518211	0.10364641	1.28E-25	-0.4001721	0.11729979	2.97E-07	Conflicting	NA
KCNJ2	221	213	TRUE	R	Q	C	P	0.54666508	0.20007373	5.37E-05	0.09155217	0.33844477	1.34E-150	NA	NA
KCNJ13	226	195	TRUE	R	Q	C	P	-0.8277082	0.27759991	0.000211	0.68552006	0.55227255	5.55E-17	VUS	NA
KCNJ2	226	218	TRUE	R	Q	C	P	-0.8277082	0.27759991	0.000211	0.68552006	0.55227255	5.55E-17	Pathog.	NA
KCNJ13	234	203	TRUE	H	Q	C	P	-0.1045322	0.62993389	2.22E-16	-0.0076486	0.04503593	1.03E-84	VUS	NA
KCNJ2	236	228	TRUE	R	Q	C	P	-0.1262753	0.19868278	2.78E-17	-0.2917952	0.10192291	2.43E-24	NA	NA
KCNJ5	243	242	TRUE	R	Q	C	P	0.66262998	0.27486984	2.78E-17	2.0510676	0.26541578	1.94E-16	VUS	NA
KCNJ10	252	230	TRUE	P	Q	NP	P	-0.0517757	0.07935168	6.39E-138	-0.0360662	0.24494881	2.44E-30	VUS	NA
KCNJ13	276	241	TRUE	T	Q	P	P	NA	NA	NA	NA	NA	NA	VUS	NA
KCNJ5	320	319	TRUE	R	Q	C	P	-0.9115812	0.32457824	8.33E-17	0.59169972	0.49044089	2.64E-05	VUS	NA
KCNJ2	327	319	TRUE	E	Q	C	P	0.00154191	0.12308261	1.53E-08	-1.1698837	0.44379526	3.35E-86	NA	NA
KCNJ2	373	365	TRUE	K	Q	C	P	0.35924758	0.14850246	1.77E-32	1.53164756	0.52617052	5.55E-17	NA	NA
KCNJ5	377	384	FALSE	S	Q	P	P	0.12045601	0.19778769	6.65E-11	0.52265041	0.30833609	7.62E-07	VUS	NA
KCNJ2	40	40	TRUE	R	Q	C	P	0.38445058	0.10805885	1.63E-14	0.59280329	0.24216928	2.37E-89	VUS	NA
KCNJ10	44	27	TRUE	R	Q	C	P	0.41024925	0.32731931	3.05E-16	0.25237599	0.36951933	1.71E-06	VUS	NA
KCNJ10	45	28	TRUE	S	Q	P	P	0.60699648	0.27798678	1.18E-10	0.43060084	0.48268434	1.69E-13	VUS	NA
KCNJ13	45	18	TRUE	S	Q	P	P	0.60699648	0.27798678	1.18E-10	0.43060084	0.48268434	1.69E-13	VUS	NA
KCNJ2	5	5	FALSE	R	Q	C	P	-0.110338	0.18109326	8.72E-08	-0.3455816	0.11941815	4.97E-72	VUS	NA
KCNJ2	5	5	TRUE	R	Q	C	P	-0.110338	0.18109326	8.72E-08	-0.3455816	0.11941815	4.97E-72	NA	NA
KCNJ11	63	50	TRUE	E	Q	C	P	0.27077659	0.12203421	0	1.73204654	0.2906335	1.20E-69	Pathog.	NA
KCNJ2	67	67	TRUE	R	Q	C	P	NA	0.22981402	0	NA	1.23588301	3.88E-74	Pathog.	NA
KCNJ11	7	10	FALSE	N	Q	P	P	0.8688729	0.36648904	5.55E-17	0.06803085	0.04366372	1.06E-53	Benign	NA
KCNJ2	82	82	TRUE	R	Q	C	P	0.22959289	0.89361994	0	0.66934443	0.48783591	7.95E-29	Pathog.	NA
KCNJ2	101	101	TRUE	C	R	P	C	NA	NA	NA	NA	NA	NA	VUS	NA
KCNJ10	110	93	TRUE	H	R	C	C	-0.1185863	0.33301199	2.78E-17	-0.6177206	0.20222546	1.53E-09	VUS	NA
KCNJ2	110	110	TRUE	H	R	C	C	-0.1185863	0.33301199	2.78E-17	-0.6177206	0.20222546	1.53E-09	NA	NA
KCNJ11	124	103	FALSE	S	R	P	C	0.41670796	0.17001787	3.55E-08	-2.6031453	0.45875783	6.64E-09	VUS	NA
KCNJ16	151	132	TRUE	I	R	NP	C	-0.9160929	0.23840049	2.94E-29	2.07270519	0.44542722	0	Pathog.	NA
KCNJ5	152	151	TRUE	G	R	NP	C	0.01807352	0.28992943	0.00087857	-0.6027265	0.23376946	5.55E-09	Pathog.	NA
KCNJ5	152	151	TRUE	G	R	NP	C	0.01807352	0.28992943	0.00087857	-0.6027265	0.23376946	5.55E-09	Pathog.	NA
KCNJ10	162	140	TRUE	C	R	P	C	-0.5859797	0.65268537	1.52E-79	-5.3048493	0.32958772	0	Pathog.	NA
KCNJ5	169	168	TRUE	V	R	NP	C	NA	0.21271887	4.47E-06	NA	1.06727628	0	Pathog.	NA
KCNJ6	169	171	TRUE	V	R	NP	C	NA	0.21271887	4.47E-06	NA	1.06727628	0	Pathog.	NA
KCNJ11	176	156	TRUE	G	R	NP	C	NA	1.3193749	1.44E-77	NA	0.13375082	1.20E-22	Pathog.	NA
KCNJ11	190	170	TRUE	K	R	C	C	0.32069724	0.47800719	0	-0.1956935	0.27292945	1.18E-73	Pathog.	NA
KCNJ2	214	206	TRUE	G	R	NP	C	-0.4577752	0.01435293	0	0.96302869	0.14988208	1.86E-19	NA	NA
KCNJ1	228	219	TRUE	S	R	P	C	-0.1268836	0.23943715	8.22E-27	0.22229499	0.27419075	1.80E-16	Pathog.	NA
KCNJ1	229	220	TRUE	H	R	C	C	-0.2577727	0.04456277	1.24E-182	0.27356525	0.64247403	0	Pathog.	NA
KCNJ5	248	247	TRUE	G	R	NP	C	0.58518246	0.169647	2.56E-21	0.22270183	0.24615362	2.86E-12	Conflicting	NA
KCNJ2	256	248	TRUE	I	R	NP	C	NA	1.34657216	0	NA	0.47584934	1.70E-29	NA	NA
KCNJ11	260	240	TRUE	V	R	NP	C	NA	0.14104141	0	NA	1.14687979	0	VUS	NA
KCNJ10	274	252	TRUE	P	R	NP	C	NA	1.31435133	0	NA	NA	NA	VUS	NA
KCNJ11	279	259	TRUE	H	R	C	C	-0.8799472	0.29600795	0	-4.7675695	0.54781824	0	Pathog.	NA
KCNJ10	3	2	FALSE	S	R	P	C	NA	0.27584734	2.20E-08	NA	1.28754145	4.02E-109	VUS	NA
KCNJ1	309	300	TRUE	M	R	NP	C	-0.2868253	0.00983036	2.64E-134	0.64374621	0.27886892	1.70E-34	VUS	NA
KCNJ10	309	286	TRUE	M	R	NP	C	-0.2868253	0.00983036	2.64E-134	0.64374621	0.27886892	1.70E-34	VUS	NA

KCNJ2	309	301	TRUE	M	R	NP	C	-0.2868253	0.00983036	2.64E-134	0.64374621	0.27886892	1.70E-34	Pathog.	NA
KCNJ2	318	310	TRUE	Q	R	P	C	-0.1812575	0.40927079	6.69E-73	-0.0389876	0.58086708	1.66E-39	VUS	NA
KCNJ2	33	33	FALSE	G	R	NP	C	0.3123512	0.24903528	1.06E-115	0.19559171	0.20457906	1.04E-43	VUS	NA
KCNJ2	33	33	TRUE	G	R	NP	C	0.3123512	0.24903528	1.06E-115	0.19559171	0.20457906	1.04E-43	NA	NA
KCNJ2	33	33	TRUE	G	R	NP	C	0.3123512	0.24903528	1.06E-115	0.19559171	0.20457906	1.04E-43	NA	NA
KCNJ10	331	308	TRUE	G	R	NP	C	-0.3158634	0.5183987	1.67E-16	-3.4097305	0.55974974	2.31E-104	VUS	NA
KCNJ2	34	34	FALSE	K	R	C	C	0.30855711	0.12780772	5.92E-53	0.52381231	0.14105176	1.04E-17	VUS	NA
KCNJ2	34	34	TRUE	K	R	C	C	0.30855711	0.12780772	5.92E-53	0.52381231	0.14105176	1.04E-17	NA	NA
KCNJ1	343	316	TRUE	H	R	C	C	0.55430129	0.5234075	0	0.25770651	0.06306767	7.21E-29	VUS	NA
KCNJ11	343	324	TRUE	H	R	C	C	0.55430129	0.5234075	0	0.25770651	0.06306767	7.21E-29	VUS	NA
KCNJ2	353	345	TRUE	H	R	C	C	NA	0.09003176	6.94E-18	NA	1.18991452	0	NA	NA
KCNJ2	372	364	TRUE	K	R	C	C	0.39946739	0.00139901	3.29E-43	0.71394322	0.30167436	2.12E-09	VUS	NA
KCNJ18	373	366	TRUE	K	R	C	C	0.73055186	0.37872094	8.85E-20	0.77811976	0.2064519	3.74E-09	Pathog.	NA
KCNJ10	374	341	FALSE	Y	R	A	C	-0.0939108	0.18207296	1.93E-36	2.41242284	0.7116637	0	VUS	NA
KCNJ5	377	384	FALSE	S	R	P	C	NA	1.0356861	4.44E-16	NA	0.49498491	6.30E-62	VUS	NA
KCNJ5	380	387	FALSE	N	R	P	C	0.99488737	0.17487817	1.30E-102	0.03199843	0.4329497	2.93E-33	Conflicting	NA
KCNJ10	383	350	FALSE	C	R	P	C	0.57417574	0.40717217	1.67E-16	1.30285404	0.40234538	5.55E-17	VUS	NA
KCNJ8	384	382	FALSE	Y	R	A	C	-0.1753688	0.16539323	5.57E-05	0.45457689	0.45174206	4.23E-43	VUS	NA
KCNJ10	387	354	FALSE	E	R	C	C	0.43626237	0.19150923	6.67E-105	-0.9997942	0.73912423	1.49E-28	VUS	NA
KCNJ2	392	384	TRUE	S	R	P	C	-0.0949467	0.22125439	1.11E-21	1.48659393	0.59202603	0	NA	NA
KCNJ5	400	407	FALSE	E	R	C	C	1.33011519	0.12131108	0	0.21852497	0.59171893	2.05E-52	VUS	NA
KCNJ2	41	41	TRUE	Q	R	P	C	NA	1.17302104	0	NA	0.48770244	1.27E-29	NA	NA
KCNJ2	43	43	TRUE	C	R	P	C	2.57555034	0.49912518	0	0.32584989	0.47902512	0	NA	NA
KCNJ2	53	53	TRUE	H	R	C	C	NA	NA	NA	NA	NA	NA	VUS	NA
KCNJ11	54	42	TRUE	C	R	P	C	-0.220711	0.35716088	2.78E-17	0.47790627	0.25726118	3.59E-21	Pathog.	NA
KCNJ2	57	57	TRUE	Q	R	P	C	1.02183737	0.67623199	1.49E-18	-0.438059	0.76985041	4.69E-51	NA	NA
KCNJ11	65	52	FALSE	G	R	NP	C	NA	1.00000668	0	NA	0.72243286	0	Pathog.	NA
KCNJ11	66	53	FALSE	Q	R	P	C	-0.1435105	0.39195234	0	2.67191319	0.80245595	0	Pathog.	NA
KCNJ11	75	62	TRUE	T	R	P	C	NA	1.1609014	1.33E-15	NA	0.55794541	3.42E-08	Pathog.	NA
KCNJ2	75	75	TRUE	T	R	P	C	NA	1.1609014	1.33E-15	NA	0.55794541	3.42E-08	Pathog.	NA
KCNJ10	94	77	TRUE	L	R	NP	C	-1.307555	0.68322546	0	-4.5182065	0.35015376	5.22E-17	Pathog.	NA
KCNJ2	94	94	TRUE	L	R	NP	C	-1.307555	0.68322546	0	-4.5182065	0.35015376	5.22E-17	NA	NA
KCNJ10	109	92	TRUE	L	S	NP	P	0.58729739	0.08843671	2.32E-89	1.9820412	0.33837486	6.29E-08	VUS	NA
KCNJ11	111	98	TRUE	G	S	NP	P	0.15942105	0.04984059	1.46E-67	-2.2252016	0.41584718	7.78E-10	VUS	NA
KCNJ10	126	101	FALSE	V	S	NP	P	0.3632812	0.05010249	2.05E-66	-0.6226335	0.64461423	9.48E-48	VUS	NA
KCNJ12	129	122	FALSE	A	S	NP	P	0.35299465	0.15338688	7.85E-29	-0.026106	0.08127674	1.55E-28	VUS	NA
KCNJ2	137	129	TRUE	F	S	A	P	-1.0280037	0.19881573	7.32E-66	-2.4793292	0.61529254	5.36E-38	NA	NA
KCNJ2	152	144	TRUE	G	S	NP	P	-0.7925531	0.17992375	0	-1.7184187	0.09852751	2.33E-104	Pathog.	NA
KCNJ6	152	154	TRUE	G	S	NP	P	-0.7925531	0.17992375	0	-1.7184187	0.09852751	2.33E-104	Pathog.	NA
KCNJ10	154	132	TRUE	G	S	NP	P	NA	NA	NA	NA	0.90236684	0	VUS	NA
KCNJ2	154	146	TRUE	G	S	NP	P	NA	NA	NA	NA	0.90236684	0	VUS	NA
KCNJ11	156	136	TRUE	R	S	C	P	0.60820281	0.73594437	2.59E-26	-2.2756636	0.50049347	2.44E-99	VUS	NA
KCNJ13	157	127	TRUE	C	S	P	P	-0.3477431	0.01639043	1.43E-56	0.50261263	0.22875048	0	VUS	NA
KCNJ5	157	157	TRUE	C	S	P	P	-0.3477431	0.01639043	1.43E-56	0.50261263	0.22875048	0	Pathog.	NA
KCNJ2	163	155	TRUE	P	S	NP	P	0.08679943	0.00446285	5.75E-16	-1.5206632	0.29800883	2.52E-61	NA	NA
KCNJ2	167	159	TRUE	F	S	A	P	-0.2197596	0.10815442	2.32E-15	-0.3107093	0.13534708	3.63E-83	NA	NA
KCNJ5	174	173	TRUE	I	S	NP	P	NA	0.39313788	0	NA	NA	NA	VUS	NA
KCNJ2	18	18	FALSE	G	S	NP	P	-0.0571234	0.91208214	0	-0.4270599	0.55910716	1.89E-104	VUS	NA
KCNJ2	18	18	TRUE	G	S	NP	P	-0.0571234	0.91208214	0	-0.4270599	0.55910716	1.89E-104	NA	NA
KCNJ5	180	179	TRUE	D	S	C	P	NA	NA	NA	NA	NA	NA	VUS	NA
KCNJ2	181	173	TRUE	A	S	NP	P	-0.0398378	0.57195786	0	1.4745158	0.24239512	3.13E-80	NA	NA
KCNJ2	185	177	TRUE	G	S	NP	P	0.26817772	0.12205433	7.91E-81	0.62718678	0.07762483	1.16E-72	VUS	NA
KCNJ8	186	176	TRUE	A	S	NP	P	-0.0185103	0.41898672	7.74E-71	1.30191594	0.31718159	4.09E-35	VUS	NA
KCNJ2	186	178	TRUE	A	S	NP	P	-0.0185103	0.41898672	7.74E-71	1.30191594	0.31718159	4.09E-35	NA	NA
KCNJ1	193	186	TRUE	K	S	C	P	1.21351427	0.24349242	0	0.61035028	0.90163084	0	VUS	NA
KCNJ2	200	192	TRUE	T	I	P	NP	-0.6218589	0.02573524	7.01E-79	-4.2734263	0.06090926	9.71E-28	VUS	lof_s
KCNJ6	23	26	FALSE	T	S	P	P	0.32246215	0.06437545	5.72E-71	0.5009554	0.22328221	2.41E-152	VUS	NA
KCNJ2	230	222	TRUE	L	S	NP	P	-0.2747064	0.40750043	2.00E-11	-0.3045224	0.29755472	6.94E-17	Pathog.	NA
KCNJ2	237	229	TRUE	A	S	NP	P	0.70824382	0.44558956	2.22E-16	1.31562645	0.24520334	1.91E-22	NA	NA
KCNJ10	242	220	TRUE	S	S	P	P	NA	NA	NA	NA	NA	NA	VUS	NA
KCNJ2	259	251	TRUE	N	S	P	P	0.33042112	0.07540504	1.74E-33	-0.144841	0.21487495	1.37E-131	VUS	NA
KCNJ13	268	234	TRUE	R	S	C	P	0.15085016	0.59349681	1.34E-61	0.04077545	0.30969748	7.01E-67	VUS	NA
KCNJ2	28	28	FALSE	N	S	P	P	0.00726724	0.24838588	1.94E-106	1.05011147	0.14858556	0	VUS	NA
KCNJ2	28	28	TRUE	N	S	P	P	0.00726724	0.24838588	1.94E-106	1.05011147	0.14858556	0	NA	NA
KCNJ2	298	290	TRUE	A	S	NP	P	0.65975989	0.07731139	3.25E-70	0.13905157	0.47528642	3.06E-81	NA	NA
KCNJ2	316	308	TRUE	T	S	P	P	NA	2.06152581	0	NA	0.34627024	2.12E-34	VUS	NA
KCNJ2	326	318	TRUE	N	S	P	P	0.3926778	0.05546238	4.35E-08	0.03666977	0.45388344	4.85E-116	VUS	NA
KCNJ11	331	312	TRUE	G	S	NP	P	0.24647365	0.20335328	2.78E-17	-0.9377784	0.71960672	3.07E-32	VUS	NA
KCNJ10	336	313	TRUE	P	S	NP	P	0.64241564	0.69729172	2.22E-16	1.76820033	0.36399263	1.71E-19	VUS	NA
KCNJ11	344	325	TRUE	Y	S	A	P	0.0778356	0.17446428	0.00054084	0.43918675	0.11025251	6.30E-83	VUS	NA
KCNJ2	359	351	TRUE	P	S	NP	P	0.47768964	0.04655664	7.86E-18	-0.2497749	0.12833153	1.31E-35	VUS	NA
KCNJ1	362	353	TRUE	P	S	NP	P	-1.4473659	0.30816698	0	-4.2739315	0.44661643	4.37E-08	VUS	NA
KCNJ10	362	339	TRUE	P	S	NP	P	-1.4473659	0.30816698	0	-4.2739315	0.44661643	4.37E-08	VUS	NA
KCNJ2	380	372	TRUE	N	S	P	P	0.41357152	0.00506201	3.24E-126	-0.0508585	0.55261843	5.12E-114	NA	NA
KCNJ8	391	389	FALSE	T	S	P	P	0.63111922	0.25201744	1.50E-44	0.31036128	0.35027918	1.81E-29	VUS	NA
KCNJ8	396	394	FALSE	E	S	C	P	-0.5517616	0.26441508	1.66E-28	0.37826623	0.08670253	1.27E-106	VUS	NA
KCNJ8	41	30	TRUE	Q	S	P	P	0.02198101	0.64952016	0	-0.4096233	0.04827894	3.60E-08	VUS	NA
KCNJ2	46	46	TRUE	R	S	C	P	0.41769445	0.07834946	1.94E-30	-1.9563797	0.17983145	2.13E-120	NA	NA
KCNJ8	49	38	TRUE	K	S	C	P	0.68292846	0.04063898	2.94E-23	0.1599154	0.42560915	3.35E-87	VUS	NA
KCNJ5	52	58	TRUE	G	S	NP	P	NA	NA	NA	NA	NA	NA	VUS	NA
KCNJ2	59	59	TRUE	I	S	NP	P	0.17646196	0.48682124	0	0.60892863	0.34265166	6.98E-203	NA	NA
KCNJ2	60	60	TRUE	N	S	P	P	0.14917338	0.20358047	7.07E-26	0.53960923	0.38745655	5.36E-05	NA	NA
KCNJ11	66	53	FALSE	Q	S	P	P	0.61799428	0.1868593	0.00021149	1.10011303	0.11881422	2.29E-40	Pathog.	NA
KCNJ2	200	192	TRUE	T	I	P	NP	-0.6218589	0.02573524	7.01E-79	-4.2734263	0.06090926	9.71E-28	VUS	lof_f
KCNJ11	73	60	TRUE	F	S	A	P	-0.6128985	0.41238871	1.32E-46	1.13954924	0.59292843	4.73E-80	VUS	NA
KCNJ13	73	45	TRUE	F	S	A	P	-0.6128985	0.41238871	1.32E-46	1.13954924	0.59292843	4.73E-80	VUS	NA
KCNJ13	89	62	TRUE	C	S	P	P	NA	NA	NA	NA	NA	NA	VUS	NA
KCNJ2	106	106	TRUE	I	T	NP	P	0.02209835	0.18576832	1.46E-45	1.41472386	0.27766334	3.52E-64	NA	NA
KCNJ13	109	81	TRUE	L	T	NP	P	-0.2814927	0.00188124	1.30E-26	0.6837192	0.49495254	3.30E-113	VUS	NA
KCNJ10	126	101	FALSE	V	T	NP	P	0.56618817	0.19342662	3.61E-58	-0.3396942	0.57203056	5.64E-43	VUS	NA
KCNJ10	127	102	FALSE	S	T	P	P	0.17638243	0.0216878	6.48E-32	0.74265379	0.20724278	3.38E-152	VUS	NA
KCNJ2	128	120	FALSE	K	T	C	P	0.58371936	0.50810709	0	1.07852914	0.20695994	0.00011608	VUS	NA
KCNJ2	128	120	TRUE	K	T	C	P	0.58371936	0.50810709	0	1.07852914	0.20695994	0.00011608	NA	NA

KCNJ2	136	128	TRUE	S	T	P	P	0.09518165	0.20306704	5.20E-11	0.59526027	0.22649239	1.10E-91	NA	NA
KCNJ2	214	206	TRUE	G	S	NP	P	-0.0668832	0.14162936	4.72E-16	2.41385623	0.3903405	5.55E-17	VUS	gof_s
KCNJ2	224	216	TRUE	N	I	P	NP	-0.3768672	0.30093972	2.78E-17	0.00559434	0.60349132	3.42E-180	VUS	lof_f
KCNJ5	140	139	TRUE	A	T	NP	P	-0.6449412	0.1622505	0	-4.8234192	0.63794591	4.00E-08	VUS	NA
KCNJ2	145	137	TRUE	I	T	NP	P	0.21402035	0.02274494	8.37E-67	-0.8611753	0.65664059	0	NA	NA
KCNJ13	151	120	TRUE	I	T	NP	P	-0.8560252	0.10834958	8.32E-10	0.70016923	0.19730566	2.08E-17	Pathog.	NA
KCNJ5	151	150	TRUE	I	T	NP	P	-0.8560252	0.10834958	8.32E-10	0.70016923	0.19730566	2.08E-17	VUS	NA
KCNJ2	164	156	TRUE	I	T	NP	P	0.20158884	0.11359283	5.89E-79	0.55726094	0.32707565	2.78E-17	NA	NA
KCNJ10	165	143	TRUE	A	T	NP	P	-0.1583065	0.03744314	1.92E-23	-3.0333024	0.33817413	1.18E-12	VUS	NA
KCNJ2	181	173	TRUE	A	T	NP	P	NA	NA	NA	NA	0.05622465	0	NA	NA
KCNJ2	186	178	TRUE	A	T	NP	P	NA	2.40630246	0	NA	0.23469612	0	VUS	NA
KCNJ2	188	180	TRUE	M	T	NP	P	NA	0.28203561	2.72E-54	NA	1.1529864	0	NA	NA
KCNJ10	191	169	TRUE	M	T	NP	P	NA	NA	NA	NA	NA	NA	VUS	NA
KCNJ13	191	160	TRUE	M	T	NP	P	NA	NA	NA	NA	NA	NA	VUS	NA
KCNJ2	225	217	TRUE	L	P	NP	NP	-1.137943	0.20704488	7.77E-09	0.95397598	0.4226832	1.11E-16	VUS	lof_f
KCNJ1	207	198	TRUE	A	T	NP	P	0.01966008	0.18427112	0	-1.8794627	0.21918984	1.58E-06	Pathog.	NA
KCNJ5	207	206	TRUE	A	T	NP	P	0.01966008	0.18427112	0	-1.8794627	0.21918984	1.58E-06	VUS	NA
KCNJ2	209	201	TRUE	I	T	NP	P	0.60938713	0.09755563	1.62E-59	0.12926906	0.14370249	2.15E-116	NA	NA
KCNJ11	210	190	TRUE	A	T	NP	P	NA	0.96239236	0	NA	1.21451114	0	Benign	NA
KCNJ2	210	202	TRUE	A	T	NP	P	NA	0.96239236	0	NA	1.21451114	0	NA	NA
KCNJ2	211	203	TRUE	M	T	NP	P	0.15662396	0.054424	2.69E-36	0.4817775	0.10422307	2.08E-80	NA	NA
KCNJ10	22	21	FALSE	A	T	NP	P	-0.2168955	0.29788002	0	0.73299765	0.30769395	1.07E-207	VUS	NA
KCNJ10	223	201	TRUE	G	T	NP	P	-0.3225763	0.13439218	1.73E-16	-5.8799571	0.72587903	5.74E-17	Pathog.	NA
KCNJ10	231	209	TRUE	V	T	NP	P	-0.5938722	0.17148752	0	0.60219406	0.27103959	4.16E-17	Pathog.	NA
KCNJ2	24	24	TRUE	M	T	NP	P	2.18315124	0.17922703	5.11E-47	1.11112706	0.65931064	0	NA	NA
KCNJ2	256	248	TRUE	I	T	NP	P	0.61071751	0.07938094	6.54E-71	1.18548509	0.48152757	6.46E-11	NA	NA
KCNJ1	264	255	TRUE	S	T	P	P	0.75844835	0.29946704	2.78E-17	0.3185611	0.19210694	1.84E-62	VUS	NA
KCNJ2	266	258	TRUE	I	T	NP	P	0.39282036	0.30740475	6.91E-73	0.08865843	0.51907828	2.45E-100	Benign	NA
KCNJ1	268	259	TRUE	R	T	C	P	NA	NA	NA	NA	0.49855378	0	VUS	NA
KCNJ5	290	289	TRUE	L	T	NP	P	1.05228482	0.37319938	0	0.54020589	0.39029897	3.94E-07	VUS	NA
KCNJ2	298	290	TRUE	A	T	NP	P	0.77361994	0.64241112	0	0.56051458	0.22017475	3.06E-08	VUS	NA
KCNJ2	314	306	TRUE	A	T	NP	P	-0.3262252	0.12852256	6.60E-12	-0.2217983	0.10456904	1.44E-46	NA	NA
KCNJ5	324	323	TRUE	L	T	NP	P	0.83193547	0.23620277	1.11E-11	-0.2016431	0.56598839	6.77E-50	VUS	NA
KCNJ2	325	317	TRUE	A	T	NP	P	0.28424518	0.11851695	1.68E-87	0.14265039	0.28674238	1.21E-84	NA	NA
KCNJ2	342	334	TRUE	K	T	C	P	0.56998316	0.06467256	4.34E-05	0.27954082	0.4147094	4.36E-183	NA	NA
KCNJ2	35	35	TRUE	S	T	P	P	0.11259628	0.42341159	5.55E-17	-0.4771332	0.05350084	3.18E-61	NA	NA
KCNJ10	362	339	TRUE	P	T	NP	P	0.14505433	0.32212685	1.11E-16	-3.9457501	0.21567895	1.06E-07	VUS	NA
KCNJ2	370	362	TRUE	A	T	NP	P	0.01163465	0.13428862	1.14E-11	0.1427684	0.54677014	4.71E-39	NA	NA
KCNJ1	382	357	FALSE	F	T	A	P	1.3287837	0.36156858	1.69E-43	1.84404588	0.59938741	1.67E-16	Benign	NA
KCNJ10	385	352	FALSE	E	T	C	P	0.15693011	0.06313066	7.63E-58	-0.2883323	0.60865806	2.54E-45	VUS	NA
KCNJ5	389	396	FALSE	A	T	NP	P	0.39382157	0.02856946	5.00E-64	0.17291229	0.13923123	2.95E-17	VUS	NA
KCNJ10	62	45	FALSE	G	T	NP	P	-0.1162347	0.14095902	1.22E-07	-0.1877929	0.01655462	3.78E-92	VUS	NA
KCNJ2	70	70	TRUE	A	T	NP	P	-0.164519	0.3081641	7.74E-14	-0.2125355	0.55966611	2.45E-216	VUS	NA
KCNJ10	77	60	TRUE	V	T	NP	P	-0.4798462	0.01857826	7.17E-48	0.1174641	0.41033657	2.67E-84	VUS	NA
KCNJ2	79	79	TRUE	I	T	NP	P	0.40441482	0.08377215	0	-0.0036684	0.73752954	0	Pathog.	NA
KCNJ2	84	84	TRUE	M	T	NP	P	-0.7074572	0.28312653	1.10E-12	-2.3986519	0.57666463	8.75E-28	NA	NA
KCNJ10	90	73	TRUE	L	T	NP	P	-0.334471	0.49836049	0	1.40582041	0.41428977	2.19E-15	VUS	NA
KCNJ2	95	95	TRUE	S	T	P	P	-0.632556	0.19447049	1.42E-43	3.31941666	0.600983	2.07E-30	NA	NA
KCNJ5	10	14	FALSE	S	V	P	NP	0.41308633	0.02574947	5.56E-123	-0.3307459	0.52125872	4.60E-45	VUS	NA
KCNJ2	100	100	TRUE	G	V	NP	NP	NA	1.68061017	0	NA	NA	NA	VUS	NA
KCNJ2	108	108	TRUE	L	V	NP	NP	0.41120625	0.41784193	5.55E-17	-0.6259778	0.22848797	0	NA	NA
KCNJ2	11	11	TRUE	I	V	NP	NP	-0.3754531	0.58597905	3.66E-10	0.22239834	0.31439051	2.24E-15	NA	NA
KCNJ2	115	115	TRUE	T	V	P	NP	0.56069181	0.40029753	6.05E-87	-0.0994155	0.43524387	3.34E-36	VUS	NA
KCNJ2	127	119	TRUE	S	V	P	NP	0.02941659	0.22306018	4.16E-17	1.05112974	0.26765537	1.44E-23	NA	NA
KCNJ5	145	144	TRUE	I	V	NP	NP	0.24056978	0.05429875	1.83E-25	2.6197352	0.35490907	2.73E-08	Conflicting	NA
KCNJ10	151	129	TRUE	I	V	NP	NP	NA	NA	NA	NA	NA	NA	VUS	NA
KCNJ10	164	142	TRUE	I	V	NP	NP	0.13994054	0.28796659	2.78E-17	1.38134018	0.31711053	6.93E-15	VUS	NA
KCNJ2	164	156	TRUE	I	V	NP	NP	0.13994054	0.28796659	2.78E-17	1.38134018	0.31711053	6.93E-15	NA	NA
KCNJ10	166	144	TRUE	V	V	NP	NP	NA	NA	NA	NA	NA	NA	VUS	NA
KCNJ2	168	160	TRUE	M	V	NP	NP	0.99042949	0.02671707	1.67E-08	-0.731182	0.79537195	4.11E-84	NA	NA
KCNJ2	174	166	TRUE	I	V	NP	NP	NA	NA	NA	NA	1.35834804	0	NA	NA
KCNJ2	179	171	TRUE	I	V	NP	NP	NA	NA	NA	NA	NA	NA	VUS	NA
KCNJ2	183	175	TRUE	I	V	NP	NP	0.38404234	0.18640237	3.09E-91	0.17234427	0.41038179	1.11E-39	NA	NA
KCNJ10	189	167	TRUE	A	V	NP	NP	NA	NA	NA	NA	0.51188689	0	Pathog.	NA
KCNJ13	189	158	TRUE	A	V	NP	NP	NA	NA	NA	NA	0.51188689	0	VUS	NA
KCNJ10	2	1	FALSE	G	V	NP	NP	1.76156389	0.86870089	0	-2.5838537	0.13468574	1.04E-17	VUS	NA
KCNJ11	202	182	TRUE	V	V	NP	NP	-0.0325777	0.03161741	6.14E-30	0.04271552	0.12506578	2.88E-52	Pathog.	NA
KCNJ11	207	187	TRUE	A	V	NP	NP	-0.4461688	0.08481589	1.43E-94	-6.4128002	0.64313574	1.57E-19	Pathog.	NA
KCNJ5	209	208	TRUE	I	V	NP	NP	0.03067198	0.13986271	4.60E-152	-0.1594614	0.08671348	8.83E-30	VUS	NA
KCNJ1	223	214	TRUE	G	V	NP	NP	-0.2656066	0.52429619	0	0.5970073	0.22451012	8.17E-58	Pathog.	NA
KCNJ13	239	208	TRUE	L	V	NP	NP	0.65248375	0.05213728	1.52E-07	-0.0145948	0.32558665	3.08E-24	VUS	NA
KCNJ2	24	24	TRUE	M	V	NP	NP	NA	NA	NA	NA	NA	NA	NA	NA
KCNJ11	25	28	FALSE	A	V	NP	NP	1.16439907	0.64594197	2.22E-16	0.27174292	0.29322195	3.21E-43	VUS	NA
KCNJ10	251	229	TRUE	I	V	NP	NP	-0.2636265	0.08488757	1.38E-29	1.12464499	0.47469451	0	VUS	NA
KCNJ2	253	245	TRUE	L	V	NP	NP	-0.1628317	0.21600515	2.62E-54	0.93983464	0.29324411	5.55E-17	NA	NA
KCNJ2	231	223	TRUE	V	G	NP	NP	-0.3691811	0.30801811	2.78E-17	-0.2154182	0.21606531	6.68E-64	VUS	lof_f
KCNJ2	270	262	TRUE	F	V	A	NP	0.40868768	0.2833027	2.78E-17	0.10168922	0.14594997	1.43E-113	VUS	NA
KCNJ2	275	267	TRUE	I	V	NP	NP	0.21609787	0.29639374	1.73E-12	-0.5595222	0.54762629	1.22E-69	VUS	NA
KCNJ2	277	269	TRUE	I	V	NP	NP	0.57454507	0.48114417	1.44E-08	0.27672431	0.92207763	1.31E-12	NA	NA
KCNJ2	281	273	TRUE	I	V	NP	NP	NA	NA	NA	NA	1.01333776	0	NA	NA
KCNJ2	282	274	TRUE	D	V	C	NP	-0.1122013	0.80779854	3.12E-69	1.18529834	0.6157615	1.82E-13	VUS	NA
KCNJ11	290	270	TRUE	L	V	NP	NP	0.42185362	0.01545075	1.45E-18	0.18889538	0.14672132	3.84E-44	Benign	NA
KCNJ2	307	299	TRUE	E	V	C	NP	0.42050221	0.59221523	1.50E-07	0.63838007	0.03391521	5.03E-187	Pathog.	NA
KCNJ11	308	289	TRUE	G	V	NP	NP	-0.5443399	0.51787394	2.76E-13	-0.0204745	0.70423339	0	Pathog.	NA
KCNJ2	308	300	TRUE	G	V	NP	NP	-0.5443399	0.51787394	2.76E-13	-0.0204745	0.70423339	0	Pathog.	NA
KCNJ2	269	261	TRUE	I	V	NP	NP	-0.3799041	0.62069396	2.00E-20	0.77570555	0.0754483	6.41E-53	VUS	lof_f
KCNJ1	315	306	TRUE	M	V	NP	NP	-0.5209843	0.01909854	8.04E-06	-0.0590375	0.32528496	2.84E-144	VUS	NA
KCNJ11	315	296	TRUE	M	V	NP	NP	-0.5209843	0.01909854	8.04E-06	-0.0590375	0.32528496	2.84E-144	Pathog.	NA
KCNJ2	309	301	TRUE	M	L	NP	NP	-0.6957045	0.49204599	0	-0.1393457	0.38497113	1.25E-83	Conflicting	lof_f
KCNJ2	329	321	TRUE	L	V	NP	NP	0.02986839	0.35568533	0	0.97738161	0.32667398	1.52E-12	NA	NA
KCNJ6	44	53	TRUE	R	V	C	NP	1.20905984	0.33924969	2.60E-84	0.54573752	0.54997524	0	Benign	NA
KCNJ11	47	35	TRUE	F	V	A	NP	0.71691636	0.38068003	5.55E-17	-0.6776668	0.35700004	6.94E-90	Pathog.	NA
KCNJ15	5	6	FALSE	R	V	C	NP	0.08232901	0.05698406	1.42E-13	-0.9922843	0.50803161	1.11E-16	Benign	NA

KCNJ2	309	301	TRUE	M	V	NP	NP	-0.6693282	0.19420483	2.02E-07	0.01573106	0.40628209	2.02E-98	Conflicting	lof_f
KCNJ2	315	307	TRUE	M	I	NP	NP	-0.7175479	0.09290881	1.99E-34	-0.481593	0.12160307	1.38E-33	VUS	lof_f
KCNJ8	57	46	TRUE	Q	V	P	NP	NA	NA	NA	NA	0.39448643	6.34E-68	VUS	NA
KCNJ2	71	71	TRUE	D	V	C	NP	1.00340855	0.85017164	2.22E-16	-1.0252169	0.2968519	4.06E-74	Pathog.	NA
KCNJ2	85	85	TRUE	L	V	NP	NP	0.27657576	0.36230995	6.49E-14	-0.6348007	0.30310343	0	NA	NA
KCNJ2	87	87	TRUE	I	V	NP	NP	0.14704835	0.09265711	3.92E-33	0.12908661	0.43399975	1.11E-16	VUS	NA
KCNJ2	91	91	TRUE	A	V	NP	NP	0.4535043	0.06087486	3.92E-36	0.24243356	0.57248274	1.32E-65	NA	NA
KCNJ2	98	98	TRUE	F	V	A	NP	0.48549801	0.42873784	0	-0.3763099	0.386465	0	NA	NA
KCNJ11	186	166	TRUE	A	W	NP	A	-0.8453095	0.62411791	1.11E-16	0.32397819	0.19439502	0	Pathog.	NA
KCNJ10	19	18	FALSE	M	W	NP	A	0.12648476	0.06042266	4.36E-05	-2.0238281	0.28166805	3.15E-83	VUS	NA
KCNJ10	193	171	TRUE	K	W	C	A	0.13171266	0.27994746	3.00E-10	-0.2004754	0.84091396	0	VUS	NA
KCNJ13	193	162	TRUE	K	W	C	A	0.13171266	0.27994746	3.00E-10	-0.2004754	0.84091396	0	Pathog.	NA
KCNJ5	212	211	TRUE	R	W	C	A	0.27986015	0.278617	0	-0.0793948	0.24729635	1.04E-09	VUS	NA
KCNJ5	221	220	TRUE	R	W	C	A	-0.4560462	0.10802933	3.39E-11	-1.94495	0.3794728	1.40E-67	VUS	NA
KCNJ2	226	218	TRUE	R	W	C	A	0.19756449	0.55813353	0	-0.1926924	0.26260942	9.19E-13	Pathog.	NA
KCNJ5	236	235	TRUE	R	W	C	A	-0.0787073	0.78303552	0.0008113	0.29973448	0.10473114	0	VUS	NA
KCNJ5	243	242	TRUE	R	W	C	A	NA	0.6317913	3.78E-117	NA	NA	NA	VUS	NA
KCNJ10	252	230	TRUE	P	W	NP	A	-0.1815275	0.29840475	9.92E-08	5.03654636	0.40913285	0	VUS	NA
KCNJ2	290	282	TRUE	L	W	NP	A	0.98491073	0.40905832	2.98E-20	0.61974861	0.39075808	1.68E-33	VUS	NA
KCNJ1	3	6	FALSE	S	W	P	A	-0.7700401	0.76472234	4.44E-16	-4.5934661	0.8304699	0	VUS	NA
KCNJ11	43	31	TRUE	C	W	P	A	-0.2069305	0.22551873	2.21E-40	-2.5670829	0.40805221	1.67E-16	VUS	NA
KCNJ10	44	27	TRUE	R	W	C	A	0.11121399	0.09370754	8.67E-18	0.44337584	0.05443669	9.52E-06	VUS	NA
KCNJ2	67	67	TRUE	R	W	C	A	-0.451578	0.11157025	5.46E-08	-0.5923685	0.07908518	8.54E-16	Pathog.	NA
KCNJ5	67	72	TRUE	R	W	C	A	-0.451578	0.11157025	5.46E-08	-0.5923685	0.07908518	8.54E-16	VUS	NA
KCNJ2	82	82	TRUE	R	W	C	A	0.05653513	0.10582424	1.63E-65	0.91338758	0.57536506	0	Pathog.	NA
KCNJ2	315	307	TRUE	M	V	NP	NP	-0.5209843	0.01909854	8.04E-06	-0.0590375	0.32528496	2.84E-144	Conflicting	lof_f
KCNJ2	320	312	TRUE	R	H	C	C	-1.0766496	0.23778485	0	0.36217952	0.28633596	2.79E-05	Conflicting	lof_f
KCNJ1	130	121	TRUE	C	Y	P	A	-0.5721161	0.30153904	0	-1.393564	0.30187403	1.92E-34	VUS	NA
KCNJ2	322	314	TRUE	S	F	P	A	0.00762798	0.52934667	0	-5.6902336	0.94147175	4.44E-16	VUS	lof_s
KCNJ2	334	326	TRUE	Y	N	A	P	-0.2505895	0.25987178	2.78E-17	-2.6558446	0.11581231	3.01E-43	VUS	lof_s
KCNJ2	357	349	TRUE	E	K	C	C	0.18102372	0.08803897	4.70E-08	-1.3287225	0.26255468	2.08E-109	VUS	lof_s
KCNJ10	182	160	TRUE	F	Y	A	A	0.28509142	0.33906686	0	-0.273535	0.15651211	2.08E-17	VUS	NA
KCNJ11	186	166	TRUE	A	Y	NP	A	NA	0.02221711	6.47E-64	NA	1.02236761	4.86E-89	Pathog.	NA
KCNJ2	254	246	TRUE	D	Y	C	A	-1.1908554	0.522666	0	0.39607077	0.2609136	0	NA	NA
KCNJ1	27	30	FALSE	A	Y	NP	A	0.37204555	0.88879096	0	-0.7394914	0.84563894	1.78E-116	VUS	NA
KCNJ13	270	236	TRUE	F	Y	A	A	0.25348327	0.43131981	1.11E-16	-0.7705225	0.15576727	2.18E-38	VUS	NA
KCNJ2	297	289	TRUE	N	Y	P	A	0.53498714	0.44835728	1.11E-16	-0.6996906	0.09562638	4.59E-10	NA	NA
KCNJ2	326	318	TRUE	N	Y	P	A	0.32799972	0.07318408	7.27E-46	0.01572495	0.30684738	5.43E-112	NA	NA
KCNJ11	346	327	TRUE	K	Y	C	A	0.05951968	0.11161787	2.79E-36	-1.5363827	0.68051062	8.82E-222	VUS	NA
KCNJ2	38	38	TRUE	H	Y	C	A	-0.4344452	0.99418305	0	-1.9377759	0.48055852	0	NA	NA
KCNJ2	43	43	TRUE	C	Y	P	A	-0.0557136	0.12115544	0	0.91054931	0.22182247	0	VUS	NA
KCNJ11	73	60	TRUE	F	Y	A	A	0.05992666	0.20735178	0	-0.3808293	0.09432038	1.50E-44	Pathog.	NA
KCNJ2	78	78	TRUE	D	Y	C	A	-0.3850291	0.10987519	2.34E-59	-0.5878599	0.33285326	3.69E-55	Pathog.	NA
	7954														

Supplemental Table 3: Primers used in study.

>Landing_pad_genome_amplification_for

GGAGCAATTCCACAACACTTTTGTC

Landing_pad_genome_amplification_rev

TTGGTCCTGGATTTTCCTCCACATCACC

>Library_swap_to_landing_bsmbi_for

acgacCGTCTCcccgtcagatccgGCCACC

>Library_swap_to_landing_bsmbi_rev

agacaCGTCTCccttgtacagctcgtccatgcc

>backbone_swap_to_landing_bsmbi_for

cacagCGTCTCccaagagcggagctactaacttcagc

>backbone_swap_to_landing_bsmbi_rev

acagcCGTCTCcacggggtggcgtgtagttgcgg

>Kir_geneP_Mut-1_R Frag2-51 55.8C

ATACGTCTCCCATGGTGGCcggatc

>Kir_geneP_Mut-1_F Frag2-51 57.7C

ATACGTCTCTGGCCACTGTAATGTGCAGTT

>Kir_geneP_Mut-2_R Frag52-101 61.5C

ATACGTCTCCATCTTTCTTGACAAAGCGTGACC

>Kir_geneP_Mut-2_F Frag52-101 59.7C

ATACGTCTCCGTTTTTTGGTTGATCGCTTTGTTG

>Kir_geneP_Mut-3_R Frag102-151 59.5C

ATACGTCTCCGCAGCCAAAGAAGAGCCA

>Kir_geneP_Mut-3_F Frag102-151 59.3C

ATACGTCTCCGGATACGGGTTCCGATGC

>Kir_geneP_Mut-4_R Frag152-201 59.0C

ATACGTCTCCGATAGTGGTTTGTGTTTCGA

>Kir_geneP_Mut-4_F Frag152-201 59.1C

ATACGTCTCGGTTTTCAGTCACAACGCTGTG

>Kir_geneP_Mut-5_R Frag202-251 59.5C

ATACGTCTCCCAATGTCTCATTTCTTTTTTTGGGCT

>Kir_geneP_Mut-5_F Frag202-251 59.5C

ATACGTCTCACCACTCGATCAGATTGATATCAATGTG

>Kir_geneP_Mut-6_R Frag252-301 62.0C

ATACGTCTCGTATGTACTCTCCTTCTGAAGTTATGCG

>Kir_geneP_Mut-6_F Frag252-301 57.5C

ATACGTCTCAATTGTCGTTATACTGGAAGGGATG

>Kir_geneP_Mut-7_R Frag302-351 61.1C

ATACGTCTCTTTCGAAATCAGCGTTGTCGATGT

>Kir_geneP_Mut-7_F Frag302-351 59.1C

ATACGTCTCGTTCCACAAAACATACGAAGTTCCT

>Kir_geneP_Mut-8_R Frag352-401 59.5C

ATACGTCTCACCTAGAGTAGTCGACCTTATAATAGT

>Kir_geneP_Mut-8_F Frag352-401 58.6C

ATACGTCTCCGGAGTTCCCGAGTCAACC

>Kir_oligoP_Mut-1_F Frag2-51_58.6C

TTGGTCATGTGCTTTTCGTTGG

>Kir_oligoP_Mut-1_R Frag2-51_56.7C

ATACTCAGAATCGATTCCCCG

>Kir_oligoP_Mut-2_F Frag52-101_57.0C

TCCGACGGGGAGTATATACTC

>Kir_oligoP_Mut-2_R Frag52-101_58.2C

TCAGGCCAAAATAATCTCCGTTC

>Kir_oligoP_Mut-3_F Frag102-151_57.6C

GTACATGAAACGATGGACGGTAA

>Kir_oligoP_Mut-3_R Frag102-151_58.8C

TCCTCAGCGATGATCCTATGC

>Kir_oligoP_Mut-4_F Frag152-201_56.5C

GGCGAGAGGAGATATAGAGC

>Kir_oligoP_Mut-4_R Frag152-201_56.5C

GCTGTGCACATATATGGTCACA

>Kir_oligoP_Mut-5_F Frag202-251_56.9C

TTATAATCATCCTCCCCGGCT

>Kir_oligoP_Mut-5_R Frag202-251_59.4C

GTGTGCTCGACAGTTGACACTT

>Kir_oligoP_Mut-6_F Frag252-301_56.7C

AAGTTTGTGGGGTAGGGAATGA

>Kir_oligoP_Mut-6_R Frag252-301_56.5C

ACCTTTGCTAGGGAGCATAAG

>Kir_oligoP_Mut-7_F Frag302-351_56.5C

TGTCAGGGGTAGTGTAACACTAA

>Kir_oligoP_Mut-7_R Frag302-351_58.7C

AAATCGCTTCTAGGCAAGTTTATTG

>Kir_oligoP_Mut-8_F Frag352-401_56.3C

AGACCAGGATGGCTGATAAGT

>Kir_oligoP_Mut-8_R Frag352-401_56.6C

ACATATACCATCTAAACCACGACC